

CITATION: Stewart, M.S., Hannington, M.D., Emberley, J., Baxter, A.T., Krätschell, A., Petersen, S., Brandl, P.A., Anderson, M.O., Mercier-Langevin, P., Mensing, R., Breker, K., and Fassbender, M.L., 2022, A new geological map of the Lau Basin (southwestern Pacific Ocean) reveals crustal growth processes in arc-backarc systems: *Geosphere*, v. 18, no. 2, p. 910–943, <https://doi.org/10.1130/GES02340.1>.

Science Editor: Andrea Hampel
Associate Editor: Gianreto Manatschal

Received 1 September 2020
Revision received 16 December 2020
Accepted 12 October 2021

Published online 11 February 2022



This paper is published under the terms of the CC-BY-NC license.

© 2022 The Authors

A new geological map of the Lau Basin (southwestern Pacific Ocean) reveals crustal growth processes in arc-backarc systems

Margaret S. Stewart^{1,*}, Mark D. Hannington^{1,2}, Justin Emberley¹, Alan T. Baxter¹, Anna Krätschell², Sven Petersen², Philipp A. Brandl², Melissa O. Anderson^{2,3}, Patrick Mercier-Langevin⁴, Rebecca Mensing^{1,2}, Kaitlyn Breker¹, and Marc L. Fassbender¹

¹Department of Earth and Environmental Sciences, University of Ottawa, Ottawa, Ontario K1N 6N5, Canada

²GEOMAR Helmholtz Centre for Ocean Research Kiel, Wischhofstraße 1-3, 24148 Kiel, Germany

³Department of Earth Sciences, University of Toronto, Toronto, Ontario M5S 3B1, Canada

⁴Geological Survey of Canada, Québec, Québec G1K 9A9, Canada

ABSTRACT

A 1:1,000,000-scale lithostratigraphic assemblage map of the Lau Basin (southwestern Pacific Ocean) has been created using remote predictive mapping (RPM) techniques developed by geological surveys on land. Formation-level geological units were identified in training sets at scales of 1:100,000–1:200,000 in different parts of the basin and then extrapolated to the areas where geological data are sparse. The final compilation is presented together with a quantitative analysis of assemblage-level crustal growth based on area-age relationships of the assigned units. The data sets used to develop mapping criteria and an internally consistent legend for the compilation included high-resolution ship-based multibeam, satellite- and ship-based gravity, magnetics, seafloor imaging, and sampling data. The correlation of units was informed by published geochronological information and kinematic models of basin opening. The map covers >1,000,000 km² of the Lau-Tonga arc-backarc system, subdivided into nine assemblage types: forearc crust (9% by area), crust of the active volcanic arc (7%), backarc rifts and spreading centers (20%), transitional arc-backarc crust (13%), relict arc crust (38%), relict backarc crust (8%), and undivided arc-backarc assemblages (<5%), plus oceanic assemblages, intraplate volcanoes, and carbonate platforms. Major differences in the proportions of assemblage types compared to other intraoceanic subduction systems (e.g., Mariana backarc, North Fiji Basin) underscore the complex geological makeup of the Lau Basin. Backarc crust formed and is forming simultaneously at 12 different locations in the basin in response to widely distributed extension, and this is considered to be a dominant pattern of crustal accretion in large arc-backarc systems. Accelerated basin opening and a microplate breakout north of the Peggy Ridge has been accommodated by seven different spreading centers. The result is an intricate mosaic of small intact assemblages in the north of the basin, compared to fewer and larger

assemblages in the south. Although the oldest rocks are Eocene (~40 m.y. old basement of the Lau and Tonga Ridges), half of the backarc crust in the map area formed within the last 3 m.y. and therefore represents some of the fastest growing crust on Earth, associated with prolific magmatic and hydrothermal activity. These observations provide important clues to the geological evolution and makeup of ancient backarc basins and to processes of crustal growth that ultimately lead to the emergence of continents.

INTRODUCTION

Geological maps are critical to our understanding of Earth evolution and processes, from plate tectonics and crustal growth to basin evolution and the formation of mineral and energy resources, including in the oceans. The geomorphology of the global oceans has been determined from satellite altimetry and derived gravity models (Sandwell et al., 2014), but <5% of the seafloor has been explored in detail, leaving the vast majority unmapped and its geological makeup poorly understood at a meaningful scale (Mayer et al., 2018). Large-scale geological compilations covering the oceans have so far been limited to the 1:35,000,000-scale publication of the Commission for the Geological Map of the World (Bouysse, 2014) and the 1:17,000,000-scale map sheets of the Circum-Pacific Council for Energy and Resources (Scheibner et al., 2013). At these scales, the smallest features depicted are on the order of 100 km. Geological formations are mostly unclassified or limited to broad tectonic assemblages (e.g., Harrison et al., 2011; Petrov et al., 2016), sediment composition (e.g., Dutkiewicz et al., 2015), or geomorphology (Harris et al., 2014). Detailed geological maps of the ocean floor have been created in areas where high-resolution multibeam bathymetry, acoustic backscatter data, and direct seafloor observations were acquired (e.g., Parson et al., 1994; Pelletier et al., 2001; Clague et al., 2013; McClinton et al., 2013; Anderson et al., 2016, 2017; Embley and Rubin, 2018; Klischies et al., 2019). However, most of these maps are of limited areal extent (e.g., 1:100,000 scale) and rarely correlate units across a basin or regionally. To illustrate how lithostratigraphic correlations can be achieved for a larger area, we have prepared the first geological map of

*Present address: Department of Earth and Environmental Sciences, Mount Royal University, Calgary, Alberta T3E 6K6, Canada

Margaret Stewart <https://orcid.org/0000-0002-0633-252X>

the Lau Basin at 1:1,000,000 scale on a single sheet (Item S1¹) and correlated assemblage- and formation-level geological units across the entire basin.

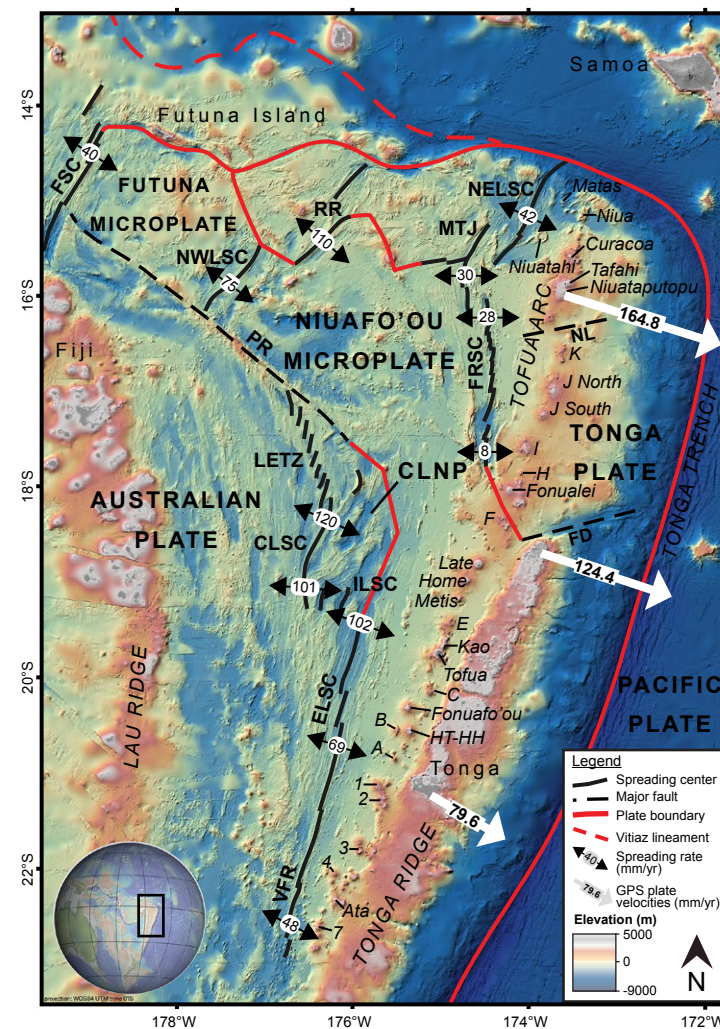
The Lau Basin (southwestern Pacific Ocean) is the type locality for intra-oceanic backarc basin formation, first recognized by Karig (1970). It was subsequently identified as the location of some of the fastest-growing crust on Earth (Hawkins, 1995; Taylor et al., 1996) and a region of prolific magmatic and hydrothermal activity (Lupton et al., 2012, 2015; Baker et al., 2019). After more than 50 research cruises since 1970, it is now one of the best-studied regions of the deep ocean. The available geophysical and sampling data provide the basis for recognition of discrete geological formations throughout the basin and for development of the first internally consistent geological legend. Using well-mapped areas as training sets, we assigned formation-level geological units to >1,000,000 km² of the Lau-Tonga arc-backarc system. The approach closely follows the techniques developed for remote predictive geological mapping (RPM) on land—and of other planets—in particular using well-established terrane classifications from terrestrial volcanic systems (e.g., Wilhelms and McCauley, 1971; Sabins, 1999; Schetselaar et al., 2007; Rogge et al., 2009; van der Meer et al., 2012; Tanaka et al., 2014). In many areas, the extrapolations are constrained by ship-based multibeam, magnetics, gravity, seismic reflection and refraction, and geological sampling data, including from drilling. In other areas where site-specific geological information is sparse, the extrapolation of formations was guided by remotely acquired geophysical data, including

¹Supplemental Material. Item S1: Geological map of the Lau Basin at 1:1,000,000 scale. Item S2: Geological map of the Mangatolu Triple Junction at 1:200,000 scale. Item S3: Cruise listing and data sources. Item S4: Ground-truthing dataset for the geological map of the Lau Basin. Please visit <https://doi.org/10.1130/GEOS.S.16869167> to access the supplemental material, and contact editing@geosociety.org with any questions.

Figure 1. Multibeam bathymetry compilation and regional tectonic map of the Lau Basin with interpreted plate boundaries, emerging microplates, spreading centers, major structures, and active volcanoes. Active volcanoes are indicated with italic labels. Names of the volcanoes are compiled from the literature, and therefore some volcanoes are referred to with names, some with numbers, and some with letters. Major plate boundaries are from Bird (2003); inferred microplate boundaries are from Conder and Wiens (2011) and Baxter et al. (2020). GPS velocities and azimuths (white arrows) for the Tonga plate (with Australia fixed) are from Phillips (2003). Spreading rates and spreading vectors (black arrows) for Rochambeau rifts (RR) and the Northwest Lau Spreading Center (NWLSC) are from Bird (2003). Spreading rates for the Central Lau Spreading Center (CLSC), Fonualei Rift and Spreading Center (FRSC), Eastern Lau Spreading Center (ELSC), Valu Fa Ridge (VFR), Mangatolu triple junction (MTJ) southern arm, and Northeast Lau Spreading Center (NELSC) are from Sleeper and Martinez (2016). The spreading rate for the Futuna Spreading Center (FSC) is from Pelletier et al. (2001). Ship tracks used in the compilation are indicated in Figure 2. Where ship track data does not exist, background is the slope-shaded GEBCO 2019 grid (GEBCO Bathymetric Compilation Group, 2019). Illumination is from the northwest (315°), and projection is WGS84 Universal Transverse Mercator Zone 01S. CLNP—Central Lau nanoplate (Conder and Wiens, 2011); FD—Fonualei discontinuity; HT-HH—Hunga Tonga-Hunga Ha'apai; ILSC—Intermediate Lau Spreading Center; LETZ—Lau extensional transform zone; NL—Niuatapu lineament; PR—Peggy Ridge.

satellite altimetry and derived vertical gravity gradient (Smith and Sandwell, 1997; Sandwell et al., 2014).

The Lau Basin is part of the Tonga subduction zone, between the active Tonga volcanic arc in the east and the remnant arc of the Lau Ridge in the west (Fig. 1). Opening of the basin started ~6 m.y. ago, initiated by retreat of the Tonga Trench. The characteristic V shape reflects progressive splitting of the older arc crust toward the south and asymmetric opening toward the west. Bathymetric and magnetic data show that early crustal accretion behind the arc occurred along



a major backarc spreading center, similar to a mid-ocean ridge (Hawkins, 1995; Taylor et al., 1996). Drilling by the Ocean Drilling Program (ODP) confirmed that the crust in the west of the basin formed through a combination of early-stage rifting followed by seafloor spreading (Hawkins, 1995). However, the sampled rocks have a range of ages spanning several millions of years that do not increase linearly with distance from the inferred spreading center as is typical at mid-ocean ridges. Instead, seafloor morphology and highly variable thickness and composition of sediment fill in numerous sub-basins throughout the backarc region indicate a more complex opening history. Chase (1971) was the first to postulate that several tectonic plates and triple junctions were needed to accommodate the rapid opening of the basin; however, many aspects of the structure and kinematics remained unresolved. Little was known about the more recent structure, particularly in the northern Lau Basin where a lack of high-resolution multibeam and high-quality magnetic data prevented a straightforward interpretation until recently (Zellmer and Taylor, 2001; Sleeper and Martinez, 2016). Seafloor mapping also provided particular insight into the crustal structure and composition as part of the Ridge2000 Integrated Studies Site in the central Lau Basin (e.g., Martinez et al., 2006) and more recently in the northeastern part of the basin (e.g., Embley and Rubin, 2018; Chadwick et al., 2019). One of the major results of the Ridge2000 research was the finding that arc proximity strongly influences morphology and thickness (Martinez and Taylor, 2002), chemistry (Pearce et al., 1995; Eason and Dunn, 2015), and seismic crustal structure (Dunn and Martinez, 2011; Arai and Dunn, 2014) in the near-ridge backarc. In addition, new refraction and multichannel reflection seismic data, ship-based gravity and magnetic data, multibeam bathymetry, and sediment echosounder data have been obtained in several long profiles crossing the northeastern Lau Basin (Hannington et al., 2019; Schmid et al., 2020), and an analysis of shallow seismicity has highlighted the kinematics of several emerging microplate boundaries in the area (Baxter et al., 2020). These data, together with compiled information from the past 50 years of research cruises, form the basis for the first comprehensive geological map of the Lau Basin, presented in this paper.

REGIONAL GEOLOGICAL SETTING

Opening of the Lau Basin was triggered by the collision of the Ontong Java and Melanesian Borderland plateaus with the Australian plate in the Miocene (Ruellan et al., 2003; Ruellan and Lagabrielle, 2005). The Pacific plate has been converging with the Australian plate at as much as 80 mm/yr at the northern end of the Tonga Trench when measured with respect to the Lau Ridge, which is part of the Australian plate. Opening of the Lau Basin, which is partitioned among several spreading systems, reaches a total rate of ~160 mm/yr at the northern end of the basin, but this involves spreading on microplates that are not part of the Australian plate. The combination sums to a total subduction rate of ~240 mm/yr (Pacific-Tonga convergence; Bevis et al., 1995). Tomographic images show the Pacific plate subducting below the active Tofua volcanic arc with dips of 60°–70° (Zhao et al., 2007). Rollback of the Pacific slab induced

upper-plate extension and separation of the former Vitiaz arc beginning at ca. 6 Ma. Because of the abrupt curvature of the trench at the northern edge of the Tonga platform, the slab is torn through the entire lithospheric thickness (Millen and Hamburger, 1998; Bonnardot et al., 2007). At the point of tearing, a STEP (subduction-transform edge propagator) fault (Govers and Wortel, 2005) developed along the northern Lau Basin after extinction of the Vitiaz subduction zone. The Vitiaz lineament is a relict feature of the extinct subduction zone and is presently inactive as shown by the lack of seismicity along it (e.g., Baxter et al., 2020). Transcurrent motion has stepped into the North Fiji Basin along the Fiji transform fault, and this deformation has left a trail of spreading centers, rift basins, and multiple microplates in the North Fiji Basin (Isacks et al., 1969; Millen and Hamburger, 1998).

Seafloor spreading started between 6 and 5.5 Ma in the north of the Lau Basin and has since propagated 700 km south following asymmetric rollback of the Pacific plate (Parson and Hawkins, 1994; Ruellan et al., 2003). The now-inactive Lau Ridge in the west (former Vitiaz arc) was separated from the Tonga Ridge in the east (Taylor et al., 1996). Because rifting of the Vitiaz crust initiated at the forearc, almost all of the original Eocene arc is now part of the Lau Ridge, which remained active even as the early backarc basin opened in front of it (Hawkins, 1995). Volcanism at the Lau Ridge continued for at least several million years after initial opening (until ca. 2.5 Ma; Parson et al., 1992a), and cores recovered during ODP Leg 135 confirm that volcanoclastic sediments in the local basins were derived first from the west and then from the east (Clift and Dixon, 1994). The active arc magmatism eventually stepped across the basin and reinitiated closer to its present position along the Tofua arc (Martinez and Taylor, 2006). Although it stabilized relatively recently, the Tofua arc has already begun to rift again at several locations in the northeastern part of the Lau Basin. A variety of geophysical data sets, including magnetization and GPS measurements, show that seafloor spreading is occurring in the south with a total opening rate of between 159 ± 10 and 91 ± 5 mm/yr and a maximum total opening of ~160 mm/yr between the northern Tonga Ridge and the Lau Ridge (Australian plate; Bevis et al., 1995). However, different models disagree on the precise locations where the strain is being taken up (Pelletier et al., 2001; Zellmer and Taylor, 2001; Conder and Wiens, 2011; Sleeper and Martinez, 2016).

Whereas only one major backarc spreading center was recognized in the 1980s, now at least 10 have been identified throughout the basin (Fig. 1). They include, in the south, the Eastern Lau Spreading Center (ELSC) and its southern extension, the Valu Fa Ridge, the Central Lau Spreading Center (CLSC), and the Lau extensional transform zone (LETZ), with a short relay zone (Intermediate Lau Spreading Center) between the ELSC and CLSC. This geometry was first described from GLORIA side-scan sonar surveys (Parson et al., 1990) and has since been refined by analysis of regional magnetics, gravity, and SeaMARC II side-scan sonar data (Zellmer and Taylor, 2001; Martinez and Taylor, 2006; Sleeper and Martinez, 2014, 2016; Sleeper et al., 2016). Based on spreading fabric and magnetic anomalies, the ELSC initially formed near 17°S and propagated south. Its northern segment has since been taken over by the CLSC near 18°S, which is now the main spreading center as far north as 19.5°S (Sleeper

and Martinez, 2014). Spreading at the ELSC was abandoned north of 19°S, but the overlap with the CLSC is marked by numerous sub-basins and a zone of right-lateral shearing (Parson et al., 1990). The different spreading centers are generally very similar to mid-ocean ridges in degree of segmentation, volcanic architecture, composition, and axial depths (minimum ~1800 m and maximum ~3200 m; average 2200–2300 m). Both the ELSC and CLSC are propagating south at an estimated rate of 120 mm/yr (Parson et al., 1990). In the northeastern Lau Basin, there are at least three additional spreading centers of different ages: the Mangatolu triple junction (MTJ), which includes both active and inactive arms; the Northeast Lau Spreading Center (NELSC); and the Fonualei Rift and Spreading Center (FRSC). Because there appears to be only one dominant spreading segment of the MTJ, we refer generally to this system as a single spreading center; however, the precise configuration remains to be determined. Farther west, the Northwest Lau Spreading Center (NWLSC), the Rochambeau rifts (RR), and the Futuna Spreading Center (FSC) have also been identified (Parson and Tiffin, 1993; Pelletier et al., 2001). Although the opening rate of the basin is comparable to that of ultrafast-spreading segments of the East Pacific Rise (Bevis et al., 1995), the individual spreading centers are much slower, with the extension distributed across many different structures. Sleeper and Martinez (2016) presented a revised kinematic model based on reinterpretation of the seafloor magnetization patterns and ridge morphology, which confirms the slow spreading in the east along the FRSC compensated by faster spreading in the west along the CLSC and LETZ. Focal mechanisms (centroid moment tensors) indicate a predominance of strike-slip motion, indicating significant rotation throughout the region (Parson et al., 1990; Wetzel et al., 1993; Sleeper and Martinez, 2014). Shallow seismicity shows that the main extensional faulting is occurring only at the northern and southern terminations of the spreading segments (Conder and Wiens, 2011; Baxter et al., 2020).

Zellmer and Taylor (2001) first proposed a three-plate kinematic model involving the Australian plate to the west, the Niuafo'ou microplate between the CLSC and the FRSC, and the Tonga plate to the east (Fig. 1). They postulated a paleo-spreading axis located near the arc during magnetic anomaly 2, which moved away from the arc toward the currently dominant spreading system (CLSC-LETZ) as the basin opened. More recently, seafloor spreading has reoccupied a position close to magnetic anomaly 2A in the FRSC (Sleeper et al., 2016). However, the ages of the magnetic anomalies are not well known in this region, and the seafloor features associated with those anomalies have only recently been mapped (Hannington et al., 2019). Among other complications, the region between the southern tip of the FRSC and the northern extension of the ELSC should be accommodating ~45 mm/yr of strain (Conder and Wiens, 2011), but it has been difficult to define a plate boundary at this location. Sleeper and Martinez (2016) predicted much slower opening rates (~8 mm/yr) at the southern tip of the FRSC, which is in better agreement with the lack of seismicity in the area, and Baxter et al. (2020) suggested a significant amount of non-rigid deformation throughout the northeastern Lau Basin region. North of the Niuafo'ou microplate, a complex pattern of small, poorly defined microplates has been recognized that formed in response to left-lateral

shear related to the transition from subduction to transform faulting at the northern termination of the Tonga Trench (Conder and Wiens, 2011; Baxter et al., 2020). This is an area of intense deformation, left-lateral strike-slip faulting, plate rotation, and extension in the forearc crustal blocks, suggesting that the northern margin of the basin is highly unstable and actively breaking up (Baxter et al., 2020).

METHODS AND DATA

The mapped formations were identified in training areas (e.g., MTJ; Item S2 [footnote 1]) using ship-based data sets, including multibeam bathymetry, acoustic backscatter (reflectivity), and side-scan sonar images of the seafloor integrated with gravity and magnetics. Additional data are from regional-scale side-scan sonar surveys (GLORIA and SeaMARC II) and airborne magnetics (Parson et al., 1990; Zellmer and Taylor, 2001; Martinez and Taylor, 2006). More than 650,000 km² of the map area is covered by ship-based multibeam and other geophysical data (Fig. 2), which were closely inspected to derive the mapped units. Digital enhancement techniques were used extensively (e.g., slope maps, terrain texture shading; see Lecours et al., 2016; Anderson et al., 2016, 2017). In the training areas, seafloor observations have been made from crewed submersibles (*Alvin*, *Pisces*, *Nautil*), remotely operated vehicles (ROVs), and autonomous underwater vehicles (AUVs), including at the Ridge2000 Integrated Studies Site (Martinez and Taylor, 2006; Baker et al., 2006; German et al., 2006), as part of the U.S. National Oceanographic and Atmospheric Administration (NOAA) Submarine Ring of Fire Program (R/Vs *Thompson*, *Kilo Moana*, *Roger Revelle*, and *Falkor*; Baker et al., 2006, 2011; Embley et al., 2007; Merle et al., 2010, 2013; Resing et al., 2011) and during operations aboard R/V *Ka'imikai-O-Kanaloa* (Stoffers et al., 2006). Extensive commercial surveys have also been carried out by Nautilus Minerals Inc. in partnership with the TELVE, NoToVE, and NoLauVE cruises led by Australian National University (R/V *Southern Surveyor*; Arculus, 2003, 2004, 2008, 2009). Ten research cruises of R/V *Sonne* (I and II) have been conducted in the area (cruise SO35: von Stackelberg et al., 1985; SO48: von Stackelberg et al., 1987; SO67: von Stackelberg et al., 1990; SO135: Stoffers et al., 1999; SO167: Stoffers et al., 2003; SO192: Schwarz-Schampera et al., 2007; SO195: Grevenmeyer and Flüh, 2008; SO215: Peirce et al., 2011; SO263: Haase et al., 2018; SO267: Hannington et al., 2019). ROVs and AUVs that were used to map the active arc and backarc spreading centers include Canadian ROV *ROPOS* (R/V *Sonne* cruise SO192: Schwarz-Schampera et al., 2007; R/V *Falkor* cruise FK160320: Kwasnitschka et al., 2016), ROV *Quest* from the University of Bremen (R/V *Roger Revelle* cruise RR1211: Merle et al., 2013; R/V *Sonne* cruise SO263: Haase et al., 2018), ROV *SuBastian* from the Schmidt Ocean Institute (R/V *Falkor* cruise FK171110: Rubin et al., 2018), ROV *Jason* and AUV *Sentry* from the Woods Hole Oceanographic Institution (R/V *Thompson* cruise TN234: Merle et al., 2009; R/V *Falkor* cruise FK171110: Rubin et al., 2018), AUV *D. Allen B.* from the Monterey Bay Aquarium Research Institute (R/V *Thompson* cruise TN234: Merle et al.,

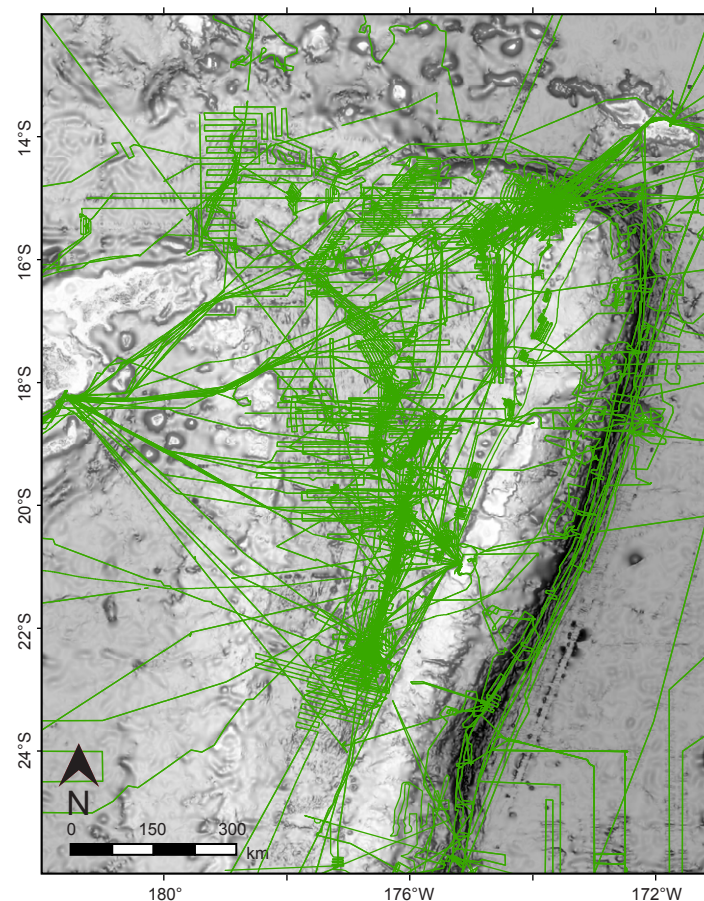


Figure 2. Locations of ship tracks where multibeam bathymetry and other geophysical data are available and were used in the creation of the 1:1,000,000-scale geological map. The total area covered by the ship-based multibeam is estimated to be ~650,000 km², based on 195,000 line km of ship tracks. Selected multibeam data sets were reprocessed with 35 m to 50 m grid spacing (listed in Item S1 [text footnote 1]). Primary data sets were obtained from publicly available national repositories, cruise reports, and chief scientists of the respective expeditions. Background is the slope-shaded GEBCO 2019 grid (GEBCO Bathymetric Compilation Group, 2019).

2009), and GEOMAR's AUV *Abyss* (R/V *Kilo Moana* cruise KM1129A: Martinez et al., 2013; R/V *Sonne* cruise SO267: Hannington et al., 2019). Research cruises of IFREMER with the submersible *Nautilus* were conducted in the French territorial waters of Futuna in 1999, 2000, 2010, and 2012 (R/V *L'Atalante*; Pelletier et al., 2000, 2001; Fouquet et al., 2015; Konn et al., 2016, 2018); more recent cruises have focused on the FRSC (Hannington et al., 2019) and the NELSC and Mata

volcanoes (cruise RR1211: Merle et al., 2013; cruise FK160320: Kwasnitschka et al., 2016; cruise SO267: Haase et al., 2018; R/V *Kilo Moana* cruises KM1024 and KM1129A: Embley and Rubin, 2018; cruise FK171110: Rubin et al., 2018; Chadwick et al., 2019). Extensive dredging, sediment coring, and grab sampling has also been conducted. The distribution of geological sampling and seafloor observations is shown in Figure 3, and a complete listing of the data sources is provided in Items S3 and S4 (footnote 1).

These data were compiled from the literature and from cruise reports as georeferenced layers in ESRI ArcGIS software. Geological formations were then assigned on the basis of structure, crustal type (and thickness, where known), magnetic character, spreading fabric, composition, age, and sediment cover. Where multibeam data were available for reprocessing and gridding, detailed maps were prepared at 1:100,000–1:200,000 scale for training purposes and to establish an internally consistent classification system and legend. The interpreted formations and structures in the training areas were then digitized in ArcGIS and extrapolated to areas with fewer data to create the 1:1,000,000-scale map. The digitized map consists of 1159 polygons grouped into 49 different formations. Surface areas of the mapped features were calculated using the *Calculate Geometry* tool of ArcGIS using a Lambert cylindrical equal-area projection. At 1:1,000,000 scale, the average area of the mapped formations is 1014 km² per polygon (excluding individual volcanoes); for the backarc crust, it is 540 km² per polygon. The spatial resolution is comparable to that of regional (1:2,000,000 to 1:5,000,000 scale) quantitative bedrock maps on land, which ranges from 297 km² to 801 km² per polygon (Peucker-Ehrenbrink and Miller, 2002, 2003, 2004, 2007a, 2007b). The average number of polygons per formation type, approximately 35, provides a statistically meaningful basis for spatial analysis in a map of this scale, following the criteria of Peucker-Ehrenbrink and Miller (2003) and Peucker-Ehrenbrink and Miller (2004). By comparison, the ocean areas of the current *Geological Map of the World* (Bouysse, 2014) are represented by polygons with an average size of 74,700 km², based on 5215 polygons. The resolution of the 1:1,000,000-scale Lau Basin map is at least an order of magnitude higher than that of the *Tectonic Map of the Circum-Pacific Region* at 1:17,000,000 scale (Scheibner et al., 2013) and 50 times higher than that of the offshore areas depicted in the *Geological Map of the World*.

Regional Bathymetric Data

Global bathymetric data for the study area were compiled from Shuttle Radar Topography Mission (SRTM) 30+ and SRTM 15+ data sets (Becker et al., 2009; Tozer et al., 2019), the *General Bathymetric Chart of the Oceans* (GEBCO Bathymetric Compilation Group, 2019), and the Global Multi-Resolution Topography data synthesis (GMRT version 3.6; Ryan et al., 2009). All four data sets use global marine gravity based on satellite altimetry, including the most recent data collected during the CryoSat-2 and Jason-1 missions, which have significantly improved the global gravity model (Sandwell et al., 2014). These data are

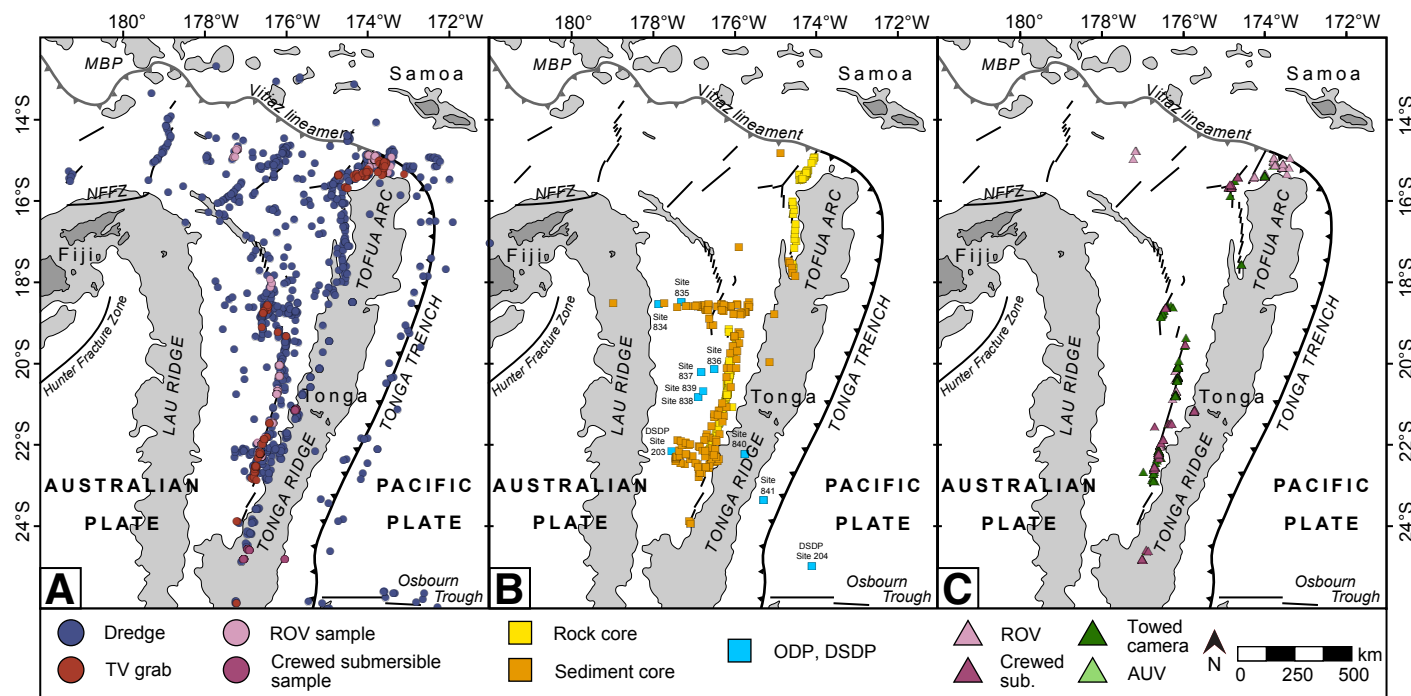


Figure 3. Summary of data used for ground truthing in the Lau Basin. (A) Samples collected by dredge, remotely operated vehicles (ROVs), human-occupied submersibles, and TV grabs. (B) Wax cores, sediment cores, and drill cores from the Deep Sea Drilling Project (DSDP; Sites 203, 204) and Ocean Drilling Program (ODP; Sites 834–841). (C) Seafloor observation data from towed cameras, submersibles, ROVs, and autonomous underwater vehicles (AUVs). More than 2600 discrete data points exist for the Lau Basin, with 2460 samples (including wax and sediment cores), 11 drill sites (DSDP and ODP), and 210 seafloor observations. The complete data set is summarized in Item S4 of the Supplemental Material (text footnote 1). MBP—Melanesian Borderland Plateau; NFFZ—North Fiji fracture zone.

calibrated with depth soundings to predict the bathymetry of the global seafloor at 30 arc-second and 15 arc-second resolution (SRTM 30+ and 15+, respectively). The GEBCO 2019 grid uses SRTM 15+ as a base. The GMRT grid (version 3.6) also incorporates ship-based multibeam data processed and gridded at 100 m resolution. In areas with no ship-based multibeam coverage, GMRT uses the GEBCO 2014 compilation with 30 arc-second resolution. Version 3.7 of the GMRT grid was released in October 2019, after completion of our map, but there are no significant changes in the newer version in the Lau Basin region.

Ship-Based Multibeam and Acoustic Backscatter Data

Ship-based multibeam echo-sounder (MBES) data were also compiled from cruise data and public repositories (Fig. 2). Where available, raw data received as a point cloud were edited using Quality Positioning Services Fledermaus or

Qimera software to generate bathymetric grids. Approximately 195,000 line km of multibeam data, with an average swath of 4 km, have been compiled for the Lau Basin, including data not currently available in GMRT. In selected areas used for training at 1:100,000–1:200,000 scale, we reprocessed the data at 35 m to 50 m resolution. For the 1:1,000,000-scale map, the multibeam data were gridded at 100 m and integrated with GMRT version 3.6 to create the final bathymetric base. Data enhancements in ArcGIS, designed to capture the complex structure of the seafloor, were applied. These included the slope raster, implemented with the *Slope* tool, and the shaded-relief raster, implemented with the *Hillshade* function.

We incorporated GLORIA and SeaMARC II side-scan sonar data in the ArcGIS base layers where available to identify hard rock substrate or sediment cover. We used the compilation of GLORIA data from Zellmer and Taylor (2001) and combined it with higher-resolution backscatter data from MBES systems where they were recorded.

Satellite-Derived Gravity Gradient

The vertical gravity gradient (VGG) and gravity anomalies derived from the CryoSat-2 and Jason-1 satellite missions were used to investigate large-scale structures with an average pixel size $>5 \text{ km}^2$. Seamounts between 1 and 2 km in height that were not visible in the older data sets are now visible in the CryoSat-2 and Jason-1 data, and buried structures (e.g., abyssal fabric with wavelengths of 2–12 km) can also be seen (Sandwell et al., 2014; MacLeod et al., 2017). The microplate boundaries typically appear as gravity lows, whereas volcanoes, seamounts, or other regions of focused crustal accretion typically appear as gravity highs. Mapping of these features based on VGG was greatly enhanced by merging the gravity gradient with bathymetric data, which was done using the GEBCO 2014 grid.

Magnetic Anomalies

Two types of magnetic data were used to guide the mapping: the 2-arc-minute-resolution Earth Magnetic Anomaly Grid (EMAG2; Maus et al., 2009) and the two-dimensional (2-D) magnetic inversions produced by Zellmer and Taylor (2001) and Sleeper and Martinez (2016). EMAG2 incorporates satellite, airborne, and marine magnetic measurements, compiled at a global scale. It was used to assist mapping of basin-scale structures; combined with VGG, the magnetic anomalies identify several of the assemblage boundaries in areas where multibeam or other data were limited. The 2-D magnetic inversions of Zellmer and Taylor (2001) and Sleeper and Martinez (2016) combine ship-based magnetic data with regional aeromagnetic data from the U.S. National Geophysical Data Center. The inversions identify regions of normal or reversed magnetic polarity (positive and negative magnetic anomalies) that can be correlated with spreading fabric. The compilation by Zellmer and Taylor (2001) covers most of the map area, whereas the study of Sleeper and Martinez (2016) is focused on the CLSC and FRSC. Both studies attempted to correlate anomalies with magnetic polarity chrons, which provided a means of assigning relative ages to formations, especially south of $\sim 18^\circ\text{S}$.

Multichannel Seismic Reflection and Seismicity

Seismic reflection data were collected in the western half of the Lau Basin as part of the site survey data for ODP Leg 135 (Parson et al., 1994), and several attempts were made to image the magma chamber of the Valu Fa Ridge and ELSC (Collier and Sinha, 1992; Turner et al., 1999; Jacobs et al., 2007). Zhao et al. (1997) and Dunn et al. (2013) conducted active-source seismic tomography experiments on the ELSC, revealing persistent seismic low-velocity volumes beneath all segments. Prior to 2019, only two refraction lines crossed the arc-to-backarc transition. The first, completed in 1994, deployed 30 ocean-bottom seismometers (OBSs) in an 840 km line across the Tonga Ridge $\sim 220 \text{ km}$ south

of the FRSC (Crawford et al., 2003). The second, completed in 2008, deployed 40 OBSs in a 327 km line across the Tonga Ridge and Tonga Trench, $\sim 100 \text{ km}$ north of the intersection with the Louisville Ridge (Grevenmeyer and Flüh, 2008; Contreras-Reyes et al., 2011). Six additional multichannel seismic lines, three with OBSs, were conducted during cruise SO267 in 2019 in the northern Lau Basin, highlighting the structure of the FRSC and the adjacent backarc basin as far west as the LETZ (Hannington et al., 2019; Schmid et al., 2020). Preliminary data from these surveys, together with Parasound (parametric sediment echosounder) data, identify a number of the backarc domains in our map, which are described below.

Global seismicity data (e.g., centroid moment tensors, CMTs) have also been used to identify major faults and their relative motions and to refine geological boundaries in the map area (Parson et al., 1990; Wetzel et al., 1993; Conder and Wiens, 2011; Sleeper and Martinez, 2014). Baxter et al. (2020) compared the CMTs of nearly 700 shallow ($<30 \text{ km}$), $M_w > 5$ seismic events to the seafloor lineaments mapped in this study, helping to identify the active deformation zones.

Geological Sampling and Seafloor Observations

Volcanic rock sampling has been carried out during 42 different cruises, using dredges, TV grabs, ROVs, and crewed submersibles. The focus of sampling has been on the active spreading centers, including more than 1100 samples from the Valu Fa Ridge, ELSC, CLSC, FRSC, MTJ, NELSC, NWLSC, and FSC (Item S4 [footnote 1]). More than 700 additional samples have also been collected from the arc front and in off-axis and intraplate areas, including via extensive dredging away from the spreading ridges in the Niufo'ou microplate during cruise SO267 in 2019 (Hannington et al., 2019). In 1973, at Site 203 of the Deep Sea Drilling Project (DSDP), one hole was drilled in the western Lau Basin area (Burns et al., 1973), and in 1990–1991, during Leg 135 of the Ocean Drilling Program (ODP), 18 holes were drilled at eight sites across the Lau Basin and Tonga Ridge (Parson et al., 1992a). Locations where direct seafloor observations and sampling have been recorded and used in this study are summarized in Figure 3 and listed in Item S4 (footnote 1).

■ GEOLOGICAL MAP OF THE LAU BASIN



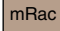


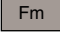
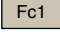
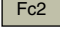
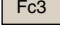
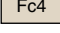
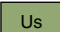
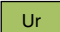
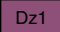


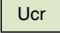


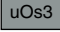
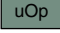

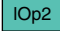
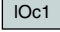
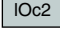




To develop the geological legend for the Lau Basin map (Table 1), we used the standard lithostratigraphic classification scheme of the International Commission on Stratigraphy (Salvador, 1994; Murphy and Salvador, 1999). Geological units were first identified as formation types and then grouped into assemblages in increasing stratigraphic rank. The approach provides the basis for a comprehensive legend and correlation of units across the entire basin, although the names used are not formally accepted units. The assemblages were assigned to a newly defined province and subprovince: the Northwest

TABLE 1. DESCRIPTION OF FORMATION TYPES IN THE LAU BASIN, WITH HEADERS INDICATING ASSEMBLAGE TYPES

CARBONATE PLATFORM	
Cp	Carbonate platform Carbonate rocks (reef complexes) built on active and extinct volcanoes and exposed arc basement
ACTIVE ARC	
<i>Upper</i>	
uAv1	Arc-front volcano Volcanic edifice at the arc front (typically active)
uAv2	Inner-arc volcano Volcanic edifice behind the arc front (may be active or inactive)
uAc	Upper arc crust Undivided crust belonging to the active arc, including volcanoclastic material, flows, and dikes
<i>Lower</i>	
lAc	Lower arc crust Earliest exposed extrusive and intrusive rocks of the active arc (may include arc basement)
BACKARC VOLCANOES	
Bav1	Conical volcano Cone-shaped edifice composed of lava flows and volcanoclastic material erupted onto backarc crust, commonly with a summit crater or caldera and/or cut by dike complexes (>1 km diameter; width:height ≤5)
Bav2	Shield volcano Mound-shaped edifice composed of lava flows extruded onto backarc crust, commonly with a central caldera (>1 km diameter; width:height >5)
Bav3	Dome volcano Dome-shaped edifice composed of lava flows extruded onto backarc crust or onto an axial volcanic ridge (>1 km diameter; length:width ~1)
Bav4	Fissure volcano Elongate volcanic edifice composed mostly of lava flows extruded onto backarc crust, commonly with a central dike (>1 km length; length:width >3)
Bavf	Volcanic field A broad area of lava flows and volcanoclastic material surrounding a number of closely spaced volcanoes
BACKARC RIFTS AND SPREADING CENTERS	
<i>Upper</i>	
uBar	Axial backarc volcanic ridge Volcanic ridge marking the active spreading center, commonly with discrete volcanic edifices (cones and domes), dike complexes, or calderas
uBac	Axial backarc crust Undivided backarc crust in the inner rift valley of an active spreading center
<i>Middle</i>	
mBar	Proximal volcanic or tectonic ridge Elongate volcanic edifice or coalesced ridges in the outer rift valley or on the flank, adjacent to an active spreading center or axial volcanic ridge
mBac	Proximal backarc crust Undivided backarc crust in the outer rift valley, adjacent to an active spreading center or axial volcanic ridge (may include products of off-axis volcanism)
mBaf	Backarc rift flank Undivided backarc crust on the flank of the outer rift valley, including volcanic ridges, volcanoclastic material, and flows (may include products of off-axis volcanism)
<i>Lower</i>	
lBar	Distal volcanic ridge Elongate volcanic edifice or coalesced ridges on distal backarc crust (may include products of off-axis volcanism or earlier seafloor spreading from a distant ridge; commonly obscured by volcanoclastic cover)
lBac1	Distal backarc crust Undivided backarc crust beyond the outer rift valley and flank of an active spreading center (may include products of off-axis volcanism)
lBac2	Outer backarc crust Outermost backarc crust distal to an active spreading center
RELICT BACKARC	
<i>Upper</i>	
uRr	Relict ridge Elongate volcanic edifice or coalesced ridges outside an identifiable area of active spreading (may be a product of intraplate volcanism, rifting of earlier backarc crust, or an unknown spreading center)
uRbc1	Upper relict backarc crust Undivided backarc crust outside an identifiable area of active spreading (may be a product of intraplate volcanism, rifting of earlier backarc crust, or an unknown spreading center)
uRbc2	Tectonized relict backarc crust Intensely deformed backarc crust outside an identifiable area of active spreading
<i>Lower</i>	
lRbc	Lower relict backarc crust Earliest exposed extrusive and intrusive rocks in the backarc and outside an identifiable area of active spreading
ARC-BACKARC TRANSITION	
<i>Upper</i>	
uTr	Ridge at the arc-backarc transition Elongate volcanic or tectonic ridge between an active or relict arc and a backarc basin (may be a product of rift volcanism or block faulting)
uTc	Upper transitional arc-backarc crust Crust immediately surrounding volcanic or tectonic ridges at the arc-backarc transition (may include both arc and backarc crust)
<i>Lower</i>	
lTc	Lower transitional arc-backarc crust Undivided crust at the arc-backarc transition (may include both arc and backarc crust)

(Continued)

TABLE 1. DESCRIPTION OF FORMATION TYPES IN THE LAU BASIN, WITH HEADERS INDICATING ASSEMBLAGE TYPES (*Continued*)

RELICT ARC	
<i>Upper</i>	
 uRav	Cross-arc volcano Part of a volcanic chain crossing all or part of a relict arc
 uRac	Upper relict-arc crust Arc (or forearc) crust, including relict arc volcanoes, belonging to the latest episode of arc construction prior to or during backarc basin opening
<i>Middle</i>	
 mRac	Middle relict-arc crust Crust surrounding relict arc volcanic edifices and belonging to a stage of arc construction prior to backarc basin opening (comprises volcanoclastic rocks and flows associated with early arc magmatism)
<i>Lower</i>	
 lRac	Lower relict-arc crust Earliest exposed extrusive and intrusive rocks in the relict arc (commonly obscured by volcanoclastic cover)
FOREARC	
 Fv	Forearc volcano Volcanic edifice composed of lava flows and volcanoclastic material erupted onto extended forearc crust
 Fm	Forearc mound Non-volcanic feature of the forearc crust that may include serpentinite mounds, mud volcanoes, or locally uplifted blocks
 Fc1	Forearc crust Undivided crust of the forearc, including sediment of the forearc slope
 Fc2	Tectonized forearc crustal block Block of forearc crust affected by intense deformation
 Fc3	Forearc crust of the inner trench wall Crust at the leading edge of the forearc that is typically heavily tectonized and may include accretionary material
 Fc4	Extended forearc crust Forearc crust affected by extension and locally associated with rift volcanism
OTHER ARC-BACKARC FORMATIONS	
 Us	Seamount Volcanic or tectonic edifice of undetermined origin
 Ur	Ridge Elongate volcanic or tectonic feature of undetermined origin
 Dz1	Leaky transform zone Lava flows and deformed crust associated with a leaky (extensional) transform fault
 Dz2	Deformation zone High-strain zone commonly associated with transcurrent faults (likely of crustal scale)
 Uc	Unassigned crust Crust that is distinguishable from adjacent formations in terms of age (e.g., sediment cover) or texture but cannot be assigned to a particular origin
 Ucr	Unassigned crust with ridges Crust that cannot be assigned to a particular origin but with a distinct fabric comprising elongate volcanic or tectonic ridges
OCEANIC FORMATIONS	
<i>Upper</i>	
 uOs1	Hot-spot volcano Intraplate volcano associated with a known hot spot
 uOs2	Intraplate volcano Intraplate volcano with no identifiable associated hot spot
 uOs3	Intraplate seamount Intraplate volcanic or tectonic edifice of undetermined origin
 uOp	Oceanic plateau Flat-topped, upper portion of intraplate volcanic edifice built on older oceanic crust
<i>Lower</i>	
 lOp1	Hot-spot volcanic plateau rise Exposed lower portion of an oceanic plateau surrounding a known hot spot
 lOp2	Volcanic plateau rise Exposed lower portion of an oceanic plateau with no identifiable associated hot spot
 lOc1	Undivided oceanic crust Crust formed at a mid-ocean ridge
 lOc2	Oceanic crust of the outer trench slope Tectonized oceanic crust exposed in the outer trench wall
SYMBOLS	
	Caldera rim
	Lineament
	Major fault zone
	Spreading center

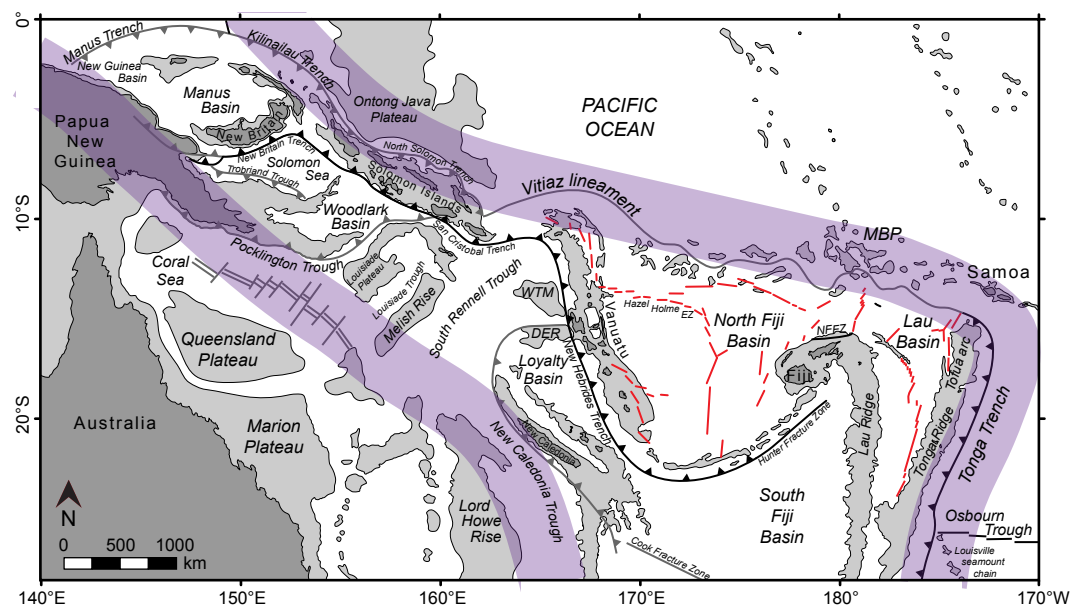


Figure 4. Geographic location and major tectonic features of the Northwest Indo-Australian Margin province and Lau-Tonga Arc-Backarc sub-province. Light gray areas are underwater areas shallower than 2000 m, and dark gray areas are land masses. Red lines are spreading centers and backarc rifts, and black barbed lines are active subduction zones. Grey lines are inactive subduction zones, spreading centers, and faults. The bold purple line is the approximate boundary of the region defined as the Northwest Indo-Australian Margin. DER—d'Entrecasteaux Ridge; Hazel Holme EZ—Hazel Holme extensional zone; MBP—Melanesian Borderland Plateau; NFFZ—North Fiji fracture zone; WTM—West Torres massif. Modified from Pelletier and Auzende (1996), Hall (2002), Schellart et al. (2006), Martin (2013), Patriat et al. (2019), and Brandl et al. (2020b).

Indo-Australian Margin province and the Lau-Tonga Arc-Backarc (LTAB) sub-province (Fig. 4; Table 2). A province is defined as a tectonically bounded region with a protracted, multistage history that is distinct from adjacent regions in terms of its age, internal makeup, structure, and metamorphism. A subprovince is a discrete region therein with distinct lithological, stratigraphic, and structural characteristics belonging to a single tectonic system. Province boundaries are commonly major orogens, whereas subprovinces may be bounded only by

large crustal-scale structures. A challenge in applying province and subprovince boundaries in the same manner as in ancient terranes is that the latter are already accreted into readily circumscribed regions bounded by major orogens and translithospheric structures, whereas the modern oceanic and continental margins are still accreting. Twenty-four (24) of the assemblages identified in Table 2 and Figure 5 are assigned to the LTAB. The number of mapped formations in the LTAB is comparable to the number of lithostratigraphic units

TABLE 2. ORGANIZATIONAL CHART OF MAPPED UNITS IN THE LAU BASIN ACCORDING TO STRATIGRAPHIC SUBDIVISIONS

Province/ subprovince	Assemblage type	Assemblage name(s)	Group	Formations
Lau-Tonga Arc-Backarc	Active arc	Tofua Arc	Upper, lower	Arc-front volcano, inner-arc volcano, arc crust
	Backarc volcanoes	Niuafu'ou, SE Futuna	—	Conical volcano, shield volcano, dome volcano, fissure volcano, volcanic field
	Backarc rifts and spreading centers	Central Lau Basin, Cikobia, East Lau Basin, Fonualei, Futuna, Mangatolu, NE Lau Basin, NW Lau Basin, Rochambeau	Upper, middle, lower	Volcanic ridge (axial, proximal, distal), backarc crust (axial, proximal, distal, outer), backarc rift flank
	Relict backarc	North Fonualei, North Futuna, Qelelevu, South Futuna, Zephyr	Upper, lower	Relict ridge, relict backarc crust, tectonized relict backarc crust
	Arc-backarc transition	West Lau Basin	Upper, lower	Ridge at the arc-backarc transition, transitional arc-backarc crust
	Relict arc	Lau Ridge, Tonga Ridge	Upper, middle, lower	Cross-arc volcano, relict-arc crust
	Forearc	North Lau Forearc, Tonga Forearc	—	Forearc volcano, forearc mound, forearc crust, tectonized forearc crustal block, forearc crust of the inner trench wall, extended forearc crust
	Other arc-backarc formations	Peggy Ridge, South Vitiiaz	—	Leaky transform zone, deformation zone, seamount, ridge, unassigned crust, unassigned crust with ridges

Note: Em dash indicates assemblages for which the Group level subdivision is not applicable.

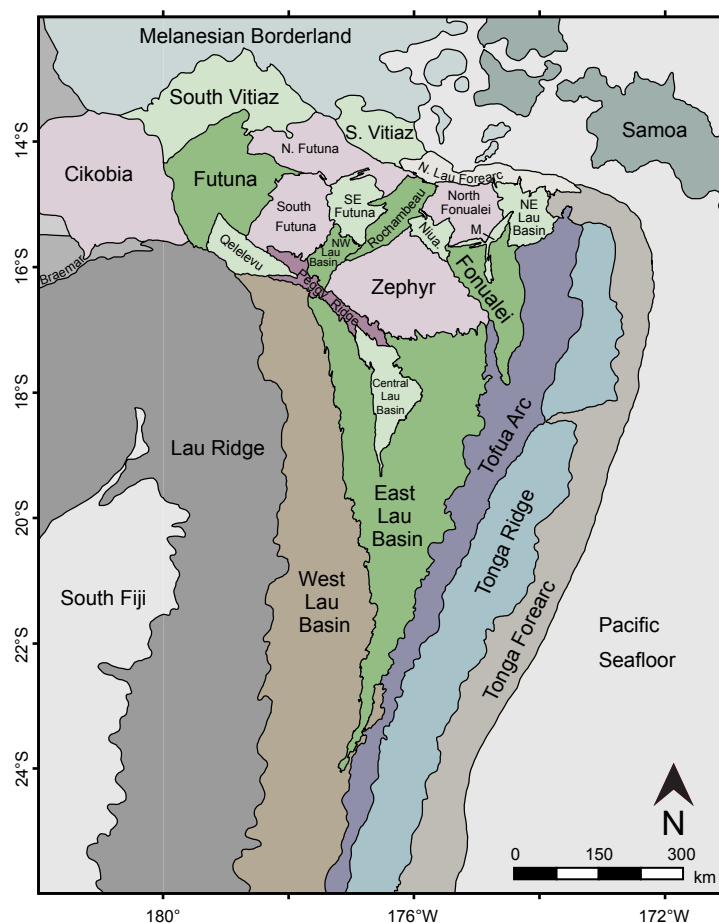


Figure 5. Assemblage map of the Lau Basin showing the distribution of 29 different groups of formations, classified herein as assemblages. Each assemblage consists of one or more geological formations grouped in terms of their origin, lithology, inferred age, and tectonic and structural regime. They are defined by inspection of marine geophysical data (hydroacoustics, magnetics, gravity) integrated with the results of structural mapping, sampling, ocean drilling, seismic surveys, and seabed observations. Colors assigned to the assemblages are for illustration purposes only and approximate those in the lithostratigraphic correlation diagram of the Lau Basin (Fig. 8). See text for assemblage descriptions. M—Mangatolu; Niua.—Niuafo’ou.

identified in similar-sized geological maps of the continents (e.g., Peucker-Ehrenbrink and Miller, 2002, 2003, 2004, 2007a, 2007b).

The northwest Indo-Australian margin comprises several large-scale arc-backarc systems and volcanic and sedimentary basins associated with west-directed subduction of the Pacific plate that began ca. 82 Ma (Schellart et al., 2006). It is distinct from regions to the north and east, which are dominated by oceanic crust of Middle Jurassic to Lower Cretaceous age (Bouysse, 2014), and to the west by the Australian continent. The region is a major geological province of the proposed continent, Zealandia (Mortimer et al., 2017). The province and subprovince divisions proposed in this study are broadly similar to the structural provinces defined by Collot et al. (2011); however, they classified the Lau-Colville Ridge, Tonga-Kermadec Ridge, and Lau Basin as separate provinces, which we have grouped into a single subprovince (LTAB; Fig. 4).

The assemblages of the LTAB subprovince include nine different types (Table 2), each consisting of one or more geological formations that are grouped in terms of their origin, lithology, inferred age, and tectonic and structural regime (e.g., an arc or a backarc spreading center and all associated geological units). In this way, the assemblages are correlatable and similar to established lithotectonic assemblages in many ancient volcanic terranes on land. The distribution of assemblages in the Lau Basin is shown in Figure 5, and they are described individually below. Assigned names are based on major tectonic or geographic features they contain. The assemblages may be in fault or depositional contact with each other and, in some cases, may be separated by major unconformities. The lithologies belonging to different assemblages may be very similar or even identical. An example is the Central Lau Basin assemblage, which is demonstrably of different age and history than the East Lau Basin assemblage but composed of very similar backarc-basin basalt.

Formations are the lowest rank in Table 2, defined by spatially and/or temporally distinct lithostratigraphic units. Formal classifications, which are based on rigorous stratigraphic relationships (Salvador, 1994; Murphy and Salvador, 1999), have not been attempted, but the mapped units invariably include recognizable volcanic or sedimentary facies as criteria for identifying formation type. Correlation of formations using these criteria, together with geomorphological expression, is particularly common practice in mapping young volcanic terranes (e.g., Thouret, 1999). The standard nomenclature of undersea features established by the International Hydrographic Organization (2013) has been used to name the formations. These include volcanic or tectonic ridges, volcanic cones, volcanic flow fields, seamounts, mounds, and deformation zones. The mapped formations also take into account available geophysical and geological data (sampling, seafloor observations) in the map area. Stratigraphic relationships between the formations are inferred from the nature of contacts between units (e.g., volcanic cones erupted onto preexisting flow fields) and their spatial relationship to eruptive centers (e.g., distance from a spreading center). Where appropriate, the formations are subdivided according to “upper” and “lower” groups (relatively younger or older, respectively), designated with lowercase “u” and “l” in the geologic unit abbreviations. Where multiple formations are mapped, a “middle” group (“m”) may also be identified.

This classification facilitates correlation of units over larger areas of the basin, including formations that have been widely separated by seafloor spreading or other tectonic processes. Boundaries of the formations are drawn where a clear distinction from an adjacent formation can be made (e.g., between a ridge and volcanic flow field) and are interpolated between formations where a clear bathymetric or geophysical change is not observed. Unless they are defined by faults or clearly separated by an unconformity, the contacts between formations are interpreted to be conformable. The formations listed in Table 1 are the basis for the geological map shown in Figure 6, which was produced at 1:1,000,000 scale and has been scaled down for publication. This figure is reproduced as a full-scale map sheet with marginal notes in the Supplemental Material to this paper (Item S1 [footnote 1]).

Where high-resolution ship-based multibeam and/or acoustic backscatter data are available, formations may be further subdivided into members. These include, for example, individual flow sequences, talus fields (e.g., breccia deposits), or sedimentary units that are mappable at 1:100,000–1:200,000 scale. Member-level mapping has been done in the training areas, such as in the NELSC and the MTJ (e.g., McClinton et al., 2013; Anderson et al., 2016, 2017; Mensing, 2019; see Item S2 [footnote 1]), and was an important step in defining the formations in the 1:1,000,000-scale map. However, individual members are typically not mappable at the 1:1,000,000 scale, and so are not included in Table 1 or Figure 6. The smallest formal lithostratigraphic units (e.g., beds or individual flows) can only be mapped in small areas with direct seafloor observations from crewed submersibles, ROVs, or AUVs (e.g., Embley and Rubin, 2018).

Mapped Formations

By comparing the mapped formations in well-studied training areas to similar features in areas where they have not been sampled or directly observed, we have been able to make informed interpretations about formation types in most parts of the map. Sediments have not been mapped, except for carbonate platforms, in order to emphasize the bedrock geology. In general, sediments having a thickness of <500 m (equivalent to ~5% of the width of the smallest polygons, excluding individual volcanoes, at 1:1,000,000 scale) have been ignored. In general, the pelagic sediment thickness is much less than 500 m. In the most heavily sedimented portions of the western Lau Basin (e.g., at ODP Sites 834 and 835), the depth to basement is only 160 m (Parson et al., 1994). In areas where significant volcanoclastic material has been identified (e.g., on or adjacent to the active arc), these units are grouped with the associated coherent volcanic rocks.

More than 3000 discrete volcanoes are mapped at the 1:1,000,000 scale in the Lau Basin (Table 3). The volcano types are: (1) active arc volcanoes (Av in unit abbreviations); (2) backarc volcanoes (Bav); (3) relict arc volcanoes (Rav); (4) forearc volcanoes (Fv); and (5) oceanic volcanoes (Os). Only volcanoes >1 km in diameter were included in the 1:1,000,000-scale compilation (drawn at the steepest inflection point nearest the base of slope). Where flows and

volcanoclastic rocks are identified beyond the base of the slope, these features are mapped as a separate formation (e.g., backarc volcanic field, unit Bavf). Volcanic fields typically occur only around the largest volcanoes (>10 km diameter) or clusters of more than five smaller volcanoes. Several different volcano morphologies are distinguished. Backarc volcanoes, in particular, are classified as cone (unit Bav1), shield (Bav2), dome (Bav3), or fissure volcanoes (Bav4; Table 1). Cones are steep sided, have a width-to-height ratio ≤ 5 , and commonly have a summit crater or caldera; many are bisected by a rift or dike complex. Shield volcanoes have gentle slopes and a width-to-height ratio >5 . They also commonly have a central caldera. Dome volcanoes are typically smaller than shield and conical volcanoes and have an aspect ratio of ~ 1 . Fissure volcanoes are elongate edifices with length-to-width ratios >3 . The arc volcanoes are classified according to their position relative to the volcanic front: along the active volcanic front (arc-front volcanoes, unit uAv1) or behind the volcanic front (inner-arc volcanoes, uAv2). Forearc volcanoes (unit Fv) and relict-arc volcanoes (uRav) include any volcanoes on forearc or relict-arc crust, respectively. The relict-arc volcanoes commonly occur as cross-arc volcanic chains. A number of volcanic or tectonic edifices are of undetermined origin and have been mapped as seamounts or “mounds”. These generic terms apply to isolated topographic features taller than 100 m that may be either volcanic or tectonic in origin (e.g., Staudigel et al., 2010; Buchs et al., 2016). They include forearc mounds (unit Fm), backarc seamounts (Us), hot spot volcanoes (uOs1), intraplate seamounts (uOs2), and intraplate seamounts (uOs3) identified according to their location with no particular genetic implications. Forearc mounds may include serpentinite mounds, mud volcanoes, or local uplifted blocks.

Below is a description of the different types of crust mapped as individual formations. Quantitative data on the different formation types and individual formations are summarized in Tables 4 and 5.

Arc crust is subdivided into upper and lower formations based on the inferred level of exposure (stratigraphic position). Upper arc crust (unit uAc) includes all flows, volcanoclastic rocks, and intrusions (exposed dike rocks) related to volcanism of the currently active arc. Lower arc crust (unit lAc) is the volcanic-dominated substrate upon which the active arc is built and mainly includes older arc crust formed at the same location. Lower arc crust is typically exposed only by crustal-scale faults in areas of arc rifting.

Backarc crust formations are classified according to their location relative to an active spreading center. Axial backarc crust (unit uBac) is located within the neovolcanic zone and typically forms the floor of an inner rift valley. Proximal backarc crust, designated “middle” (unit mBac), is located outside the neovolcanic zone but typically occupies a broader outer rift valley (Fig. 7). Backarc crust on the flank of the outer rift valley (unit mBaf) is broadly stratigraphically equivalent to middle backarc crust (mBac) but is located outside the rift. Distal backarc crust (units lBac1 and lBac2) is located outside the rift valley and generally beyond the rift flank. Where a rift valley is not clearly defined but a ridge morphology is still present, the backarc flanking crust (unit mBaf) or lower backarc crust (lBac) may occur adjacent to the axial spreading ridge.

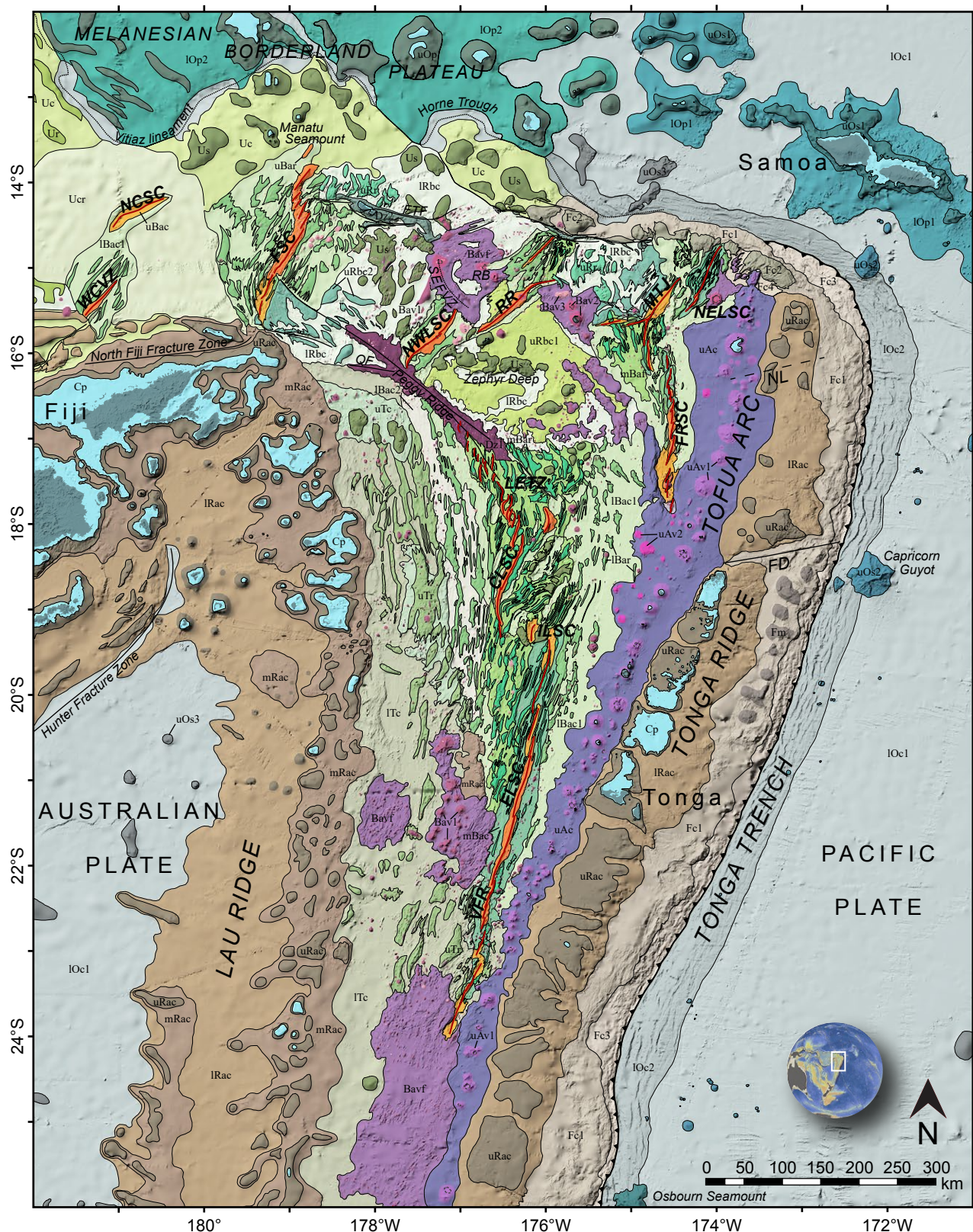


Figure 6. Reduced version of the 1:1,000,000-scale geological map of the Lau Basin at the formation level. The corresponding legend is in Table 1. The complete map sheet with marginal notes is provided at the original scale in Item S1 of the Supplemental Material (text footnote 1). CLSC—Central Lau Spreading Center; ELSC—Eastern Lau Spreading Center; FRSC—Fonualei Rift and Spreading Center; FD—Fonualei Discontinuity; FSC—Futuna Spreading Center; FTF—Futuna Transform Fault; ILSC—Intermediate Lau Spreading Center; LETZ—Lau Extensional Transform Zone; MTJ—Mangatolu Triple Junction; NCSC—North Cikobia Spreading Center; NELSC—Northeast Lau Spreading Center; NL—Niuatoputapu Lineament; NWLSC—Northwest Lau Spreading Center; QF—Qelelevu fault; RB—Rochambeau Bank; RR—Rochambeau Rifts; SEFVZ—Southeast Futuna Volcanic Zone; VFR—Valu Fa Ridge; WCVZ—West Cikobia Volcanic Zone.

TABLE 3. SUMMARY STATISTICS OF VOLCANO TYPES, DISTRIBUTIONS, SURFACE AREAS, AND VOLUMES

Formation	Legend abbreviation	Total area (km ²)	Total volume (km ³)	No. of polygons	Area/polygon (km ²)	Volume/polygon (km ³)
Forearc		3113	3574	18	173	199
Forearc mound	Fm	3020	3508	8	378	439
Forearc volcano	Fv	93	66	10	9	7
Active arc		12,143	7112	124	98	57
Arc-front volcano	uAv1	11,350	6781	109	104	62
Inner-arc volcano	uAv2	793	331	15	53	22
Backarc volcanoes		13,987	4659	3018	5	2
Backarc conical volcano	Bav1	8200	2922	1343	6	2
Backarc shield volcano	Bav2	1508	781	7	215	112
Backarc dome volcano	Bav3	2770	557	1408	2	0.4
Backarc fissure ridge	Bav4	1509	399	260	6	2
Relict arc		3655	4332	27	135	160
Cross-arc volcano	uRav	3655	4332	27	135	160
Oceanic crust		620	214	42	15	5
Intraplate volcano	uOs2	620	214	42	15	5
Total		33,518	19,891	3229		
Average					10	6

Note: Bold indicates the tectonic setting in which the volcanoes are located.

Importantly, the proximal (units mBac and mBaf) and distal (lBac) backarc crust are not always present on both sides of the axial valley, indicative of asymmetric spreading (e.g., Fig. 7). The lower backarc crust is commonly obscured by volcanoclastic and/or sedimentary cover but can be further divided (units lBac1 and lBac2) on the basis of magnetic anomalies, major structural boundaries, degree of sedimentation, or obvious changes in crustal thickness established from published seismic sections or gravity anomalies. Relict backarc crust includes all crust that is interpreted to have formed at a backarc spreading ridge but is now located outside an identifiable region of active spreading. This crust is divided into upper (unit uRbc1) and lower (lRbc) formations where younger crust is clearly built on top of preexisting crust (e.g., where rifting has exposed the older crust). In some areas, the relict backarc crust has been intensely deformed and is broken out as a separate formation (tectonized relict backarc crust, unit uRbc2).

Discrete or coalesced ridge-parallel volcanic and tectonic features, similar to the off-axis spreading fabric of mid-ocean ridges (e.g., Macdonald, 2001), are widespread throughout the Lau Basin. They are interpreted to have formed by backarc spreading, but different ridge formations are recognized in different settings. Ridges that are clearly volcanic in origin have centrally located eruptive fissures or volcanic cones. They may be related to dikes intruded into backarc crust during spreading, or they are products of off-axis volcanism associated with rifting of older backarc crust. Other ridges are simply tilted fault blocks that have exposed older volcanic crust. Axial volcanic ridges that are associated with active spreading centers (cf. Yeo, 2016) are designated “upper” backarc ridges (unit uBar). They are elongated parallel to the spreading

axis and typically occupy the center of the neovolcanic zone or inner rift valley. Proximal ridges, designated “middle” (unit mBar), are located outside the neovolcanic zone but within the outer rift valley (Fig. 7). Distal ridges, designated “lower” (unit lBar), are located beyond the rift valley on older backarc crust that was formed during an earlier episode of seafloor spreading or by off-axis volcanism. Relict ridges (uRr) occur outside identifiable areas of active spreading and may be products of intraplate volcanism, rifting of earlier backarc crust, or distal ridges related to an unknown spreading center. Other elongate volcanic or tectonic features that cannot be assigned to an identifiable spreading center or lack other data to confirm their origin are simply “undivided” ridges (unit Ur).

Transitional arc-backarc crust is the oldest crust in the basin, having formed where early arc rifting and basin opening was initiated. It is divided into upper (unit uTc) and lower (lTc) formations based on magnetic anomalies, degree of sedimentation, or obvious changes in crustal thickness, as for the backarc crust. The lower transitional crust surrounds obvious volcanic or tectonic ridges in heavily sedimented areas and includes the inferred basement in failed backarc sub-basins. The ridges may be volcanic, formed during the early opening of the basin, or fault blocks of old arc or backarc crust. In areas with limited ship-based bathymetry or other data, features of this type for which an origin is unknown are labeled “unassigned” (units Uc and Ucr; e.g., north and west of the FSC).

Arc crust formed prior to backarc basin opening is designated relict arc crust, including any eroded early-arc volcanoes (e.g., on Lau Ridge and east of the currently active Tofua arc). Relict arc crust is divided into upper (uRac), middle (mRac), and lower (lRac) formations based on level of exposure and contact

TABLE 4. SUMMARY STATISTICS AND QUANTITATIVE ANALYSIS OF MAPPED FORMATIONS IN THE LAU BASIN

Formation	Legend abbreviation	Area (km ²)	Proportion of total area (%)	Proportion of total backarc area (501,877 km ²) (%)	No. of polygons	Area/polygon (km ²)
Upper arc crust*	uAc	72,260	6.6	N/A*	1	72,260
Lower arc crust*	lAc	150	0.0	N/A*	1	150
Volcanic field	Bavf	57,390	5.2	11.4%	18	3188
Axial backarc volcanic ridge	uBar	10,696	1.0	2.1%	33	324
Axial backarc crust	uBac	6788	0.6	1.4%	15	453
Proximal volcanic or tectonic ridge	mBar	13,473	1.2	2.7%	320	42
Proximal backarc crust	mBac	11,692	1.1	2.3%	11	1063
Backarc rift flank	mBaf	21,400	2.0	4.3%	12	1783
Distal volcanic ridge	lBar	26,191	2.4	5.2%	242	108
Distal backarc crust	lBac1	73,751	6.7	14.7%	41	1799
Outer backarc crust	lBac2	10,509	1.0	2.1%	2	5255
Relict ridge	uRr	3387	0.3	0.7%	25	135
Upper relict backarc crust	uRbc1	15,859	1.4	3.2%	2	7930
Tectonized relict backarc crust	uRbc2	7072	0.6	1.4%	33	214
Lower relict backarc crust	lRbc	41,990	3.8	8.4%	14	2999
Ridge at the arc-backarc transition	uTr	17,882	1.6	3.6%	73	245
Upper transitional arc-backarc crust	uTc	11,039	1.0	2.2%	3	3680
Lower transitional arc-backarc crust	lTc	70,559	6.4	14.1%	9	7840
Upper relict-arc crust*	uRac	123,510	11.3	N/A*	121	1021
Middle relict-arc crust*	mRac	94,841	8.7	N/A*	8	11855
Lower relict-arc crust*	lRac	203,789	18.6	N/A*	4	50947
Forearc crust*	Fc1	68,499	6.3	N/A*	2	34,250
Tectonized forearc crustal block*	Fc2	5320	0.5	N/A*	8	665
Forearc crust of the inner trench wall*	Fc3	25,291	2.3	N/A*	1	25,291
Extended forearc crust*	Fc4	1277	0.1	N/A*	2	638
Seamount (undetermined origin)	Us	23,334	2.1	4.7%	62	376
Leaky transform zone	Dz1	6341	0.6	1.3%	1	6341
Deformation zone	Dz2	2423	0.2	0.5%	11	220
Unassigned crust with ridges	Ucr	37,444	3.4	7.5%	1	37,444
Unassigned crust	Uc	30,879	2.8	6.2%	4	7720
Totals		1,095,036			1080	

*Not included in backarc area calculations.

TABLE 5. SUMMARY STATISTICS AND QUANTITATIVE ANALYSIS OF FORMATION TYPES

Formation type	Total area (km ²)	Proportion of total area (%)	No. of polygons	Area/polygon (km ²)
Ridges	71,629	6.5	693	103
Crust	930,899	85.0	295	3156
Arc crust	494,549	45.2	135	3663
Forearc crust	97,367	8.9	13	7490
Backarc crust	338,983	31.0	147	2306
Deformation zones	8764	0.8	12	730
Seamounts and mounds	26,354	2.4	70	376
Volcanic fields	57,390	5.2	18	3188
Volcanoes*	33,517	N/A*	3229	10
Carbonate platforms*	72,250	N/A*	197	367

*Not included in total area calculations.

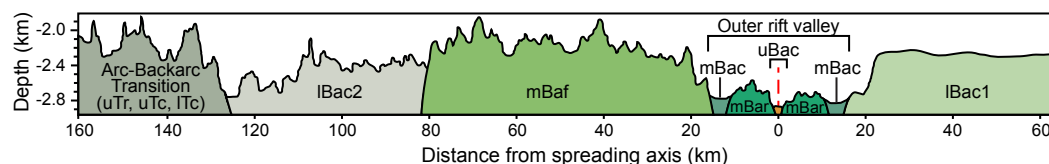


Figure 7. Schematic cross-section of a rift valley showing the relationship between the inner (unit uBac) and outer valley floor and the rift flank used to define the assemblage and formation boundaries. Refer to Table 1 for abbreviations.

relationships, similar to the crust of the active arc. Large areas between the trench and the active arc are designated forearc crust, including crust of the forearc slope (unit Fc1), tectonized forearc crustal blocks (Fc2), crust exposed on the inner trench wall (Fc3), and extended crust associated with active rifting of the forearc (Fc4). The crust exposed on the inner trench wall and the large uplifted blocks on the upper slope may include part of the arc basement (e.g., Meffre et al., 2012).

Several major deformation zones are mapped in the backarc, as in previous studies (e.g., Pelletier and Auzende, 1996; Pelletier et al., 2001). Although they are mainly structural elements of the map, they are identified here and in the legend as geological formations. In some cases, they include lava flows, for example, erupted from the leaky transform fault (unit Dz1) at the Peggy Ridge. Elsewhere, they are simply high-strain zones along one or more large-scale transcurrent faults (unit Dz2).

Oceanic formations include the Pacific plate, Samoan Plateau, and Melanesian Borderland, which comprise Cretaceous and younger oceanic crust formed at mid-ocean ridges and oceanic hot spots. A number of different types of volcanoes are mapped on this crust, including volcanoes that are associated with a hot spot (unit uOs1), intraplate volcanoes that are not clearly associated with a plume source (uOs2), and flat-topped, steep-sided volcanic edifices built on an oceanic plateau (uOp) and surrounded by a plateau rise (IOp2).

Carbonate formations of the Lau, Tonga, and Fiji platforms (unit Cp) are built on active and extinct volcanoes and exposed arc basement. A depth contour of 125 m, which is within the photic zone and encompasses all reefs in the Reefs at Risk database of the World Resources Institute (2011), was used to map the platforms.

Mapped Structures

Several major deformation zones are recognized in the north of the Lau Basin: the North Fiji fracture zone in the west, the Futuna transform fault between the FSC and RR, and the Peggy Ridge fault in the central Lau Basin. These structures are interpreted to be translithospheric and have accommodated much of the opening of the basin (Eguchi, 1984; Hamburger and Isacks, 1988; Clarke et al., 1993; Parson and Tiffin, 1993; Pelletier and Auzende, 1996; Pelletier et al., 2001). Several are marked by plate-boundary or intraplate volcanism that comprises discrete formation types (units Dz1 and Dz2) and, in

one case (Peggy Ridge), an assemblage. Other structures mappable at the 1:1,000,000 scale include large numbers of lineaments that are distinct from volcanic ridges. Baxter et al. (2020) mapped 1100 major faults in the map area, defined as having individual strike lengths of >25 km and throws of >250 m, with a cumulative strike length of 19,160 km. It is reasonable to expect that many of the longest structures are also transcrustal, given that the depths of faults in extensional environments generally scale with their strike length at surface. The full lineament database is not included with the 1:1,000,000-scale map but is available in Baxter et al. (2020).

LITHOSTRATIGRAPHIC ASSEMBLAGES

The mapped formations have been grouped into ten assemblage types: (1) active arc, (2) backarc volcanoes, (3) backarc rifts and spreading centers, (4) relict backarc, (5) arc-backarc transition, (6) relict arc, (7) forearc, (8) other arc-backarc formations, (9) oceanic formations, and (10) carbonate platforms. Each assemblage comprises a group of formations of similar age belonging to a common lithotectonic framework and crustal type. The locations of the assemblages with assigned names are indicated in Figure 5, and they are described in detail below and in Table 6. Quantitative data on the main assemblage types (excluding carbonate platforms) are given in Table 7, and data for the individual assemblages are listed in Table 8.

Active Arc Assemblage

The Tofua volcanic arc is the only active arc assemblage in the map area, covering 72,295 km² (Fig. 5). The formations grouped in this assemblage comprise all volcanic edifices, volcanoclastic rocks, flows, and dikes associated with the active volcanic front of the subduction zone, including inner arc volcanoes behind the active arc front and any exposed arc basement. The assemblage contacts are depositional and marked by the limit of the volcanoclastic apron of the active arc; to the east is the Tonga Ridge, and to the west, the East Lau Basin assemblage. South of the Fonualei discontinuity, a major structure cutting across the Tofua arc, the boundary between the Tofua arc and Tonga Ridge is sharp and defined by major uplifted portions of the Tonga Ridge. Although volcanism in the Tofua arc began at ca. 3 Ma (Tappin et al., 1994),

TABLE 6. CHARACTERISTICS OF ASSEMBLAGES IN THE LAU BASIN

Assemblage name	Age	Assemblage type	Ship-based bathymetry coverage (%)
Central Lau Basin	1.5 Ma–present	Backarc rifts and spreading centers	95
Cikobia	5.5 Ma–present	Backarc rifts and spreading centers	11
East Lau Basin	5.5 Ma–present	Backarc rifts and spreading centers	81
Fonualei	3.8 Ma–present	Backarc rifts and spreading centers	78
Futuna	4.5 Ma–present	Backarc rifts and spreading centers	69
Lau Ridge	46–31 Ma; 28–15 Ma; 14–0.3 Ma	Relict arc	10
Mangatolu	0.6 Ma–present	Backarc rifts and spreading centers	99
Niuafo'ou	1 Ma–present	Backarc volcanoes	78
North Fonualei	3.8–0.6 Ma	Relict backarc	68
North Futuna	5.5 Ma–present	Relict backarc	51
North Lau Forearc	35–28 Ma; 15–9 Ma	Forearc	71
Northeast Lau Basin	2.5 Ma–present	Backarc rifts and spreading centers	90
Northwest Lau Basin	1 Ma–present	Backarc rifts and spreading centers	85
Peggy Ridge	5.5 Ma–present	Other arc-backarc formations	84
Qelelevu	46–31 Ma; 28–15 Ma; 14–2.4 Ma	Relict backarc	61
Rochambeau	0.5 Ma–present	Backarc rifts and spreading centers	98
South Futuna	5.5 Ma–present	Backarc volcanoes	51
South Vitiaz	12 Ma–present	Other arc-backarc formations	10
Southeast Futuna	1 Ma–present	Backarc volcanoes	83
Tofua Arc	3 Ma–present	Active arc	29
Tonga Forearc	52–48 Ma; 44–35 Ma; 17 to present	Forearc	41
Tonga Ridge	46–40 Ma; 33–31 Ma; 19–17 Ma; 14–5.5 Ma	Relict arc	13
West Lau Basin	46–31 Ma; 28–15 Ma; 14–2.4 Ma	Arc-backarc transition	43
Zephyr	5.5–1 Ma	Relict backarc	51

the presently active volcanoes are all younger than 1 Ma (e.g., Stoffers et al., 2003; Arculus, 2008). Twenty-eight (28) of the larger stratovolcanoes are indicated in Figure 1, but as many as 100 smaller volcanoes were identified in this study. Most are built from effusive and explosive eruptive products, varying in composition from basaltic andesite to andesite with lesser dacite and rhyolite. Seventy-seven (77) volcanic eruptions have been recorded along the Tofua arc since 1774 CE (Global Volcanism Program, 2013), with the most

recent occurring at volcano F (Fig. 1) in August 2019, which produced a large pumice raft (Brandl et al., 2020a; Jutzeler et al., 2020).

Samples from the Tafahi and Niuatoputapu volcanoes (Beier et al., 2017) and the adjacent forearc (Meffre et al., 2012) confirm that the active arc is built on a basement of old arc crust of the Tonga Ridge. Two seismic sections across the active arc indicate that these basement rocks are as much as 20 km thick (Crawford et al., 2003; Contreras-Reyes et al., 2011).

TABLE 7. SUMMARY STATISTICS AND QUANTITATIVE ANALYSIS OF ASSEMBLAGE TYPES

Assemblage type	No. of assemblages	Area (km ²)	Proportion of total area (%)	No. of polygons	Area/polygon (km ²)
Active arc	1	72,295	6.60	2	36,147
Backarc volcanoes	2	11,769	1.07	4	2942
Backarc rifts and spreading centers	9	216,265	19.75	696	311
Relict backarc	5	82,760	7.56	111	746
Arc-backarc transition	1	143,775	13.13	93	1546
Relict arc	2	419,992	38.35	132	3182
Forearc	2	100,872	9.21	17	5934
Other arc-backarc formations	2	47,308	4.32	25	1892

TABLE 8. SUMMARY STATISTICS AND QUANTITATIVE ANALYSIS OF MAPPED ASSEMBLAGES IN THE LAU BASIN

Assemblage	Area (km ²)	Proportion of total area (%)	Proportion of backarc area (%)	No. of polygons	Area/polygon (km ²)
Central Lau Basin	11,030	1.0	2.2	72	153
Cikobia	47,275	4.3	9.4	20	2364
East Lau Basin	90,325	8.2	18.0	316	286
Fonualei	16,145	1.5	3.2	61	265
Futuna	28,922	2.6	5.8	82	353
Lau Ridge*	310,568	28.4	N/A*	110	2823
Mangatolu	1871	0.2	0.4	13	144
Niuafu'ou	3509	0.3	0.7	1	3509
North Fonualei	10,552	1.0	2.1	38	278
North Futuna	17,529	1.6	3.5	18	974
North Lau Forearc*	9384	0.9	N/A*	9	1043
Northeast Lau Basin	7916	0.7	1.6	76	104
Northwest Lau Basin	4626	0.4	0.9	10	463
Peggy Ridge	6341	0.6	1.3	1	6341
Qelelevu	7417	0.7	1.5	11	674
Rochambeau	8155	0.7	1.6	46	177
South Futuna	15,682	1.4	3.1	21	747
South Vitiaz	40,967	3.7	8.2	24	1707
Southeast Futuna	8260	0.8	1.6	3	2753
Tofua Arc*	72,295	6.6	N/A*	2	36,148
Tonga Forearc*	91,488	8.4	N/A*	8	11,436
Tonga Ridge*	109,424	10.0	N/A*	22	4974
West Lau Basin	143,775	13.1	28.6	93	1546
Zephyr	31,580	2.9	6.3	23	1373
Total area (km ²)	1,095,036		Total no. of polygons	1080	
Total backarc area (km ²)	501,877				

*Not included in total backarc area calculations.

Backarc Rift and Spreading Center Assemblages

New backarc crust is forming throughout the Lau Basin in at least 12 distinct assemblages: East Lau Basin, Central Lau Basin, Fonualei, Mangatolu, Northeast Lau Basin, Niuafu'ou, Rochambeau, Northwest Lau Basin, Southeast Futuna, Futuna, Cikobia, and Peggy Ridge (Fig. 5; Table 6). Although the Niuafu'ou and Southeast Futuna assemblages are classified as the “backarc volcanoes” assemblage type and the Peggy Ridge assemblage is classified as a deformation zone under the “other arc-backarc formations” assemblage type, these assemblages are described here because they all represent regions of significant backarc crustal growth. The growth of these assemblages has kept pace with an integrated basin opening rate of 120–145 mm/yr (Bevis et al., 1995; Hawkins, 1995; Fig. 1) and locally >160 mm/yr north of the MTJ (Sleeper and Martinez, 2016). Each assemblage encompasses an area of backarc crust with a spreading fabric that is demonstrably linked to a currently active spreading center. Although a distinction has been suggested between thick, felsic, arc-proximal crust and

thinner, mid-ocean ridge basalt (MORB)-like arc-distal crust along the spreading centers (Martinez et al., 2006), we cannot identify that transition farther off axis and therefore have grouped all of the crust that originated at the spreading center into one assemblage (i.e., East Lau Basin and Fonualei assemblages). Further refinement based on the compositions of off-axis basalts, however, is an important objective for future mapping and sampling in the basin. The spreading axes are thought to have remained generally in their present location throughout the formation of the different assemblages, although several rift zones have propagated or jumped across overlapping spreading centers in response to basin opening. The assemblage boundaries are marked by sharp changes in spreading fabric and, in some cases, pseudofaults or transform zones (Parson et al., 1990; Martinez and Taylor, 2006).

The largest of the active backarc spreading center assemblages is the East Lau Basin assemblage, covering an area of 90,325 km² (Tables 6 and 8). It contains the ELSC, which is interpreted to be the oldest active spreading center in the Lau Basin, having initiated in the north at ca. 5.5–5 Ma during the transition

from early basin rifting to spreading (Parson et al., 1992b; Hawkins, 1995; Clift et al., 1998; Martinez and Taylor, 2006; Martinez et al., 2006). The associated assemblage contains the main volcanic formations of the neovolcanic zone and rift valley (units uBar, uBac, mBac) and of the adjacent backarc crust (mBar, mBaf, lBac1, lBac2). ODP drilling and other sampling indicates that these formations are dominantly tholeiitic basalt and basaltic andesite, with an arc signature where the spreading axis approaches the Tofua arc along the Valu Fa Ridge in the south (see Item S4 [footnote 1] and references therein). The arc signature decreases sharply north of 21°S and a few tens of kilometers west of the volcanic front, and the northern segment of the ELSC is entirely backarc-basin basalt. The eastern boundary of the East Lau Basin assemblage, adjacent to the active Tofua volcanic arc, is obscured by the volcanoclastic apron associated with the arc but corresponds generally to a gravity high and sharp discontinuity in the vertical gravity gradient. It is likely that some crust of the East Lau Basin assemblage (unit lBac1) underlies the Tofua volcanic arc assemblage (uAc). The western boundary of the East Lau Basin assemblage is an ~200-km-long pseudofault marked by dozens of en echelon sub-basins (Martinez and Taylor, 2006) and separating transitional arc-backarc crust of the West Lau Basin (units uTc and lTc) from the outermost backarc crust (lBac1 and lBac2) of the East Lau Basin (Fig. 6). This boundary coincides with the edge of the Gauss magnetic polarity chron (3.58–2.58 Ma) identified by Zellmer and Taylor (2001) and Sleeper and Martinez (2016).

At its widest point, in the north, the East Lau Basin assemblage is bordered by the southern boundary of the Zephyr assemblage. Here, the north-south fabric associated with spreading at the CLSC and LETZ, including units mBaf, lBac1, mBar, and lBar, terminates at a discontinuity that separates the East Lau and Zephyr basins. The boundary broadly coincides with the Matuyama magnetic polarity chron (2.58–0.78 Ma; Zellmer and Taylor, 2001; Sleeper and Martinez, 2016), but ship-based data also reveal a dramatic change in the magnetic fabric between the two assemblages (Barckhausen et al., 2019; Hannington et al., 2019). The boundary is currently aseismic (Baxter et al., 2020) and therefore might be related to an older structure of the Niuafu'ou microplate. Three prominent northwest-trending ridges (unit lBar) at the northeastern corner of the East Lau Basin assemblage, which are notably oblique to the dominant north-south fabric, have been identified as mafic intrusions in seismic profiles and in one dredge (Hannington et al., 2019; Schmid et al., 2020). These may be related to ongoing deformation of the Niuafu'ou microplate in this area.

The Central Lau Basin assemblage contains the CLSC and LETZ and associated neovolcanic formations (unit uBar) and is dominated by proximal volcanic ridges (mBar) and their flanks (mBaf). It is generally much younger than the East Lau Basin assemblage, and the area covered is much smaller (11,030 km²; Tables 6 and 8). It is distinguished from the adjacent East Lau Basin assemblage by higher acoustic backscatter in GLORIA side-scan sonar imagery (Hughes Clarke et al., 1993; Parson and Tiffin, 1993; Hill and Tiffin, 1993; Zellmer and Taylor, 2001; Martinez and Taylor, 2006). Early workers interpreted the CLSC to have formed at 1.5 Ma (Parson and Hawkins, 1994); however, recent detailed magnetic studies suggest that it may be as young as 0.78 Ma (Sleeper and Martinez, 2016). It

is interpreted to be propagating southward and is currently rifting older crust of the East Lau Basin assemblage. The northern part of the CLSC is entirely basalt, but andesite has been sampled just south of the maximum inflation of the main propagator (see Item S4 [footnote 1]). The western boundary of the assemblage is a pseudofault defined by truncation of spreading fabric of the East Lau Basin assemblage and coinciding approximately with the Brunhes magnetic polarity chron (Zellmer and Taylor, 2001; Martinez and Taylor, 2006; Sleeper and Martinez, 2106). To the east, the assemblage boundary is marked by several deep nodal basins that belong to the northern termination of the ELSC. This area is characterized by complex intersecting fabric with a number of backarc crustal blocks (unassigned seamounts, unit Us) stranded among the basins of the overlapping spreading center. In the north, the Central Lau Basin assemblage abuts the Peggy Ridge transform and associated formations. Here, the CLSC is connected to the Peggy Ridge via the LETZ and a series of axial volcanic ridges south of the transform (Sleeper and Martinez, 2016). The Peggy Ridge is a long-lived transcrustal boundary between the currently active and relict backarc spreading centers in the north of the Lau Basin and the LETZ, CLSC, and ELSC in the south. It appears to have accommodated significant differential opening of the Lau Basin (~600 km at latitude 15°S versus only 300 km at 18°S) and is included here as an assemblage in its own right (see below).

As many as 17 different assemblages are identified in the complex northern part of the Lau Basin, north of the Peggy Ridge. They contain seven distinct backarc rifts and spreading centers (FRSC, MTJ, NELSC, NWLSC, RR, FSC, and the enigmatic North Cikobia Spreading Center [NCSC] in the far west of the basin; Figs. 5 and 6). In the east, the Fonualei assemblage (16,145 km²) contains the FRSC, which is thought to be the youngest boundary of the Niuafu'ou microplate. The rift valley of the FRSC is located behind the active volcanic front of the Tofua arc. It was first mapped in 1996 and has been the subject of only a few studies since (German et al., 2006; Keller et al., 2008; Escrig et al., 2012). The valley, which is 200 km in length, is defined by a series of en echelon sub-basins, each ~25–50 km long and ~15–30 km wide, with the basin floors at depths of 2400 m below sea level in the north and deepening to 3000 m in the south. Originally, the opening rate was estimated to be 94 mm/yr at 16°S, decreasing to 47 mm/yr at 18°S where the rift impinges on the arc (Zellmer and Taylor, 2001). However, a reinterpretation by Sleeper et al. (2016) predicts FRSC opening rates of only ~32–8 mm/yr, decreasing from north to south. At least six rift segments can be recognized, marked by axial volcanic ridges (unit uBar): two in the north, three shorter overlapping segments in the central FRSC, and a deeper sub-basin which may contain new backarc crust (unit uBac) at the southernmost tip. The rift segments step progressively eastward toward the south, with the distance to the volcanic front decreasing from ~75 km at 16°S to <20 km at 18°S. The rift is thought to be propagating to the south, but the interpretation of magnetic data by Zellmer and Taylor (2001) suggests reversed magnetization at the rift tip, which is consistent with relatively little new crust being produced. Positive magnetization is highly localized in areas where there is clearly recent volcanic activity (cones and dikes), but there are few large earthquakes associated with the spreading (Conder and Wiens, 2011).

The shift in axial morphology of the FRSC from semicontinuous volcanic ridges north of 17°S to isolated volcanic cones and dike complexes south of 17°S may reflect along-axis variation in the focusing of melt as the opening rates decrease and the FRSC axis approaches the volcanic arc (Sleeper et al., 2016). Dredged lavas from the FRSC include mainly basaltic andesite and show strong arc signatures (Keller et al., 2008; Escrig et al., 2012). This is consistent with a model where the southern portion of the FRSC is “capturing” melt from the arc front. However, the location of the rift behind the volcanic front contrasts with that of the late Miocene rift that initiated at or near the arc front. Recent seismic tomography across the FRSC reveals a coincident gravity low and low-velocity anomaly in the arc crust between the rift and the active volcanic front, which has been interpreted as a region containing partial melts (Schmid et al., 2020). This might indicate an imminent rift jump that would strand additional blocks of arc crust in the backarc region. This appears to have happened already at the current location of the FRSC, given that dredging of the high-standing western flanks of the rift indicate that they are mainly arc crust (unit uAc; Hannington et al., 2019).

At its widest point, the Fonualei assemblage is nearly 110 km across, although it has formed relatively recently (<3.8 Ma). It is abruptly terminated in the north by the three arms of the MTJ, which have produced a small amount of new backarc crust composing the Mangatolu assemblage (1871 km²; Tables 6 and 8). Detailed mapping of the MTJ (see Item S2 [footnote 1]; Mensing, 2019) shows that crustal accretion is no longer occurring along the western arm, but this structure clearly truncates older backarc crust that originated from the southern arm or from earlier spreading associated with the northernmost segment of the FRSC. The dominant accretion is now occurring along the northern arm, where the rift valley is occupied by an inflated axial high. Dredged material from the northern arm is mostly basaltic andesite, whereas samples from the southern arm are entirely basaltic (Mensing, 2019).

The Northeast Lau Basin assemblage contains the NELSC as well as the Niuatahi silicic volcanic caldera and its surrounding volcanic field, collectively 7916 km². This assemblage has been mapped in detail by Embley and Rubin (2018) and Norris-Julseth et al. (2020) who defined the region between the Tofua arc and the NELSC as “rear arc.” This assemblage is bounded by major faults that appear to have been inherited from the early stages of rifting in the northeastern Lau Basin. The southern boundary crosses the Fonualei assemblage (unit lBac1) and the northern Tofua volcanic arc (uAc). The western boundary is interrupted by the northern arm of the MTJ, which appears to be propagating into the Northeast Lau Basin assemblage. The northern boundary is at the contact with forearc blocks belonging to the North Lau Forearc assemblage and rifted Tonga forearc (i.e., the Mata Basin; Embley and Rubin, 2018). The NELSC is propagating into old forearc crust in the north and also appears to be propagating south toward the northern tip of the FRSC. The two spreading centers may eventually connect in the area of rifted arc and backarc crust at the intersection of the N-FRSC, MTJ, and NELSC (Baxter et al., 2020). This area is heavily intruded by recent backarc volcanoes (e.g., Merle et al., 2013). Samples of the crust proximal to the NELSC are backarc-basin basalt and basaltic

andesite, including the youngest lavas of the neovolcanic zone (Falloon et al., 2007; Michael et al., 2009), whereas the volcanic flow field (unit Bavf) surrounding the Niuatahi volcano is mainly dacite (Embley and Rubin, 2018).

Recently formed backarc assemblages west of Fonualei and Mangatolu include Niuafu’ou, Rochambeau, Southeast Futuna, and Northwest Lau. The formations surrounding Niuafu’ou Island are grouped as an assemblage that comprises the large Niuafu’ou shield volcano (unit Bav2), several other large submarine volcanoes, and a large volcanic field (Bavf), covering 3509 km² (Tables 6 and 8). The volcanic field surrounding Niuafu’ou consists of lava flows and pyroclastic material (airfall and surge deposits; Taylor, 1991). Niuafu’ou Island is capped by the remnants of a composite cone, where the latest eruption occurred in March 1985 (Global Volcanism Program, 1985). The alignment of several large submarine volcanoes northwest and southeast of Niuafu’ou may mark an emerging microplate boundary between the western arm of the MTJ and the northern tip of the RR (cf. Baxter et al., 2020). Samples from the volcanoes include a wide range of rock types such as normal MORB, enriched MORB, oceanic island basalt, and dacite (Hawkins, 1995).

The western limit of the Niuafu’ou assemblage interfingers with, or is overprinted by, the formations of the Rochambeau assemblage. The Rochambeau assemblage comprises the proximal backarc crust and ridges of the Rochambeau spreading centers (Rochambeau rifts, RR), which together occupy an area of 8155 km². The main RR segment is interpreted to be spreading at 110 mm/yr (Lupton et al., 2012) and has a prominent axial volcanic high (unit uBar) and large summit caldera (Lobster caldera; Arculus, 2008). A smaller en echelon rift to the northwest lacks an axial high but is floored by proximal backarc crust (unit uBac). Both of the rift valleys of the RR segments are only ~40 km wide, suggesting that they are not older than 350,000 yr. The northwestern segment terminates against the eastern extension of the Futuna transform fault and deformation zone (unit Dz2) in the north, which separates the young backarc region from the old forearc crust of the North Lau Forearc assemblage.

The Northwest Lau Basin assemblage (4626 km²) is dominated by the axial volcanic ridge of the NWLSC, which is surrounded by young backarc crust and volcanic ridges. The ridge is 97 km long and >500 m high, with two prominent summit calderas (Arculus, 2008). To the north, the assemblage is truncated by a large volcanic field belonging to the Southeast Futuna assemblage (Southeast Futuna volcanic zone). To the south, it is in contact with the Peggy Ridge. The western and eastern contacts are defined by the broad, 45-km-wide rift valley containing the NWLSC.

The large Southeast Futuna volcanic zone and Rochambeau Bank (Fouquet et al., 2015; Konn et al., 2016) are located within the Southeast Futuna assemblage at the intersection of the North Futuna, South Futuna, Northwest Lau Basin, and Rochambeau assemblages and may conceal the boundaries between these assemblages. The southern extent of the Southeast Futuna volcanic zone, in particular, represents a large volume of material possibly erupted along a crustal boundary between emerging microplates (Baxter et al., 2020). Like Niuafu’ou, the Southeast Futuna assemblage is dominated by a number of large shield volcanoes (unit Bav2; e.g., Kulo Lasi volcano), smaller

volcanic cones, domes and ridges, and several broad volcanic fields (Bavf, collectively 8260 km²). The northern boundary of the assemblage appears to be truncated by the Futuna transform fault. Several dredge samples from the perimeter of the field are all basaltic (Arculus, 2012). However, a distinctive feature of the volcanic rocks from the Southeast Futuna, Northwest Lau Basin, Rochambeau, and Niuafu'ou assemblages is a plume-like signature indicated by elevated ³He/⁴He (Lupton et al., 2015).

The Futuna assemblage, farther to the west, contains the FSC and all ridges and backarc crust thought to have formed at the spreading center (>28,922 km²; Pelletier et al., 2001). A very broad but poorly defined outer rift valley (155–190 km wide) is interpreted to be the limit of the assemblage and is consistent with its presumed age (as old as 4.5 Ma, assuming a spreading rate of 40 mm/yr on the FSC; Pelletier et al., 2001). The FSC itself is nearly 215 km long and 800 m high with an axial ridge (unit uBar) at least 15 km wide. The entire ridge covers an area >2350 km², which is the largest of the currently active spreading centers in the Lau Basin. The spreading fabric of the Futuna assemblage is truncated by the Futuna transform fault in the north and the western extension of the Peggy Ridge in the south, where it is in contact with the Qelelevu assemblage. The southern end of the FSC may be propagating into the Fiji platform, although the connection to the North Fiji fracture zone is unclear.

Another enigmatic assemblage is centered on the North Cikobia Spreading Center (NCSC) and the West Cikobia volcanic zone (WCVZ), west of Futuna. The NCSC is an active spreading center with a spreading rate of 20 mm/yr (Pelletier et al., 2001); however, its relationship to the mapped Cikobia assemblage, which is dominated by unassigned crust (unit Ucr), is not clear. Based on the mapped area (47,275 km²) and the spreading rate at the NCSC, this assemblage may have started forming as early as 12.5 Ma, assuming all of the crust was generated at the spreading center. Alternatively, the ridges and backarc crust outside the zones of active spreading may be much older, and the NCSC and WCVZ are relatively recent features. The northern boundary of the Cikobia assemblage is the Vitiaz lineament. The southern boundary is the contact with the Fiji platform. The eastern limit is drawn where volcanic ridges and backarc crust of the Futuna assemblage are clear.

Although their ages are not well constrained, the Fonualei, Futuna, and Cikobia assemblages cover the largest areas and are likely the oldest currently active backarc assemblages in the north of the Lau Basin. These older and larger assemblages likely represent an early phase of fast growth in the opening of the northern Lau Basin. The Mangatolu, Northeast Lau Basin, Northwest Lau Basin, and Rochambeau assemblages are much smaller and were probably not formed until after 1.5 Ma (Hawkins, 1995).

Relict Backarc Basin Assemblages

Five relict backarc basin assemblages have been identified in the north: Zephyr, North Fonualei, North Futuna, South Futuna, and Qelelevu (Fig. 5). They are interpreted to have formed by rifting and seafloor spreading but have less

well-defined spreading fabric than the active assemblages, and the associated spreading centers are either no longer preserved or cannot be identified. The assemblage boundaries are drawn where a clear distinction from an adjacent assemblage can be made, including changes in the spreading fabric or the magnetic signature. Commonly, the relict backarc assemblages are in fault contact with other assemblages, marked by discontinuities in the gravity gradient.

The Zephyr assemblage (31,580 km²) occupies a large region between the FRSC in the east and the NWLSC and RR in the west. It is composed of rifted arc and backarc crust (units uRbc1, uRbc2, and IRbc) that is overprinted by recent intraplate volcanism (Bav1) in its eastern half. Zephyr shoal was sampled by Hawkins (1976) and found to be mostly dacite, similar to samples recently collected west of the FRSC (Hannington et al., 2019). These observations are consistent with characteristics of many of the deep depressions in the relict backarc basin assemblages representing failed rifts in earlier arc and backarc crust (e.g., the large Zephyr Deep) and some of the large seamounts (unit Us) representing rifted blocks of arc crust. These older formations (uRbc and IRbc) are interpreted to have originated in the early history of the opening of the basin (ca. 5.5 Ma), and so the large size of the assemblage reflects its age. The more recent intraplate volcanism in the southeast of the assemblage is basaltic (Hannington et al., 2019) and likely indicates widespread rifting and intrusion of the crust that is ongoing today.

The North Fonualei assemblage (10,552 km²) consists of relict backarc crust (units uRbc1, uRbc2, and IRbc) and volcanic ridges (uRr), partly obscured by younger backarc crust (IBac1) from the Northeast Lau Basin and Mangatolu assemblages. Some of the tectonized crust in the east (depicted on the map as unit uRbc2) could be large blocks rifted from the Tofua arc by the MTJ and NELSC (Mensing, 2019; Norris-Julseth et al., 2020). In the north, the assemblage is structurally bounded by the Futuna transform fault, and in the south, it is bounded by the MTJ and the Niuafu'ou volcanic field. The western boundary is mapped along the contact with the younger backarc crust of the northern Rochambeau assemblage. Although the North Fonualei assemblage does not contain an active spreading center, the crust may be related to the Fonualei assemblage which was bisected by the formation of the MTJ. The age of North Fonualei is therefore likely bracketed by the maximum age of the Fonualei assemblage (between 3.8 Ma and 1.9 Ma).

The North Futuna assemblage is located west of the Rochambeau assemblage. It consists of a large area (17,529 km²) of relict backarc crust (unit IRbc) and, in the far west, a series of ridges (uRr) interpreted to represent old spreading fabric (Pelletier et al., 2001). It is bounded to the north by an extension of the Futuna transform fault, separating backarc crust of the northern Lau Basin and forearc crust of the former Vitiaz arc, and to the south by the Southeast Futuna volcanic field.

The South Futuna assemblage is located between the younger backarc assemblages associated with the NWLSC in the east and the FSC in the west. It is in contact with the North Futuna assemblage along the Futuna transform fault and the Qelelevu assemblage in the south along the Peggy Ridge fault. Like the North Futuna assemblage, it consists of a large area (15,682 km²) of

relict backarc crust (unit IRbc) and unassigned seamounts (Us); a clear spreading fabric is not evident, but dredge samples are all basalt (Item S4 [footnote 1]). A possible interpretation is that the South Futuna assemblage is a rifted portion of the Zephyr assemblage, separated by the NWLSC.

The Qelelevu assemblage (7417 km²) consists mainly of deformed backarc crust (units IRbc and uRbc) in a structurally bounded area trapped between the South Futuna assemblage, Peggy Ridge, the Qelelevu fault, and the North Fiji fracture zone. The origin of this assemblage is unclear, but it may be a relict of the West Lau Basin assemblage or Lau Ridge, separated from the West Lau by the Qelelevu fault.

Arc-Backarc Transition

The West Lau Basin assemblage is an areally extensive (143,775 km²) group of formations (units ITc, uTc, and uTr) at the boundary between the active backarc region, dominated by the East Lau Basin assemblage, and the Lau Ridge relict arc. It is interpreted to have formed during the initiation of backarc rifting and seafloor spreading during the earliest opening of the Lau Basin. It has a seismic velocity structure consistent with mainly rifted material and nearly identical to that of the crust from the ELSC rather than arc-type crust (Crawford et al., 2003). Thus, much of the West Lau Basin assemblage may have been magmatically accreted but in a less-organized way than at a focused spreading center. The dominant formations are similar to normal backarc and relict backarc crust but heavily deformed and sedimented, with sub-basins that are considered to be failed rifts floored by basalt (Parson et al., 1992b; Parson and Hawkins, 1994; Hawkins, 1995; Parson and Wright, 1996). Some parts may include remnants of old arc crust in addition to the basaltic crust formed during rifting (Hawkins, 1995; Martinez and Taylor, 2006). Thus, the overall assemblage is likely a mixture of rifted material from the early arc (i.e., Lau and Tonga Ridge age: 46–31 Ma, 28–15 Ma) and younger volcanic rocks formed during the transition from rifting to spreading (5.6–2.4 Ma; Table 6). We have drawn the assemblage boundaries in the east where the sediment cover decreases and the spreading fabric of younger backarc crust is visible, and in the west where elevated relict arc crust of the Lau Ridge dominates.

Three large volcanic fields (unit Bavf, individually 4411–27,010 km²) appear to overprint the West Lau Basin assemblage and partly overlap the boundary with the East Lau Basin assemblage, close to the southern ELSC and the Valu Fa Ridge. Although individual flows have not been identified, the associated formations are identified as unit Bavf, punctuated by numerous backarc volcanic cones (unit Bav1) that indicate recent intraplate volcanism within the arc-backarc transition zone. These areas have been mapped previously as “ridges and knolls,” which were interpreted to be products of rifting and diapir-like magma intrusion into the extended crust (Fujiwara et al., 2001; Martinez and Taylor, 2006). The southernmost of the fields covers 27,010 km² and is associated with a significant regional-scale bulge or inflation of the arc and backarc region. This inflation has been described by Fujiwara et al. (2001)

as a precursor of basin opening produced by MORB-like magmatism in the absence of a stable rift or spreading center. The ages of the volcanic fields are uncertain, but those in the north are more heavily sedimented than in the south.

Relict Arc Assemblages

The Lau Ridge and Tonga Ridge are relict arc assemblages that formed prior to backarc basin opening. They comprise mainly flows and volcanoclastic rocks that were products of early arc magmatism, but they also include crust that may have formed as a result of rifting of the arc, forearc, or arc-backarc transition (e.g., Taylor and Karner, 1983; Stern et al., 1984; Hawkins and Allan, 1994; Martinez and Taylor, 2006). The majority of the Lau Ridge and Tonga Ridge assemblages belong to the former Vitiaz arc and forearc and are underlain by old arc basement along their entire length (Martinez and Taylor, 2006). This contrasts with rifting of the present-day Tofua arc by the FRSC and the Valu Fa Ridge, which is occurring behind the volcanic front and isolating relatively small relicts of arc crust in the backarc basin.

The Tonga Ridge assemblage covers 109,424 km² and consists of mostly volcanoclastic and sedimentary material (units IRac and uRac; Hawkins and Allan, 1994; Meffre et al., 2012; Beier et al., 2017). Drilling at ODP Site 840 on the Tonga Ridge (Fig. 3) encountered >590 m of volcanoclastic and sedimentary rocks ranging from Holocene to late Miocene in age (Parson et al., 1992b). No crystalline rocks were encountered, but felsic igneous rocks of Eocene age were intersected on the Tonga forearc at ODP Site 841, which may suggest that similar material is present in the basement of the Tonga Ridge. In general, drilling on the Tonga Ridge at ODP Site 840 and in the forearc at ODP Site 841 recovered rocks belonging to similar formations.

The Lau Ridge assemblage (310,568 km²) is similar to the Tonga Ridge assemblage, consisting of volcanic and volcanoclastic rocks that range in age from Holocene to middle Eocene (Hawkins, 1976; Cole et al., 1990; Parson et al., 1992b; Hathway, 1994; Wharton et al., 1995; Taylor et al., 2000). Older volcanic rocks are present at the Lau Ridge, dating from 46 Ma to 31 Ma, when the ridge was part of the Vitiaz arc (Hathway, 1994; Wharton et al., 1995; Taylor et al., 2000). Volcanism continued as the crust was separated from the former Vitiaz forearc, and intermittent volcanic activity on the ridge has been dated to as young as ca. 0.3 Ma (Cole et al., 1990; Wharton et al., 1995). Cross-arc volcanic chains or coalesced volcanic ridges (unit uRav) have a west-southwest trend on the eastern side of the Lau Ridge and a west-northwest trend on the western side, implying a late-stage rotation in the direction of basin opening. Older eroded arc volcanoes are also present within the assemblage (unit uRac). To the east, the Lau Ridge is in contact with the West Lau Basin assemblage along the inferred boundary of early arc rifting, where deep, sediment-filled basins abut the Lau Ridge. To the west, the Lau Ridge descends into the South Fiji Basin, and its boundary is defined by a gravity high. The overlap with formations of the South Fiji Basin is likely conformable, marking the western limit of volcanism associated with the former Vitiaz arc.

Forearc Assemblages

The Tonga Forearc assemblage includes crust of the forearc slope (unit Fc1), tectonized forearc blocks (Fc2), crust of the inner trench wall (Fc3), forearc volcanoes (Fv), and different types of forearc mounds (Fm), including serpentinite mounds, mud volcanoes, and uplifted crustal blocks of uncertain origin. These formations, which cover 91,488 km², mostly belong to the former Vitiaz arc. The assemblage boundaries are drawn along the deepest part of the trench and at the inferred contact with the relict arc assemblage of the Tonga Ridge, described above. No accretionary material is assigned to this assemblage or anywhere in the Lau-Tonga region.

The Mata Basin, north of the Tonga Ridge, consists of extended forearc crust (unit Fc4) surrounding the active Niua arc volcano and the Mata rift volcanoes. The Mata rift volcanoes are boninitic in composition (Resing et al., 2011) and have erupted as recently as 2018 (Chadwick et al., 2019). The rifting of the forearc is thought to be related to significant left-lateral transcurrent motion and wrench tectonics associated with the STEP fault at the former Vitiaz trench (e.g., Embley et al., 2014; Baxter et al., 2020; Norris-Julseth et al., 2020). The anomalous magmatism may be related to an emerging ridge-trench-fault triple junction at this location (Escrig et al., 2012; Regelous et al., 2014). However, boninitic volcanism, like that at the Mata volcanoes, has had a protracted history in this region since at least 15.2 Ma (Meffre et al., 2012).

We separate the North Lau Forearc assemblage (9384 km²) from the Tonga forearc because of their very different structural settings. The North Lau forearc is bounded to the north by the regional Vitiaz lineament, which is a crustal-scale structure accommodating transcurrent motion between the Pacific and Australian plates and juxtaposing the arc, backarc, and oceanic assemblages (Govers and Wortel, 2005). Little or no forearc crust is preserved west of this location because most of the former Vitiaz arc was transported to the south with the rotation of the Fiji platform in the early stages of opening of the North Fiji Basin (Hawkins 1995; Schellart et al., 2006).

Other Assemblages

The South Vitiaz assemblage in the north of the Lau Basin is difficult to classify because there are few ship-based data in the area, but it can be distinguished from adjacent assemblages on the basis of magnetic fabric and major bounding structures visible in the vertical gravity gradient. One of the seamounts, Manatu seamount, has been sampled, and the rocks recovered include basalt, dolerite, talus breccia, limestone, and marl (Sinton et al., 1985), but no additional information is available.

A number of the deformation zones (units Dz1 and Dz2) have also been mapped as assemblages where a significant amount of crust is involved. The Peggy Ridge assemblage, in particular, includes voluminous lava flows associated with leaky transform faulting along much of its length (Parson and Tiffin, 1993; Taylor et al., 1996). We consider the Peggy Ridge to be a distinct

assemblage because of the extent of the erupted material (6341 km²) and the presence of several different formation types, including clearly visible dome volcanoes (unit Bav3). Eighty-four percent (84%) of the ridge is covered by ship-based bathymetry and GLORIA side-scan sonar imagery (Zellmer and Taylor, 2001; Martinez and Taylor, 2006). A strong magnetic anomaly, clear volcanic morphology, high acoustic backscatter, and fresh samples collected along the ridge are consistent with recent magmatism. The samples include tholeiitic basalt from thick flow units (Volpe et al., 1988; Falloon et al., 2007). Taylor et al. (1996) interpreted the MORB-like magmatic rocks to be younger than magnetic polarity chron 2n (1.77 Ma) but older than the Brunhes chron (0.78 Ma). One sample of basalt from the northern end of the Peggy Ridge has elevated ³He/⁴He that is intermediate between MORB and the plume signature of the NWLSC-RR basalts (Lupton et al., 2015).

All of the mapped formations on oceanic crust are grouped into a single oceanic assemblage because these were not the focus of the present study. However, we distinguish different types of volcanoes and seamounts (units uOs1–uOs3), oceanic plateaus (uOp, IOp1, IOp2), and undivided crust (units IOc1, IOc2) belonging to the Pacific and Australian plates.

TECTONIC AND LITHOSTRATIGRAPHIC CORRELATIONS

Based on this compilation, we have assigned age ranges to each of the mapped assemblages and arranged them in approximate stratigraphic order in Figure 8, with major regional tectonic events also indicated. The tectonic and lithostratigraphic correlations are constrained by historical drill-hole data, geological sampling, and absolute age data summarized in Table 6. Where necessary, relative ages have been assigned based on crosscutting structural relationships or spreading fabrics (e.g., indicating crust that formed contemporaneously or at different times) and sediment cover. Following is a summary of the age constraints for the individual assemblages. These data provide a basis for the area-age calculations in our model of crustal growth.

The initiation of subduction and formation of the proto-Vitiaz arc began as early as 46 Ma and continued in three major intervals (Hathway, 1994; Wharton et al., 1995; Taylor et al., 2000). The oldest arc crust now at the Lau Ridge formed during protracted arc volcanism in the middle Eocene (Yavuna Group at 46–31 Ma). Subsequent rifting of the proto-Vitiaz arc produced a significant unconformity at the top of the Yavuna Group, and a second stage of subduction formed the Vitiaz arc between ca. 28 and 15 Ma (Wainimala Group; Wharton et al., 1995). The latest episode of arc development started at ca. 14 Ma and continued through initial backarc basin opening. The Eocene to Miocene stratigraphy preserved on the Tonga Ridge differs slightly from that of the Lau Ridge, with volcanic episodes spanning 46–40 Ma, 33–31 Ma, and 19–17 Ma (Duncan et al., 1985). The thick sequence of volcanoclastic material at ODP Site 840 on the Tonga Ridge is interpreted to have been deposited on the forearc of the Lau Ridge before it was separated from Tonga (Parson et al., 1992b, 1994; Hawkins, 1995). The shorter volcanic episodes recorded by rocks of the Tonga

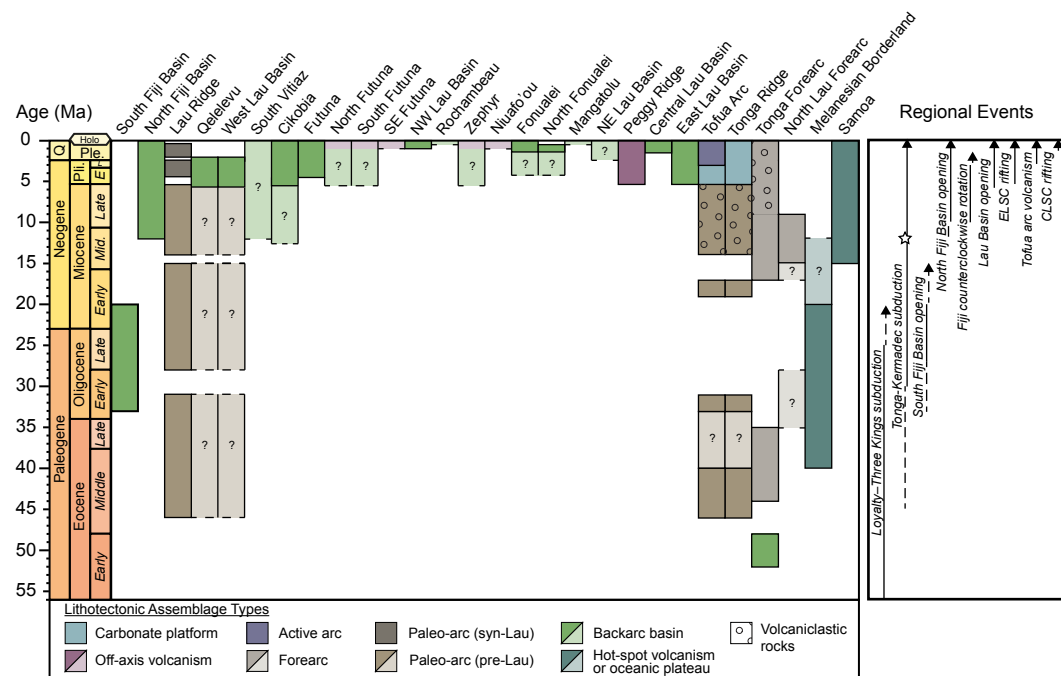


Figure 8. Lithostratigraphic correlation diagram of the Lau Basin, summarizing the general stratigraphy within each of the assemblages depicted in Figure 5, with reference to published ages of volcanic units, depositional ages of sedimentary units, and relative ages of assemblages inferred from mapped relationships. Inferred age correlations of regional tectonic events are also shown. Star indicates end of subduction at the Vitiaz trench. Note: Darker shades indicate volcanic episodes and/or deposition of volcaniclastic material with published age constraints; lighter shades are of unknown stratigraphic extent. Assemblages outside the Lau Basin (South Fiji Basin, North Fiji Basin, Melanesian Borderland, Samoa) are included for regional context. See text for descriptions of regional events. CLSC—Central Lau Spreading Center; ELSC—Eastern Lau Spreading Center. Holo—Holocene, Ple.—Pleistocene, Pli.—Pliocene, E—Eocene, Q—Quaternary, L.—Late.

Ridge may reflect incomplete preservation or less magmatism in the forearc. The crust associated with this early arc development is likely present beneath the Tofua Arc, Tonga Forearc, North Lau Forearc, West Lau Basin, and Qelelevu assemblages. Volcanic rocks on the Lau Ridge, dated between 14 and 2.5 Ma, are related to the final stage of arc development (Lau and Korobasaga Volcanic Groups; Cole et al., 1990). Volcanic activity on the Lau Ridge after 2.5 Ma is thought to be related to extension of the ridge and not subduction-related arc volcanism (Mago Volcanic Group; Cole et al., 1990). Volcanism continued on the Lau Ridge until ca. 0.3 Ma, but there is no correlation with units on the Tonga Ridge between 6 and 0.3 Ma. The ages of the prominent cross-arc volcanoes on the Lau Ridge are unknown, but the orientations of the chains appear to reflect a change in principal stress during the early history of the arc. The volcanoes on the western side, oriented northwest-southeast, may be somewhat older and reflect the prevailing stress regime at the time of subduction along the original Vitiaz arc. The switch to northeast-oriented chains might record the change in stress related to (or even triggering) the breakup of the Vitiaz arc.

The oldest rocks of the Tonga Forearc assemblage (52–48 Ma) are interpreted to represent backarc crust formed behind the east-dipping Three Kings–Loyalty arc, which became part of the forearc assemblage of the Vitiaz arc following subduction reversal (Meffre et al., 2012). Crustal ages in the forearc vary geographically, with older crust occurring in the south than in the north (Meffre

et al., 2012). Drilling of the Tonga forearc at ODP Site 841 (Parson et al., 1992b) intersected late Eocene rhyolite (44 ± 2 Ma) interpreted to be equivalent to Eocene formations on the Lau and Tonga Ridges. A major unconformity is present between late Eocene to early Oligocene sediments and volcaniclastics (44–35 Ma) and middle Miocene to middle Pleistocene sediments and volcaniclastics (17 to <1 Ma; Cunningham and Anscombe, 1985; McDougall, 1994; Clift et al., 1998). The gap in deposition and development of the unconformity may have been the result of seamount collision, which is also suggested by a change in the dip of the sediments (Clift et al., 1998). The unconformity broadly coincides with the hiatus in volcanism on the Tonga Ridge between 31 and 19 Ma and a period of active volcanism at the Lau Ridge (Fig. 8). North of the Tongan island of 'Eua, the forearc region was dominated by three episodes of crust development at 52–48 Ma, 35–28 Ma, and 15–9 Ma (Meffre et al., 2012). The North Lau Forearc assemblage has a somewhat different history more closely linked to the termination of subduction at the Vitiaz trench and lacking the more recent sediment and volcaniclastic rocks (Meffre et al., 2012).

Crust formed during the initial rifting and opening of the Lau Basin is represented by the West Lau Basin assemblage (Parson et al., 1992b; Parson and Hawkins, 1994; Hawkins, 1995; Parson and Wright, 1996; Martinez and Taylor, 2006). Hawkins (1995) proposed that the crust west of the ELSC and CLSC formed mainly through rifting rather than seafloor spreading, with numerous

sediment-filled basins characteristic for this early opening phase. Basaltic flows and sediments in the sub-basins have a broad range of ages, generally decreasing from 5.6 Ma at ODP Site 834 in the west to 0.8–0.64 Ma at ODP Site 836 in the east (Fig. 3) (Hawkins and Allan, 1994). The intervening crust is thought to be a combination of rifted arc crust from the early opening phase and basalt from the advanced stages of opening, with seafloor spreading occurring mainly distant from the volcanic arc (Hawkins, 1995; Martinez and Taylor, 2006). We interpret the Qelelevu assemblage to be a remnant of the West Lau Basin assemblage with a similar stratigraphy (Fig. 8).

The assemblages formed during recent backarc rifting and spreading have well-established ages based on magnetic data (Zellmer and Taylor, 2001; Sleeper and Martinez, 2016). The East Lau Basin assemblage began forming early in the opening history at ca. 5.5–5 Ma (Parson and Hawkins, 1994; Hawkins, 1995; Taylor et al., 1996; Sleeper and Martinez, 2016). The Central Lau Basin assemblage is considerably younger, having formed since the CLSC initiated and began propagating south from the Peggy Ridge at ca. 1.5–1.2 Ma (Parson and Hawkins, 1994; Hawkins, 1995).

Ages of the other backarc assemblages are assigned according to the oldest (most distant) crust that originated from the present-day spreading center. The Futuna assemblage, which is ~180 km wide, is interpreted to have started forming at 4.5 Ma, assuming a constant spreading rate of 40 mm/yr (Pelletier et al., 2001), and it is still growing today. In contrast, the Northwest Lau Basin assemblage is only 50 km wide and is spreading at a rate of 48 mm/yr (Taylor et al., 1996), suggesting that it is <1 m.y. old. This is consistent with the positive magnetization, corresponding to the Brunhes-Matuyama magnetic polarity reversal at 0.78 Ma (Zellmer and Taylor, 2001). The age of the Rochambeau assemblage is poorly constrained. The global plate-boundary model suggests a spreading rate as high as 110 mm/yr (Lupton et al., 2012, citing Bird, 2003), which is probably too high considering that the entire basin is widening at 159 mm/yr (Pelletier et al., 1998) to 174 mm/yr (Zellmer and Taylor, 2001). Even if crustal accretion were occurring at half the rate cited above, the Rochambeau assemblage, which is only 22 km wide, would still be considerably younger than 1 Ma.

Different estimates for the rate of extension of the FRSC result in a range of ages for the Fonualei assemblage. At a width of ~106 km in the north and an opening rate of 28 mm/yr at this location (Sleeper and Martinez, 2016), the maximum age of the Fonualei assemblage is 3.8 Ma, whereas in the south, where the rift valley is 15 km wide and the opening rate is 8 mm/yr (Sleeper and Martinez, 2016), the crust is younger than 1.9 Ma. This discrepancy in age between the northern and southern regions of the Fonualei assemblage is consistent with southward propagation of the FRSC (Sleeper and Martinez, 2016), similar to what has been documented for the ELSC and CLSC (Parson et al., 1990). At the rift tip where the FRSC is propagating into the Tofua arc, the magnetic polarity is reversed (Zellmer and Taylor, 2001), indicating that significant new crust has not yet formed there. Spreading on the MTJ is occurring at an average rate of 30 mm/yr (Sleeper and Martinez, 2016) and, based on the width of the rift valley (18 km), is younger than 600,000 yr. This

crust has formed contemporaneously with the Rochambeau and Northwest Lau Basin assemblages.

Spreading rates for the NELSC are poorly constrained but estimated to be ~42 mm/yr (Baker et al., 2019). We estimate the age of the Northeast Lau Basin assemblage to be 2.5 Ma, assuming a full width of 105 km. Our mapping suggests that the border of the Northeast Lau Basin assemblage truncates the northern portion of the Tofua arc, and the NELSC appears to propagate into arc crust, which would indicate that the backarc assemblage is younger than 3 Ma, the maximum age of the Tofua arc. Thus, we consider the Northeast Lau Basin assemblage to be the same age as the Fonualei assemblage. The North Fonualei assemblage does not contain an active spreading center, but it may be the northern extension of the Fonualei assemblage, bracketed by the maximum age of Fonualei crust (3.8 Ma) and the maximum age of the Mangatolu assemblage (<1 Ma).

The Niuafu'ou assemblage cross-cuts the Fonualei assemblage and therefore has a maximum age between 3.8 and 1.9 Ma. However, we suggest that it may be significantly younger, given that it contains the active Niuafu'ou volcano. The Southeast Futuna assemblage is similarly an active volcanic center (Fouquet et al., 2015; Konn et al., 2016). The relationship to the NWLSC and southern RR strongly suggests that the Southeast Futuna, Northwest Lau Basin, and Rochambeau assemblages are of similar age and mostly younger than 1 Ma.

The age of the Peggy Ridge assemblage is uncertain, but Parson and Hawkins (1994) proposed that basin opening was initiated on the trace of this structure, and therefore it must have been present as early as 5.5 Ma. It is still an important locus of deformation in the northern Lau Basin, connecting the northern spreading centers (notably the FSC and NWLSC) to the LETZ and CLSC in the south. Fresh volcanic rocks have been recovered from the ridge (Hawkins, 1995; Falloon et al., 2007), and most of the Peggy Ridge assemblage is characterized by high acoustic backscatter, indicating little sedimentation (Zellmer and Taylor, 2001). The fact that the Peggy Ridge transform cuts some of the oldest crust in the basin (e.g., the Qelelevu assemblage) and also the youngest in the Central Lau Basin assemblage confirms that it is one of the longest-lived structures in the region and has been key to basin opening. The northern edge of the Fiji platform might have been an important crustal boundary along which the Peggy Ridge was initiated. For example, Martin (2013), citing data in Malahoff et al. (1982), Inokuchi et al. (1992), and Taylor et al. (2000), suggested that rotation of the Fiji platform started at or before 10 Ma and ceased after collision with the Lau Ridge between 2.7 Ma and 1.56 Ma, with the pole of rotation close to the north end of the Peggy Ridge.

The Cikobia assemblage straddles the boundary between the Lau and North Fiji Basins and therefore might have begun forming during the opening of the North Fiji Basin and prior to the formation of the Lau Basin. If the entire assemblage formed by spreading at ~20 mm/yr (Pelletier et al., 2001), the maximum age of the assemblage would be 12.5 Ma, which approximately coincides with the end of subduction at the Vitiaz trench at ca. 12 Ma and the beginning of opening of the North Fiji Basin (Malahoff et al., 1982; Taylor et al., 2000; Martin, 2013). The ages of the Zephyr, North Futuna, and South Futuna

assemblages are also poorly constrained due to limited sampling and the lack of identifiable spreading. The Zephyr assemblage is interpreted to be older than the Northwest Lau Basin and Fonualei assemblages and may date from the beginning of basin opening (ca. 5.5 Ma). However, small volcanic cones and ridges in the eastern half of the Zephyr assemblage have high acoustic backscatter, suggesting that some younger intraplate volcanism continued after 1 Ma. The South Futuna assemblage is interpreted here to be the extension of the Zephyr assemblage and therefore the same age. It also shows signs of widespread, late-stage intraplate volcanism. The North Futuna assemblage has an uncertain tectonic history but is considered to be similar in age to the South Futuna assemblage. There are no constraints on the age of the South Vitiaz assemblage; however, some of the unassigned seamounts in the South Vitiaz assemblage may have been accreted from the Melanesian Borderland during subduction at the Vitiaz trench. Therefore, we interpret the maximum age of the South Vitiaz assemblage as the termination of subduction at the Vitiaz trench (12 Ma).

The South Fiji Basin, North Fiji Basin, Melanesian Borderland, and Samoa are included in the correlation diagram (Fig. 8) to provide a larger tectonic context. The South Fiji Basin crust west of the Lau Ridge is early Oligocene to early Miocene in age, based on magnetic anomalies 13–8 (Meffre et al., 2012; van de Lagemaat et al., 2018). The North Fiji Basin crust has been produced during the opening of the North Fiji Basin since 12 Ma and is still forming (Yan and Kroenke, 1993; Taylor et al., 2000; Meffre et al., 2012; van de Lagemaat et al., 2018). The Samoa assemblage has a maximum age of 14.8 Ma in the area surrounding the Samoan Islands (Finlayson et al., 2018) but also includes crust associated with the active Samoan hot spot. In the vicinity of the Melanesian Borderland assemblage, the Samoan and Rarotongan hot-spot tracks span 20–40 Ma (Finlayson et al., 2018). One of the volcanic features in the Melanesian Borderland assemblage (Alexa Bank) has been dated at 37 Ma (Duncan, 1985), and all of the crust in the area has a thick sedimentary cover, suggesting that it is old (Pelletier and Auzende, 1996).

■ QUANTITATIVE ANALYSIS

Early models of the Lau Basin focused on the rate of basin opening as the complete picture of crustal accretion, but new research has shown that crustal growth has been highly episodic and, in the last 1.5 m.y., dominated by extension distributed across many active spreading segments and deformation zones (e.g., Martinez and Taylor, 2006). In the southern Lau Basin, >100,000 km² of backarc crust has been created at the ELSC and CLSC in the last 5 m.y. In the same time period, 202,000 km² of backarc crust was created among the different assemblages of the northern Lau Basin, including 33,450 km² in the last 1.5 m.y. Our mapping also suggests that important episodes of crustal growth and basin opening were not the result of simple backarc spreading but included significant non-volcanic rifting, magmatism at leaky transform faults and deformation zones, and intraplate volcanism.

The greatest part of the map area is occupied by relict arc crust (310,568 km² and 109,424 km² in the Lau and Tonga Ridges, respectively), reflecting the long history of construction of the Vitiaz arc prior to opening of the Lau Basin. The Lau Ridge covers 28% of the map area, and the Tonga Ridge 10%. Assemblages that can be confidently identified as originating from a backarc spreading center account for only ~28% of the map area (Table 7). The earliest backarc crust (143,775 km² of transitional arc-backarc crust of the West Lau Basin assemblage) covers 13% of the map area and accounts for 29% of the total backarc crust. This large area of crust formed over a period of steady crustal growth from at least 5.5 Ma to ca. 2.5 Ma. Subsequent episodes of crustal accretion between 2.5 and 1.5 Ma were dominated by the East Lau Basin assemblage (90,325 km²) in the south and the Cikobia (47,275 km²) and Futuna (28,922 km²) assemblages in the north, corresponding to a period of rapid growth. The young backarc assemblages that appeared in the northern Lau Basin within the last 1.5 m.y. are far more numerous but also much smaller. The Fonualei assemblage is the largest, covering 16,145 km²; the Mangatolu, Northeast Lau Basin, Northwest Lau Basin, and Rochambeau assemblages are the smallest, from 1871 to 8155 km². Based on the total width (~222 km) and inferred ages of these assemblages, the average spreading rate in the last 1.5 m.y. was 148 mm/yr, consistent with published values. However, because opening of the basin has been partitioned across five different spreading centers (FSC, RR, FRSC, NWLSC, NELSC), the individual spreading rates were much slower (8–110 mm/yr; Pelletier et al., 1998; Zellmer and Taylor, 2001; Bird, 2003; Lupton et al., 2012; Sleeper and Martinez, 2016). Large areas of relict backarc crust older than 1.5 Ma (North Futuna, South Futuna, Qelelevu, and Zephyr assemblages) cover 72,208 km² and account for almost 15% of the total backarc crust. They belong to an episode of protracted crustal growth in the early history of opening before the emergence of the presently active arc-backarc spreading centers.

The mapped areas of different assemblage types confirm that crustal accretion has occurred simultaneously at widely spaced zones of extension and at major centers of intraplate volcanism. More than 10% (66,154 km²) of the backarc comprises formations associated with intraplate volcanism, non-volcanic rifting, leaky transforms, and deformation zones. The large volcanic fields of the Niufo'ou and Southeast Futuna assemblages cover 11,769 km². This does not include >3200 individual volcanoes that have a total area of 29,877 km² (Table 3) and 60 other seamounts that cover an area of 23,334 km², equivalent to some of the largest mapped assemblages. Unassigned, relict backarc, and transitional arc-backarc crust cover 64,921–81,598 km², and a significant area consists of foundered blocks of old arc crust stranded in the backarc region (e.g., Sleeper and Martinez, 2016; Schmid et al., 2020). However, these crust types cannot be confidently related to specific episodes of basin opening. The undivided crust of the South Vitiaz assemblage alone covers 40,967 km², highlighting the need for additional surveys in these areas.

The rates of crustal growth can be quantified in terms of area-age relationships (e.g., Peucker-Ehrenbrink and Miller, 2002; Dürr et al., 2005; Wilkinson et al., 2009). Crustal growth during the evolution of the Lau Basin is tracked by

comparing the cumulative areas of the assemblages with their inferred ages. This approach is useful for identifying changes in far-field tectonic stresses that are commonly correlated with pulses of growth. An early stage of rapid crustal growth in the early Eocene produced the Lau Ridge, Tonga Ridge, Tonga Forearc, and North Lau Forearc assemblages (Fig. 8). After 12 Ma, at the end of subduction along the Vitiaz trench and in the earliest stages of opening to form the Lau Basin, a protracted episode of slow crustal growth produced the South Vitiaz, West Lau Basin, Zephyr, and Qelelevu assemblages (Fig. 9). At ca. 5 Ma, a rapid transition from rifting to spreading formed the East Lau Basin assemblage, followed by initiation of the Tofua arc at ca. 3 Ma. Spreading at the FSC and possibly the NCSC also occurred at this time to produce the large Futuna and Cikobia assemblages. The significant expansion of the basin between 5 Ma and 3 Ma correlated with the appearance of the Peggy Ridge as a major structure accommodating basin opening. During the last

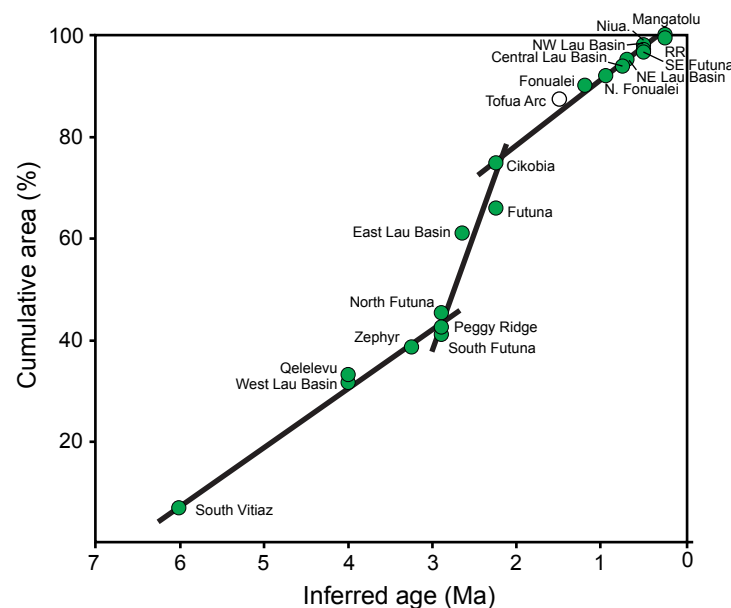


Figure 9. Model of crustal growth within the Lau backarc basin based on area-age relationships of the mapped assemblages. The area-age plot shows rates of crustal growth, which can be quantified by comparing the cumulative areas of the assemblages with their inferred ages. The plot shows a significant increase in the rate of crustal growth coinciding with the formation of the Peggy Ridge and the emergence of the large East Lau Basin, Futuna, and Cikobia assemblages during the initial opening of the Lau Basin. Current rates of crustal growth are lower, with accretion distributed across many active spreading centers. The Tofua Arc assemblage is shown for reference, but it is not part of the crustal growth of the backarc assemblages. Note: To improve diagram clarity, inferred ages are averages of the minimum and maximum age for each assemblage; actual ages are referenced in the text. MTJ—Mangatolu triple junction; Niua.—Niuafo’ou; RR—Rochambeau.

3 m.y., the rate of crustal growth has been $\sim 115,600 \text{ km}^2/\text{m.y.}$ (Fig. 9), with many small assemblages emerging as a result of the microplate breakout in the north (Figs. 10 and 11).

The predominance of a few large assemblages in the initial period of rapid crustal growth in the Lau Basin is consistent with the inferred long ridge lengths at that time (e.g., Taylor et al., 1996; Martinez and Taylor, 2006). The more abundant and smaller assemblages in the last few million years agrees well with the models of microplate formation as basin opening progressed (Conder and Wiens, 2011; Sleeper and Martinez, 2016). The Peggy Ridge marks the boundary between the two domains of relatively fast early crustal growth in the south and the more recent breakup and apparent slower growth in the north. The strong deformation in the north is partly decoupled from the more organized basin opening in the south by rotation of non-rigid domains of the crust (Wetzel et al., 1993; Baxter et al., 2020). This style of crustal accretion has been difficult to model based on magnetic inversions because of the lack of obvious reversals in the available data (e.g., Sleeper and Martinez, 2016). A number of studies suggest that changes in the rate and distribution of crustal growth have a direct link to mantle flow, such as the sudden release of enriched mantle material that resulted in the switch from mainly arc rifting to backarc spreading along the ELSC (Dunn and Martinez, 2011; Sleeper et al., 2016). Significant along- and across-strike changes in upper crustal seismic velocity and gravity imply discontinuities in the mantle supplying the melts (Dunn and Martinez, 2011; Schmid et al., 2020), and in the north, the complex organization of crustal assemblages may reflect a lack of a stable zone of upwelling.

DISCUSSION AND CONCLUSIONS

The Lau Basin is arguably one of the most important settings for understanding crustal growth in the oceans today (Martinez and Taylor, 2006). Early pictures of the crustal accretion focused on a simple two-stage model of arc rifting and seafloor spreading, first producing the West Lau Basin and then the East Lau Basin assemblages. However, it is clear that more complex growth soon emerged, with early rift segments taken over by multiple spreading centers and highly distributed extension in the north. Basin opening was diachronous and neither symmetric nor unidirectional. Major structures along which new crust was accreting jumped repeatedly both to the west (e.g., from the ELSC to the CLSC and LETZ) and to the east (e.g., toward the arc along the Valu Fa Ridge and FRSC). Identical units have formed in different assemblages at the same time (e.g., at multiple spreading centers simultaneously) and even at different times in the same location (e.g., rifting of preexisting backarc crust at the MTJ). The result is a mix of active and relict arc and backarc crust with extensive overprinting and inheritance, as indicated by low-velocity andesitic material dominating some backarc crustal blocks (Schmid et al., 2020). Rates of deformation associated with the different phases of opening of the basin have been deduced from studies of magnetic data (Sleeper and Martinez, 2016) and teleseismic data (Conder and Wiens, 2011; Baxter et al., 2020). In

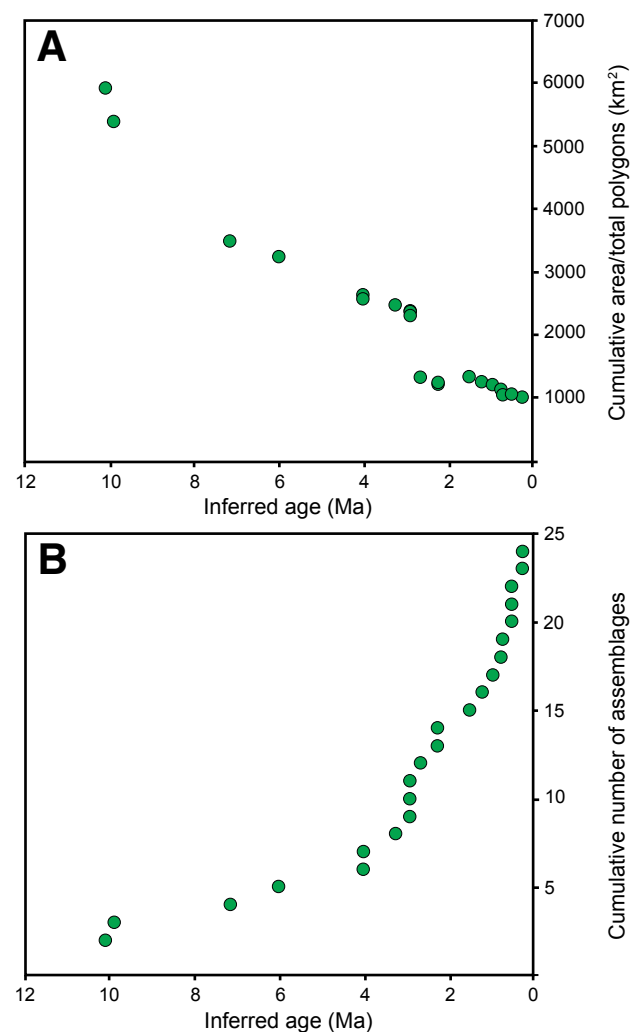


Figure 10. Plots showing the partitioning of crustal growth in the Lau Basin into smaller increments through time, measured in terms of the sizes and numbers of polygons in the geological map. **Note:** To improve diagram clarity, inferred ages are averages of the minimum and maximum for each assemblage; actual ages are referenced in the text. (A) Plot of cumulative area divided by the number of polygons in age increments corresponding to the mapped assemblages. (B) Plot of the cumulative number of assemblages. The sizes of the mapped polygons decrease from 12 Ma to present, corresponding to the increasing number of active spreading centers and deformation zones. A particularly rapid increase in the number of assemblages in the basin has occurred since ca. 4 Ma.

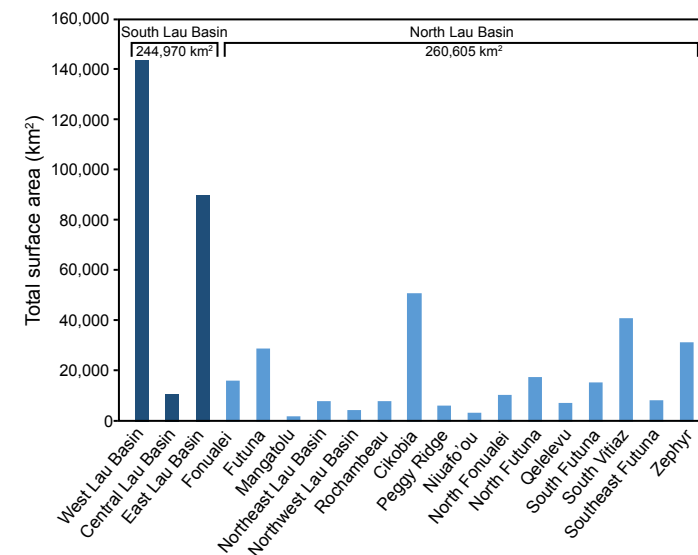


Figure 11. Histogram of assemblage sizes in the Lau Basin, showing a small number of large assemblages in the south and a large number of small assemblages in the north.

the last 2–3 m.y., failed rifts, ridge jumps, and deformation zones linked to distributed extension have resulted in mainly slow rates of accretion at the individual spreading centers. The large number of spreading centers led to high rates of basin opening observed in the north, despite the slow spreading. The incremental opening has been accommodated in part by the Peggy Ridge, which separated the northern Lau Basin from the southern Lau Basin following acute rotation of the Fiji platform. Ruellan et al. (2003) previously suggested that subduction of the Louisville seamount chain (LSC) has temporarily locked backarc spreading in the south, where the arc experiences the most compression today, whereas farther north, the LSC has already passed, unlocking the backarc rift and allowing basin opening to accelerate. The LSC would have migrated past the Peggy Ridge at ca. 3.5 Ma, when maximum basin opening commenced in the north.

The formation-level geological map of the Lau Basin provides new insight into the nature of crustal growth in this iconic arc-backarc system. At 1:1,000,000 scale, the spatial and temporal resolution of the map is sufficient for performing quantitative analysis of the area-age relationships and identifying lithostratigraphic correlations that track where, when, and how the backarc crust was created. The makeup of the crust (38% relict arc, 9% forearc, 7% active arc, 20% active backarc rift and spreading centers, 13% transitional arc-backarc, and 8% relict backarc; Table 7) differs markedly from that of other intraoceanic subduction systems such as the Mariana backarc and the North Fiji Basin, which are dominated by crust of relatively uniform

structure and composition originating at long-lived spreading centers. The mapped assemblages of the Lau Basin are a product of microplate tectonics, as originally defined in this area by Conder and Wiens (2011) and Sleeper and Martinez (2016). Early workers initially identified four microplates, but Baxter et al. (2020) suggested there may be as many as six microplates actively developing in the northern part of the basin alone (Fig. 1).

Microplates are structural rather than lithostratigraphic domains, and so they typically contain elements of several different assemblages. For example, the Futuna microplate (Fig. 1), bounded by the FSC in the west and the NWLSC in the east, contains parts of four different assemblages: the eastern half of the Futuna assemblage, all of the South Futuna assemblage, and portions of both the Southeast Futuna and Northwest Lau Basin assemblages. Where new microplates are forming, such as in the area between the CLSC and the northern termination of the ELSC (identified by Conder and Wiens [2011] as an emerging “nanoplate”), crust from both the Central Lau Basin assemblage and the East Lau Basin assemblage is being transferred to the new microplate. Thus, the proliferation of microplates in the north of the Lau Basin is the main control on the large number of assemblages in the map area (Figs. 10 and 11). Several seismic studies of the backarc crust in the Lau Basin have identified unexpected high-velocity zones (7.3–7.6 km/s; Dunn and Martinez, 2011; Arai and Dunn, 2014; Schmid et al., 2020), which are interpreted to indicate magmatic underplating (Handy and Streit, 1999; Mjelde et al., 2002). This has been observed in other backarc regions, including the Izu-Bonin-Mariana arc-backarc system in the western Pacific Ocean (Takahashi et al., 2008) and the Yamato Basin in the southern Japan Sea (Sato et al., 2014), and several authors have suggested it is a consequence of elevated upper-mantle temperatures (Fujiwara et al., 2001; Ruellan et al., 2003). Thus, the complex pattern of crustal growth and microplate formation may reflect structurally controlled mantle domains that in turn influence the distribution of magmatic and hydrothermal activity.

The rate of crustal accretion across the basin is on the order of 0.3 km³/yr, or nearly 2% of the amount of new oceanic crust formed globally at the mid-ocean ridges (~18 km³/yr; Cogné and Humler, 2006; Deligne and Sigurdsson, 2015). The cumulative length of active spreading centers in the basin (~1500 km) exceeds the entire length of the adjacent Tofua arc by nearly 500 km, and the length of new and emerging microplate boundaries, combining results of Conder and Wiens (2011) and Baxter et al. (2020), is now >860 km longer than in the original plate model of Bird (2003). The large number of crustal-scale faults associated with emerging microplate boundaries contributes to significant crustal permeability and provides extensive pathways for melt and fluid flow from the mantle to the seafloor. We believe this explains the high density of hydrothermal sites, which is notably greater than at mid-ocean ridges (German et al., 2006; Kim et al., 2009; Baker et al., 2019), and the regional ³He/⁴He anomaly (in the volcanic rocks and in the water column) that encompasses the entire northwest of the Lau Basin, including the Rochambeau, Northwest Lau Basin, Southeast Futuna, Niuafo’ou, and Peggy Ridge assemblages and rivals the helium plume of the East Pacific Rise (Lupton et al., 2012, 2015). Large new hydrothermal fields have now been discovered at plume-related backarc

volcanoes in the South Futuna assemblage at Kulo Lasi (Fouquet et al., 2015; Konn et al., 2018), providing further support for this model.

In addition to the proof of concept that geological mapping of the seafloor can be done at 1:1,000,000 scale using RPM techniques, the new geological map of the Lau Basin shows the benefits of regional seafloor mapping for understanding crustal growth and composition at a scale that is appropriate for tectonic interpretations, emphasizing the lack of such maps in the published record. Although it is hard to assess limitations in terms of identifying formation types from the remote-sensing data, with the different data sets now available for the Lau Basin, we believe that the uncertainties are not large enough to challenge the geological model. Geological maps at this scale are of fundamental importance for quantitative assessment of crustal makeup and evolution and can be analyzed directly in terms of area-age relationships. The 1:1,000,000-scale map of the Lau Basin provides a further useful reference and legend for future geologic studies in the region.

ACKNOWLEDGMENTS

This project was funded through the Canada First Research Excellence Fund (CFREF, Metal Earth) and the Marine Mineral Resources Group at the GEOMAR Helmholtz Centre for Ocean Research Kiel (Germany). The Helmholtz Association, the Natural Sciences and Engineering Research Council of Canada (NSERC), CFREF, and the German Federal Ministry of Education and Research (project number 03G0267) are acknowledged for support of this work through research grants and project funding to the authors. We particularly thank W.W. Chadwick and an anonymous referee for insightful comments that improved the manuscript. This is Metal Earth contribution MERC-ME-2020-103.

REFERENCES CITED

- Anderson, M.O., Hannington, M.D., Haase, K., Schwarz-Schampera, U., Augustin, N., McConachy, T.F., and Allen, K., 2016, Tectonic focusing of voluminous basaltic eruptions in magma-deficient backarc rifts: Earth and Planetary Science Letters, v. 440, p. 43–55, <https://doi.org/10.1016/j.epsl.2016.02.002>.
- Anderson, M.O., Chadwick, W.W., Jr., Hannington, M.D., Merle, S.G., Resing, J.A., Baker, E.T., Butterfield, D.A., Walker, S.L., and Augustin, N., 2017, Geological interpretation of volcanism and segmentation of the Mariana back-arc spreading center between 12.7°N and 18.3°N: Geochemistry Geophysics Geosystems, v. 18, p. 2240–2274, <https://doi.org/10.1002/2017GC006813>.
- Arai, R., and Dunn, R.A., 2014, Seismological study of Lau back arc crust: Mantle water, magmatic differentiation, and a compositionally zoned basin: Earth and Planetary Science Letters, v. 390, p. 304–317, <https://doi.org/10.1016/j.epsl.2014.01.014>.
- Arculus, R.J., 2003, Voyage summary SS02/2003: Submarine hydrothermal plume activity and petrology of the Eastern Lau Spreading Centre and neighbouring Tofua Arc, Tonga: Hobart, Tasmania, Australia, Marine National Facility, 19 p.
- Arculus, R.J., 2004, Voyage summary SS11/2004: NoToVE-2004 (Northern Tonga Vents Expedition)—Submarine hydrothermal plume activity and petrology of the northern Tofua Arc, Tonga: Hobart, Tasmania, Australia, Marine National Facility, 18 p.
- Arculus, R.J., 2008, Voyage summary SS07/2008: Northern Lau Vents Expedition (NoLauVE): Hobart, Tasmania, Australia, Marine National Facility, 23 p.
- Arculus, R.J., 2009, Voyage summary SS02/2009: Hydrothermal plume and structural geology mapping in the Tonga/Fiji region: Hobart, Tasmania, Australia, Marine National Facility, 39 p.
- Arculus, R.J., 2012, Voyage summary SS2012/V02: Northern Lau Transit Expedition (NoLauTE): Hobart, Tasmania, Australia, Marine National Facility, 26 p.
- Baker, E.T., Resing, J.A., Walker, S.L., Martinez, F., Taylor, B., and Nakamura, K.-i., 2006, Abundant hydrothermal venting along melt-rich and melt-free ridge segments in the Lau back-arc basin: Geophysical Research Letters, v. 33, L07308, <https://doi.org/10.1029/2005GL025283>.

- Baker, E.T., Lupton, J.E., Resing, J.A., Baumberger, T., Lilley, M.D., Walker, S.L., and Rubin, K.H., 2011, Unique event plumes from a 2008 eruption on the Northeast Lau Spreading Center: *Geochemistry Geophysics Geosystems*, v. 12, Q0AF02, <https://doi.org/10.1029/2011GC003725>.
- Baker, E.T., Walker, S.L., Massoth, G.J., and Resing, J.A., 2019, The NE Lau Basin: Widespread and abundant hydrothermal venting in the back-arc region behind a superfast subduction zone: *Frontiers in Marine Science*, v. 6, 382, <https://doi.org/10.3389/fmars.2019.00382>.
- Barkhausen, U., Heyde, I., Kopp, H., and Hannington, M.D., 2019, Seafloor spreading and crustal extension of the Central and Northern Lau Basin: Some insights from new magnetic data: Abstract T33F-0424 presented at 2019 Fall Meeting, American Geophysical Union, San Francisco, California, 9–13 December.
- Baxter, A.T., Hannington, M.D., Stewart, M.S., Emberley, J.M., Breker, K., Krättschell, A., Petersen, S., Brandl, P.A., Klischies, M., Mensing, R., and Anderson, M.O., 2020, Shallow seismicity and the classification of structures in the Lau back-arc basin: *Geochemistry Geophysics Geosystems*, v. 21, e2020GC008924, <https://doi.org/10.1029/2020GC008924>.
- Becker, J.J., Sandwell, D.T., Smith, W.H.F., Braud, J., Binder, B., Depner, J., Fabre, D., Factor, J., Ingalls, S., Kim, S.-H., Ladner, R., Marks, K., Nelson, S., Pharaoh, A., Trimmer, R., Von Rosenberg, J., Wallace, G., and Weatherall, P., 2009, Global bathymetry and elevation data at 30 arc seconds resolution: SRTM30_PLUS: *Marine Geodesy*, v. 32, p. 355–371, <https://doi.org/10.1080/01490410903297766>.
- Beier, C., Turner, S.P., Haase, K.M., Pearce, J.A., Münker, C., and Regelous, M., 2017, Trace element and isotopic geochemistry of the northern and central Tongan islands with an emphasis on the genesis of high Nb/Ta signatures at the northern volcanoes of Tafahi and Niuatoputapu: *Journal of Petrology*, v. 58, p. 1073–1106, <https://doi.org/10.1093/petrology/egx047>.
- Bevis, M., Taylor, F.W., Schutz, B.E., Recy, J., Isacks, B.L., Helu, S., Singh, R., Kendrick, E., Stowell, J., Taylor, B., and Calmant, S., 1995, Geodetic observations of very rapid convergence and back-arc extension at the Tonga arc: *Nature*, v. 374, p. 249–251, <https://doi.org/10.1038/374249a0>.
- Bird, P., 2003, An updated digital model of plate boundaries: *Geochemistry Geophysics Geosystems*, v. 4, 1027, <https://doi.org/10.1029/2001GC000252>.
- Bonnardot, M.-A., Régnier, M., Ruellan, E., Christova, C., and Tric, E., 2007, Seismicity and state of stress within the overriding plate of the Tonga-Kermadec subduction zone: *Tectonics*, v. 26, TC5017, <https://doi.org/10.1029/2006TC002044>.
- Bouysse, P., 2014, *Geological Map of the World* (third edition, revised): Paris, France, Commission for the Geological Map of the World, 2 sheets, scale 1:35,000,000, <https://doi.org/10.14682/2014CGM3R>.
- Brandl, P.A., Schmid, F., Augustin, N., Grevenmeyer, I., Arculus, R.J., Devey, C.W., Petersen, S., Stewart, M., Kopp, H., and Hannington, M.D., 2020a, The 6–8 Aug 2019 eruption of ‘Volcano F’ in the Tofua Arc, Tonga: *Journal of Volcanology and Geothermal Research*, v. 390, 106695, <https://doi.org/10.1016/j.jvolgeores.2019.106695>.
- Brandl, P.A., Hannington, M.D., Geersen, J., Petersen, S., and Gennerich, H.-H., 2020b, The submarine tectono-magmatic framework of Cu-Au endowment in the Tabar-to-Feni island chain, PNG: *Ore Geology Reviews*, v. 121, 103491, <https://doi.org/10.1016/j.oregeorev.2020.103491>.
- Buchs, D.M., Hoernle, K., and Grevenmeyer, I., 2016, Seamounts, *in* Harff, J., Meschede, M., Petersen, S., and Thiede, J., eds., *Encyclopedia of Marine Geosciences*: Dordrecht, Netherlands, Springer, p. 754–760, https://doi.org/10.1007/978-94-007-6238-1_34.
- Burns, R.E., Andrews, J.E., van der Lingen, G.J., Churkin, M., Jr., Galehouse, J.S., Packham, G.H., Davies, T.A., Kennett, J.P., Dumitrica, P., Edwards, A.R., and Von Herzen, R.P., 1973, Initial Reports of the Deep Sea Drilling Project, Volume 21: Washington, D.C., United States Government Printing Office, 931 p., <https://doi.org/10.2973/dsdp.proc.21.1973>.
- Chadwick, W.W., Jr., Rubin, K.H., Merle, S.G., Bobbitt, A.M., Kwasnitschka, T., and Embley, R.W., 2019, Recent eruptions between 2012 and 2018 discovered at West Mata submarine volcano (NE Lau Basin, SW Pacific) and characterized by new ship, AUV, and ROV data: *Frontiers in Marine Science*, v. 6, 495, <https://doi.org/10.3389/fmars.2019.00495>.
- Chase, C.G., 1971, Tectonic history of the Fiji Plateau: *Geological Society of America Bulletin*, v. 82, p. 3087–3110, [https://doi.org/10.1130/0016-7606\(1971\)82\[3087:THOTFP\]2.0.CO;2](https://doi.org/10.1130/0016-7606(1971)82[3087:THOTFP]2.0.CO;2).
- Clague, C.A., Dreyer, B.M., Paduan, J.B., Martin, J.F., Chadwick, W.W., Caress, D.W., Portner, R.A., Guilderson, T.P., McGann, M.L., Thomas, H., Butterfield, D.A., and Embley, R.W., 2013, Geologic history of the summit of Axial Seamount, Juan de Fuca Ridge: *Geochemistry Geophysics Geosystems*, v. 14, p. 4403–4443, <https://doi.org/10.1002/ggge.20240>.
- Clarke, J.E.H., Jarvis, P., Tiffin, D., Price, R., and Kroenke, L., 1993, Tectonic activity and plate boundaries along the northern flank of the Fiji Platform: *Geo-Marine Letters*, v. 13, p. 98–106, <https://doi.org/10.1007/BF01204551>.
- Clift, P.D., and Dixon, J.E., 1994, Variations in arc volcanism and sedimentation related to rifting of the Lau Basin (southwest Pacific), *in* Hawkins, J.W., Parson, L.M., Allan, J.F., et al., *Proceedings of the Ocean Drilling Program, Scientific Results, Volume 135*: College Station, Texas, Ocean Drilling Program, p. 23–49, <https://doi.org/10.2973/odp.proc.sr.135.102.1994>.
- Clift, P.D., MacLeod, C.J., Tappin, D.R., Wright, D.J., and Bloomer, S.H., 1998, Tectonic controls on sedimentation and diagenesis in the Tonga Trench and forearc, southwest Pacific: *Geological Society of America Bulletin*, v. 110, p. 483–496, [https://doi.org/10.1130/0016-7606\(1998\)110<0483:TCOSAD>2.3.CO;2](https://doi.org/10.1130/0016-7606(1998)110<0483:TCOSAD>2.3.CO;2).
- Cogné, J.-P., and Humler, E., 2006, Trends and rhythms in global seafloor generation rate: *Geochemistry Geophysics Geosystems*, v. 7, Q03011, <https://doi.org/10.1029/2005GC001148>.
- Cole, J.W., Graham, I.J., and Gibson, I.L., 1990, Magmatic evolution of Late Cenozoic volcanic rocks of the Lau Ridge, Fiji: Contributions to Mineralogy and Petrology, v. 104, p. 540–554, <https://doi.org/10.1007/BF00306663>.
- Collier, J.S., and Sinha, M.C., 1992, Seismic mapping of a magma chamber beneath the Valu Fa Ridge, Lau Basin: *Journal of Geophysical Research*, v. 97, p. 14,031–14,053, <https://doi.org/10.1029/91JB02751>.
- Collot, J., Vendé-Leclerc, M., Rouillard, P., Lafoy, Y., and Géli, L., compilers, 2011, Structural provinces of the Southwest Pacific (first edition): Noumea, New Caledonia, Geological Survey of New Caledonia, Direction de l’Industrie, des Mines et de l’Energie de Nouvelle Calédonie (DIMENC), L’Institut Français de Recherche pour l’Exploitation de la Mer (IFREMER).
- Conder, J.A., and Wiens, D.A., 2011, Shallow seismicity and tectonics of the central and northern Lau Basin: *Earth and Planetary Science Letters*, v. 304, p. 538–546, <https://doi.org/10.1016/j.epsl.2011.02.032>.
- Contreras-Reyes, E., Grevenmeyer, I., Watts, A.B., Flüß, E.R., Peirce, C., Moeller, S., and Papenberg, C., 2011, Deep seismic structure of the Tonga subduction zone: Implications for mantle hydration, tectonic erosion, and arc magmatism: *Journal of Geophysical Research*, v. 116, B10103, <https://doi.org/10.1029/2011JB008434>.
- Crawford, W.C., Hildebrand, J.A., Dorman, L.M., Webb, S.C., and Wiens, D.A., 2003, Tonga Ridge and Lau Basin crustal structure from seismic refraction data: *Journal of Geophysical Research*, v. 108, 2195, <https://doi.org/10.1029/2001JB001435>.
- Cunningham, J.K., and Anscombe, K.J., 1985, Geology of ‘Eua and other islands, Kingdom of Tonga, *in* Scholl, D.W., and Vallier, T.L., eds., *Geology and Offshore Resources of Pacific Island Arcs—Tonga Region*: Circum-Pacific Council for Energy and Mineral Resources Earth Science Series 2, p. 221–257.
- Deligne, N.I., and Sigurdsson, H., 2015, Global rate of volcanism and volcanic episodes, *in* Sigurdsson, H., Houghton, B., McNutt, S.R., Rymer, H., and Stix, J., eds., *Encyclopedia of Volcanoes* (second edition): San Diego, Academic Press, p. 265–272, <https://doi.org/10.1016/B978-0-12-385938-9.00014-6>.
- Duncan, R.A., 1985, Radiometric ages from volcanic rocks along the New Hebrides–Samoa Lineament, *in* Brocher, T.M., ed., *Geological Investigations of the Northern Melanesian Borderland*: Circum-Pacific Council for Energy and Mineral Resources Earth Science Series 3, p. 67–76.
- Duncan, R.A., Vallier, T.L., and Falvey, D.A., 1985, Volcanic episodes at ‘Eua, Tonga Islands, *in* Scholl, D.W., and Vallier, T.L., eds., *Geology and Offshore Resources of Pacific Island Arcs—Tonga Region*: Circum-Pacific Council for Energy and Mineral Resources Earth Science Series 2, p. 281–290.
- Dunn, R.A., and Martinez, F., 2011, Contrasting crustal production and rapid mantle transitions beneath back-arc ridges: *Nature*, v. 469, p. 198–202, <https://doi.org/10.1038/nature09690>.
- Dunn, R.A., Martinez, F., and Conder, J., 2013, Crustal construction and magma chamber properties along the Eastern Lau Spreading Center: *Earth and Planetary Science Letters*, v. 371–372, p. 112–124, <https://doi.org/10.1016/j.epsl.2013.04.008>.
- Dürr, H.H., Meybeck, M., and Dürr, S.H., 2005, Lithologic composition of the Earth’s continental surfaces derived from a new digital map emphasizing riverine material transfer: *Global Biogeochemical Cycles*, v. 19, GB4S10, <https://doi.org/10.1029/2005GB002515>.
- Dutkiewicz, A., Müller, R.D., O’Callaghan, S., and Jónasson, H., 2015, Census of seafloor sediments in the world’s ocean: *Geology*, v. 43, p. 795–798, <https://doi.org/10.1130/G36883.1>.
- Eason, D.E., and Dunn, R.A., 2015, Petrogenesis and structure of oceanic crust in the Lau back-arc basin: *Earth and Planetary Science Letters*, v. 429, p. 128–138, <https://doi.org/10.1016/j.epsl.2015.07.065>.
- Eguchi, T., 1984, Seismotectonics of the Fiji Plateau and Lau Basin: *Tectonophysics*, v. 102, p. 17–32, [https://doi.org/10.1016/0040-1951\(84\)90006-4](https://doi.org/10.1016/0040-1951(84)90006-4).
- Embley, R.W., and Rubin, K.H., 2018, Extensive young silicic volcanism produces large deep submarine lava flows in the NE Lau Basin: *Bulletin of Volcanology*, v. 80, 36, <https://doi.org/10.1007/s00445-018-1211-7>.
- Embley, R.W., Baker, E.T., Butterfield, D.A., Chadwick, W.W., Jr., Lupton, J.E., Resing, J.A., de Ronde, C.E.J., Nakamura, K.-i., Tunncliffe, V., Dower, J.F., and Merle, S.G., 2007, Exploring

- the submarine Ring of Fire: Mariana Arc—Western Pacific: *Oceanography* (Washington, D.C.), v. 20, p. 68–79, <https://doi.org/10.5670/oceanog.2007.07>.
- Embley, R.W., Merle, S.G., Baker, E.T., Rubin, K.H., Lupton, J.E., Resing, J.A., Dziak, R.P., Lilley, M.D., Chadwick, W.W., Jr., Shank, T., Greene, R., Walker, S.L., Haxel, J., Olson, E., and Baumberger, T., 2014, Eruptive modes and hiatus of volcanism at West Mata seamount, NE Lau basin: 1996–2012: *Geochemistry Geophysics Geosystems*, v. 15, p. 4093–4115, <https://doi.org/10.1002/2014GC005387>.
- Escrig, S., Bézou, A., Langmuir, C.H., Michael, P.J., and Arculus, R., 2012, Characterizing the effect of mantle source, subduction input and melting in the Fonualei Spreading Center, Lau Basin: Constraints on the origin of the boninitic signature of the back-arc lavas: *Geochemistry Geophysics Geosystems*, v. 13, Q10008, <https://doi.org/10.1029/2012GC004130>.
- Falloon, T.J., Danyushevsky, L.V., Crawford, T.J., Maas, R., Woodhead, J.D., Eggins, S.M., Bloomer, S.H., Wright, D.J., Zlobin, S.K., and Stacey, A.R., 2007, Multiple mantle plume components involved in the petrogenesis of subduction-related lavas from the northern termination of the Tonga Arc and northern Lau Basin: Evidence from the geochemistry of arc and backarc submarine volcanics: *Geochemistry Geophysics Geosystems*, v. 8, Q09003, <https://doi.org/10.1029/2007GC001619>.
- Finlayson, V.A., Konter, J.G., Konrad, K., Koppers, A.A.P., Jackson, M.G., and Rooney, T.O., 2018, Sr-Pb-Nd-Hf isotopes and $^{40}\text{Ar}/^{39}\text{Ar}$ ages reveal a Hawaii-Emperor-style bend in the Rurutu hotspot: *Earth and Planetary Science Letters*, v. 500, p. 168–179, <https://doi.org/10.1016/j.epsl.2018.08.020>.
- Fouquet, Y., Alix, A.-S., Birot, D., Chéron, S., Charlou, J.-L., Donval, J.-P., Etoubeau, J., Germain, Y., Guillou, M., Guerin, C., Guyader, V., Konn, C., Labanieh, S., Pelleter, E., Pierre, D., Dupré, S., Scalabrini, C., Cambon, M.A., Menot, L., Pradillon, F., Chazot, G., Dymont, J., Szitkar, F., and Gouin, J., 2015, Discovery of extensive hydrothermal fields in the Wallis and Futuna back-arc environment (SW Pacific), in André-Mayer, A.-S., Cathelineau, M., Muchez, P., Pirard, E., and Sindern, S., eds., *Mineral Resources in a Sustainable World: Proceedings of the 13th Biennial SGA Meeting, 24–27 August 2015, Nancy, France: Geneva, Society for Geology Applied to Mineral Deposits*, v. 3, p. 1223–1226.
- Fujiwara, T., Yamazaki, T., and Joshima, M., 2001, Bathymetry and magnetic anomalies in the Havre Trough and southern Lau Basin: From rifting to spreading in back-arc basins: *Earth and Planetary Science Letters*, v. 185, p. 253–264, [https://doi.org/10.1016/S0012-821X\(00\)00378-2](https://doi.org/10.1016/S0012-821X(00)00378-2).
- GEBCO Bathymetric Compilation Group, 2019, The GEBCO 2019 grid—A continuous terrain model of the global oceans and land: Liverpool, UK, British Oceanographic Data Centre, National Oceanography Centre, NERC, <https://doi.org/10.5285/836f016a-33be-6ddc-e053-6c86abc0788e>.
- German, C.R., Baker, E.T., Connelly, D.P., Lupton, J.E., Resing, J., Prien, R.D., Walker, S.L., Edmonds, H.N., and Langmuir, C.H., 2006, Hydrothermal exploration of the Fonualei Rift and Spreading Center and the Northeast Lau Spreading Center: *Geochemistry Geophysics Geosystems*, v. 7, Q11022, <https://doi.org/10.1029/2006GC001324>.
- Global Volcanism Program, 1985, Report on Niuafu'ou (Tonga): Scientific Event Alert Network Bulletin (National Museum of Natural History, Smithsonian Institution), v. 10, no. 9, <https://doi.org/10.5479/si.GVP.SEAN198509-243110>.
- Global Volcanism Program, 2013, Venzke, E., ed., *Volcanoes of the World*, Smithsonian Institution, v. 4.8.2, <https://doi.org/10.5479/si.GVP.VOTW4-2013>.
- Govers, R., and Wortel, M.J.R., 2005, Lithosphere tearing at STEP faults: Response to edges of subduction zones: *Earth and Planetary Science Letters*, v. 236, p. 505–523, <https://doi.org/10.1016/j.epsl.2005.03.022>.
- Grevemeyer, I., and Flüß, E.R., 2008, FS *Sonne* Fahrtbericht / cruise report SO195TOTAL: Tonga Thrust earthquake Asperity at Louisville Ridge, Suva/Fiji—Suva/Fiji, 07.01–16.02.2008: Kiel, Germany, Leibniz-Institut für Meereswissenschaften, IFM-GEOMAR, 106 p., https://doi.org/10.3289/ifm-geomar_rep_14_2008.
- Haase, K.M., Beier, C., Bach, W., Kleint, C., Anderson, M., Büttner, H., Dede, B., Diehl, A., Ernst, D., Fungani, C., Giguere, T., Gonzales Porras, M.A., Günther, T., Hüttich, D., Krumm, D.H., Leymann, T., Meierhoff, I., Moje, A., Monien, P., Murdock, S., Nowald, N., Peters, C., Planer-Friedrich, B., Ratmeyer, V., Reuter, C., Reuter, M., Rubin, K., Schade, T., Schleifer, B.K., Schönhofen, M., Sopke, S., Storch, B., Ücker, M., Türke, A., and Wilckens, F., 2018, RV *Sonne* cruise report: Tonga Rift, cruise no. SO263, 01.06–2018–27.06.2018, Suva, Fiji—Suva, Fiji: Erlangen, Germany, GeoZentrum Nordbayern, Friedrich-Alexander Universität Erlangen-Nürnberg, 222 p.
- Hall, R., 2002, Cenozoic geological and plate tectonic evolution of SE Asia and the SW Pacific: Computer-based reconstructions, model and animations: *Journal of Asian Earth Sciences*, v. 20, p. 353–431, [https://doi.org/10.1016/S1367-9120\(01\)00069-4](https://doi.org/10.1016/S1367-9120(01)00069-4).
- Hamburger, M.W., and Isacks, B.L., 1988, Diffuse back-arc deformation in the southwestern Pacific: *Nature*, v. 332, p. 599–604, <https://doi.org/10.1038/332599a0>.
- Handy, H.R., and Streit, J.E., 1999, Mechanics and mechanisms of magmatic underplating: Inferences from mafic veins in deep crustal mylonite: *Earth and Planetary Science Letters*, v. 165, p. 271–286, [https://doi.org/10.1016/S0012-821X\(98\)00272-6](https://doi.org/10.1016/S0012-821X(98)00272-6).
- Hannington, M.D., Kopp, H., and Schnabel, M., 2019, RV *SONNE* Fahrtbericht / cruise report SO267: ARCHIMEDES I: Arc Rifting, Metallogeny and Microplate Evolution—An Integrated Geodynamic, Magmatic and Hydrothermal Study of the Fonualei Rift System, NE Lau Basin, Suva (Fiji)—Suva (Fiji), 11.12.2018–26.01.2019: Kiel, Germany, GEOMAR Helmholtz-Zentrum für Ozeanforschung, GEOMAR Report N. Ser. 049, 275 p., https://doi.org/10.3289/GEOMAR_REP_NS_49_2019.
- Harris, P.T., Macmillan-Lawler, M., Rupp, J., and Baker, E.K., 2014, Geomorphology of the oceans: *Marine Geology*, v. 352, p. 4–24, <https://doi.org/10.1016/j.margeo.2014.01.011>.
- Harrison, J.C., St-Onge, M.R., Petrov, O.V., Strelnikov, S.I., Lopatin, B.G., Wilson, F.H., Tella, S., Paul, D., Lynds, T., Shokalsky, S.P., Hufts, C.K., Bergman, S., Jepsen, H.F., and Solli, A., 2011, Geological map of the Arctic: Geological Survey of Canada “A” Series Map 2159A, 9 sheets, scale 1:5,000,000, 1 DVD, <https://doi.org/10.4095/287868>.
- Hathway, B., 1994, Sedimentation and volcanism in an Oligocene–Miocene intra-oceanic arc and fore-arc, southwestern Viti Levu, Fiji: *Journal of the Geological Society*, v. 151, p. 499–514, <https://doi.org/10.1144/gsjgs.151.3.0499>.
- Hawkins, J.W., 1976, Petrology and geochemistry of basaltic rocks of the Lau Basin: *Earth and Planetary Science Letters*, v. 28, p. 283–297, [https://doi.org/10.1016/0012-821X\(76\)90190-4](https://doi.org/10.1016/0012-821X(76)90190-4).
- Hawkins, J.W., 1995, Evolution of the Lau Basin—Insights from ODP Leg 135, in Taylor, B., and Natland, J., eds., *Active Margins and Marginal Basins of the Western Pacific: American Geophysical Union Geophysical Monograph* 88, p. 125–173, <https://doi.org/10.1029/GM088p0125>.
- Hawkins, J.W., and Allan, J.F., 1994, Petrologic evolution of Lau Basin Sites 834 through 839, in Hawkins, J.W., Parson, L.M., Allan, J.F., et al., *Proceedings of the Ocean Drilling Program, Scientific Results, Volume 135: College Station, Texas, Ocean Drilling Program*, p. 427–470, <https://doi.org/10.2973/odp.proc.sr.135.136.1994>.
- Hill, P.J., and Tiffin, D.L., 1993, Geology, sediment patterns, and widespread deformation on the sea floor off Western Samoa revealed by wide-swath imagery: *Geo-Marine Letters*, v. 13, p. 116–125, <https://doi.org/10.1007/BF01204553>.
- Inokuchi, H., Yaskawa, K., and Rodda, P., 1992, Clockwise and anticlockwise rotation of Viti Levu, Fiji—In relation to the tectonic development of the North and South Fiji Basin: *Geophysical Journal International*, v. 110, p. 225–237, <https://doi.org/10.1111/j.1365-246X.1992.tb00869.x>.
- International Hydrographic Organization, 2013, Standardization of Undersea Feature Names: Guidelines, Proposal Form, Terminology (edition 4.1.0): Monaco, International Hydrographic Organization and Intergovernmental Oceanographic Commission Bathymetric Publication B-6, 40 p.
- Isacks, B.L., Sykes, L.R., and Oliver, J., 1969, Focal mechanisms of deep and shallow earthquakes in the Tonga-Kermadec region and the tectonics of island arcs: *Geological Society of America Bulletin*, v. 80, p. 1443–1470, [https://doi.org/10.1130/0016-7606\(1969\)80\[1443:FMODAS\]2.0.CO;2](https://doi.org/10.1130/0016-7606(1969)80[1443:FMODAS]2.0.CO;2).
- Jacobs, A.M., Harding, A.J., and Kent, G.M., 2007, Axial crustal structure of the Lau back-arc basin from velocity modeling of multichannel seismic data: *Earth and Planetary Science Letters*, v. 259, p. 239–255, <https://doi.org/10.1016/j.epsl.2007.04.021>.
- Jutzeler, M., Marsh, R., van Sebille, E., Mittal, T., Carey, R.J., Fauria, K.E., Manga, M., and McPhie, J., 2020, Ongoing dispersal of the 7 August 2019 pumice raft from the Tonga Arc in the southwestern Pacific Ocean: *Geophysical Research Letters*, v. 47, e1701121, <https://doi.org/10.1029/2019GL086768>.
- Karig, D.E., 1970, Ridges and basins of the Tonga-Kermadec Island Arc System: *Journal of Geophysical Research*, v. 75, p. 239–254, <https://doi.org/10.1029/JB075i002p00239>.
- Keller, N.S., Arculus, R.J., Hermann, J., and Richards, S., 2008, Submarine back-arc lava with arc signature: Fonualei Spreading Center, northeast Lau Basin, Tonga: *Journal of Geophysical Research*, v. 113, B08S07, <https://doi.org/10.1029/2007JB005451>.
- Kim, J., Son, S.-K., Son, J.-W., Kim, K.-H., Shim, W.J., Kim, C.H., and Lee, K.-Y., 2009, Venting sites along the Fonualei and Northeast Lau Spreading Centers and evidence of hydrothermal activity at an off-axis caldera in the northeastern Lau Basin: *Geochemical Journal*, v. 43, p. 1–13, <https://doi.org/10.2343/geochemj.0164>.
- Klischies, M., Petersen, S., and Devey, C.W., 2019, Geological mapping of the Menez Gwen segment at 37°50'N on the Mid-Atlantic Ridge: Implications for accretion mechanisms and associated hydrothermal activity at slow-spreading mid-ocean ridges: *Marine Geology*, v. 412, p. 107–122, <https://doi.org/10.1016/j.margeo.2019.03.012>.

- Konn, C., Fourré, E., Jean-Baptiste, P., Donval, J.P., Guyader, B., Birot, D., Alix, A.S., Gaillot, A., Perez, F., Dapigny, A., Pelleter, E., Resing, J.A., Charlou, J.L., and Fouquet, Y., 2016, Extensive hydrothermal activity revealed by multi-tracer survey in the Wallis and Futuna region (SW Pacific): Deep-Sea Research: Part I, Oceanographic Research Papers, v. 116, p. 127–144, <https://doi.org/10.1016/j.dsr.2016.07.012>.
- Konn, C., Donval, J.P., Guyader, V., Roussel, E., Fourré, Jean-Baptiste, P., Pelleter, E., Charlou, J.L., and Fouquet, Y., 2018, Organic, gas, and element geochemistry of hydrothermal fluids of the newly discovered extensive hydrothermal area in the Wallis and Futuna Region (SW Pacific): *Geofluids*, v. 2018, 7692839, <https://doi.org/10.1155/2018/7692839>.
- Kwasnitschka, T., and the Shipboard Scientific Party, 2016, Virtual Vents: The changing face of hydrothermalism revealed, R/V Falkor FK160320, March 20–April 1, 2016, Suva, Fiji to Suva, Fiji: Palo Alto, California, Schmidt Ocean Institute, 13 p., <https://doi.org/10.7284/906663>.
- Lecours, V.L., Dolan, M.F.J., Micallef, A., and Lucieer, V.L., 2016, A review of marine geomorphometry, the quantitative study of the seafloor: *Hydrology and Earth System Sciences*, v. 20, p. 3207–3244, <https://doi.org/10.5194/hess-20-3207-2016>.
- Lupton, J., Rubin, K.H., Arculus, R., Lilley, M., Butterfield, D., Resing, J., Baker, E., and Embley, R., 2015, Helium isotope, C³He, and Ba-Nb-Ti signatures in the northern Lau Basin: Distinguishing arc, back-arc, and hotspot affinities: *Geochemistry Geophysics Geosystems*, v. 16, p. 1133–1155, <https://doi.org/10.1002/2014GC005625>.
- Lupton, J.E., Arculus, R.J., Resing, J., Massoth, G.J., Greene, R.R., Evans, L.J., and Buck, N., 2012, Hydrothermal activity in the Northwest Lau Backarc Basin: Evidence from water column measurements: *Geochemistry Geophysics Geosystems*, v. 13, Q0AF04, <https://doi.org/10.1029/2011GC003891>.
- Macdonald, K.C., 2001, Mid-ocean ridge tectonics, volcanism and geomorphology, in Thorpe, S.A., and Turekian, K.K., eds., *Encyclopedia of Ocean Sciences*: Cambridge, Massachusetts, Academic Press, p. 1798–1813, <https://doi.org/10.1006/rwos.2001.0094>.
- MacLeod, S.J., Williams, S.E., Matthews, K.J., Müller, R.D., and Qin, X., 2017, A global review and digital database of large-scale extinct spreading centers: *Geosphere*, v. 13, p. 911–949, <https://doi.org/10.1130/GES01379.1>.
- Malahoff, A., Hammond, S.R., Naughton, J.J., Keeling, D.L., and Richmond, R.N., 1982, Geophysical evidence for post-Miocene rotation of the island of Viti Levu, Fiji, and its relationship to the tectonic development of the North Fiji Basin: *Earth and Planetary Science Letters*, v. 57, p. 398–414, [https://doi.org/10.1016/0012-821X\(82\)90159-5](https://doi.org/10.1016/0012-821X(82)90159-5).
- Martin, A.K., 2013, Double-saloon-door tectonics in the North Fiji Basin: *Earth and Planetary Science Letters*, v. 374, p. 191–203, <https://doi.org/10.1016/j.epsl.2013.05.041>.
- Martinez, F., and Taylor, B., 2002, Mantle wedge control on back-arc crustal accretion: *Nature*, v. 416, p. 417–420, <https://doi.org/10.1038/416417a>.
- Martinez, F., and Taylor, B., 2006, Modes of crustal accretion in back-arc basins: Inferences from the Lau Basin, in Christie, D.M., Fisher, C.R., Lee, S.-M., and Givens, S., eds., *Back-Arc Spreading Systems: Geological, Biological, Chemical, and Physical Interactions*: American Geophysical Union Geophysical Monograph 166, p. 5–30, <https://doi.org/10.1029/166GM03>.
- Martinez, F., Taylor, B., Baker, E.T., Resing, J.A., and Walker, S.L., 2006, Opposing trends in crustal thickness and spreading rate along the back-arc Eastern Lau Spreading Center: Implications for controls on ridge morphology, faulting, and hydrothermal activity: *Earth and Planetary Science Letters*, v. 245, p. 655–672, <https://doi.org/10.1016/j.epsl.2006.03.049>.
- Martinez, F., and the Shipboard Scientific Party, 2013, R/V Kilo Moana KM1129 [cruise data], available from Rolling Deck to Repository (R2R), <https://doi.org/10.7284/903698>.
- Maus, S., Barkhausen, U., Berkenbosch, H., Bournas, N., Brozena, J., Childers, V., Dostaler, F., Fairhead, J.D., Finn, C., von Frese, R.R.B., Gaina, C., Golymsky, S., Kucks, R., Lühr, H., Milligan, P., Mogren, S., Müller, R.D., Olesen, O., Pilkington, M., Saltus, R., Schreckenberger, B., Thébaud, E., and Carratori Tontini, F., 2009, EMAG2: A 2-arc min resolution Earth Magnetic Anomaly Grid compiled from satellite, airborne, and marine magnetic measurements: *Geochemistry Geophysics Geosystems*, v. 10, Q08005, <https://doi.org/10.1029/2009GC002471>.
- Mayer, L., Jakobsson, M., Allen, G., Dorschel, B., Falconer, R., Ferrini, V., Lamarche, G., Snaith, H., and Weatherall, P., 2018, The Nippon Foundation—GEBCO Seabed 2030 Project: The quest to see the world's oceans completely mapped by 2030: *Geosciences*, v. 8, 63, 18 p., <https://doi.org/10.3390/geosciences8020063>.
- McClinton, T., White, S.M., Coleman, A., and Sinton, J.M., 2013, Reconstructing lava flow emplacement processes at the hot spot-affected Galápagos Spreading Center, 95°W and 92°W: *Geochemistry Geophysics Geosystems*, v. 14, p. 2731–2756, <https://doi.org/10.1002/ggge.20157>.
- McDougall, I., 1994, Dating of rhyolitic glass in the Tonga forearc (Hole 841B), in Hawkins, J.W., Parson, L.M., Allan, J.F., et al., *Proceedings of the Ocean Drilling Program, Scientific Results*, Volume 135: College Station, Texas, Ocean Drilling Program, p. 923, <https://doi.org/10.2973/odp.proc.sr.135.140.1994>.
- Meffre, S., Falloon, T.J., Crawford, T.J., Hoernle, K., Hauff, F., Duncan, R.A., Bloomer, S.H., and Wright, D.J., 2012, Basalts erupted along the Tonga fore arc during subduction initiation: Evidence from geochronology of dredged rocks from the Tonga fore arc and trench: *Geochemistry Geophysics Geosystems*, v. 13, Q12003, <https://doi.org/10.1029/2012GC004335>.
- Mensing, R., 2019, The tectonic and volcanic evolution of the Mangatolu Triple Junction [M.S. thesis]: Halle, Germany, Martin Luther University Halle-Wittenberg, 78 p.
- Merle, S., and the Shipboard Scientific Party, 2009, Northeast Lau Basin Response Cruise (NELRC), R/V Thomas G. Thompson TN234, May 5–May 14, 2009, Apia, Samoa to Apia, Samoa: Washington, D.C., National Oceanic and Atmospheric Administration, 243 p., <https://doi.org/10.7284/903993>.
- Merle, S., and the Shipboard Scientific Party, 2010, NE Lau Basin rock dredging expedition, R/V *Kilo Moana* KM1024, Dec 9–Dec 15, 2010, Nuku'alofa Tonga to Pago Pago American Samoa: Washington, D.C., National Oceanic and Atmospheric Administration, 55 p., <https://doi.org/10.7284/900840>.
- Merle, S., Resing, J., and Embley, R., 2013, Submarine Ring of Fire 2012 (SRoF-12) Northeast Lau Basin: R/V *Roger Revelle* Expedition RR1211, Captain Wes Hill, Sept 9–25, 2012, Suva Fiji to Apia Samoa: Washington, D.C., National Oceanic and Atmospheric Administration, 260 p., <https://doi.org/10.7284/903953>.
- Michael, P.J., Escrig, S., Rubin, K.H., Cooper, L.B., Langmuir, C.H., Clague, D.A., Keller, N.S., and Plank, T., 2009, Major and trace elements and volatiles in glasses from the 2009 rapid response expedition to West Mata volcano and Northeast Lau Spreading Center (NELSC): Abstract V51D-1720 presented at 2009 Fall Meeting, American Geophysical Union, San Francisco, California, 14–18 December.
- Millen, D.W., and Hamburger, M.W., 1998, Seismological evidence for tearing of the Pacific plate at the northern termination of the Tonga subduction zone: *Geology*, v. 26, p. 659–662, [https://doi.org/10.1130/0091-7613\(1998\)026<0659:SEFTOT>2.3.CO;2](https://doi.org/10.1130/0091-7613(1998)026<0659:SEFTOT>2.3.CO;2).
- Mjelde, R., Kasahara, J., Shimamura, H., Kamimura, A., Kanazawa, T., Kodaira, S., Raum, T., and Shiobara, H., 2002, Lower crustal seismic velocity-anomalies: Magmatic underplating or serpentinized peridotite? Evidence from the Vøring Margin, NE Atlantic: *Marine Geophysical Researches*, v. 23, p. 169–183, <https://doi.org/10.1023/A:1022480304527>.
- Mortimer, N., Campbell, H.J., Tulloch, A.J., King, P.R., Stagpoole, V.M., Wood, R.A., Rattenbury, M.S., Sutherland, R., Adams, C.J., Collot, J., and Seton, M., 2017, Zealandia: Earth's hidden continent: *GSA Today*, v. 27, no. 3, p. 27–35, <https://doi.org/10.1130/GSATG321A.1>.
- Murphy, M.A., and Salvador, A., 1999, *International Stratigraphic Guide—An abridged edition: Episodes*, v. 22, p. 255–271, <https://doi.org/10.18814/epiiugs/1999/v22i4/002>.
- Norris-Julseth, C., Anderson, M.O., Rubin, K., Haase, K., Hannington, M., Baxter, A., and Stewart, M., 2020, The influence of wrench tectonics on submarine volcanism in the NE Lau Basin (Tonga): Abstract presented at Virtual 2020 Goldschmidt Conference, 21–26 June, <https://doi.org/10.46427/gold2020.1949>.
- Parson, L., Hawkins, J., and Allan, J., and Shipboard Scientific Party, 1992a, Introduction, background, and principal results of Leg 135, Lau Basin, in Parson, L., Hawkins, J., Allan, J., et al., *Proceedings of the Oceanic Drilling Program, Initial Reports, Volume 135*, College Station, Texas, Ocean Drilling Program, p. 5–47, <https://doi.org/10.2973/odp.proc.ir.135.101.1992>.
- Parson, L.M., and Hawkins, J.W., 1994, Two-stage propagation and the geological history of the Lau backarc basin, in Hawkins, J.W., Parson, L.M., Allan, J.F., et al., *Proceedings of the Ocean Drilling Program, Scientific Results, Volume 135*: College Station, Texas, Ocean Drilling Program, p. 819–828, <https://doi.org/10.2973/odp.proc.sr.135.153.1994>.
- Parson, L.M., and Tiffin, D.L., 1993, Northern Lau Basin: Backarc extension at the leading edge of the Indo-Australian Plate: *Geo-Marine Letters*, v. 13, p. 107–115, <https://doi.org/10.1007/BF01204552>.
- Parson, L.M., and Wright, I.C., 1996, The Lau-Havre-Taupo back-arc basin: A southward-propagating, multi-stage evolution from rifting to spreading: *Tectonophysics*, v. 263, p. 1–22, [https://doi.org/10.1016/S0040-1951\(96\)00029-7](https://doi.org/10.1016/S0040-1951(96)00029-7).
- Parson, L.M., Pearce, J.A., Murton, B.J., Hodgkinson, R.A., Bloomer, S., Ernwein, M., Huggett, Q.J., Miller, S., Johnson, L., Rodda, P., and Helu, S., 1990, Role of ridge jumps and ridge propagation in the tectonic evolution of the Lau back-arc basin, southwest Pacific: *Geology*, v. 18, p. 470–473, [https://doi.org/10.1130/0091-7613\(1990\)018<0470:ROBJAR>2.3.CO;2](https://doi.org/10.1130/0091-7613(1990)018<0470:ROBJAR>2.3.CO;2).
- Parson, L.M., Hawkins, J.W., and Hunter, P.M., 1992b, Morphotectonics of the Lau Basin seafloor—Implications for the opening history of backarc basins, in Parson, L., Hawkins, J., Allan, J., et al., *Proceedings of the Oceanic Drilling Program, Initial Reports, Volume 135*: College Station, Texas, Ocean Drilling Program, p. 81–82, <https://doi.org/10.2973/odp.proc.ir.135.103.1992>.

- Parson, L.M., Rothwell, R.G., and MacLeod, C.J., 1994, Tectonics and sedimentation in the Lau Basin (southwest Pacific), in Hawkins, J.W., Parson, L.M., Allan, J.F., et al., Proceedings of the Ocean Drilling Program, Scientific Results, Volume 135: College Station, Texas, Ocean Drilling Program, p. 9–21, <https://doi.org/10.2973/odp.proc.sr.135.111.1994>.
- Patriat, M., Falloon, T., Danyushevsky, L., Collot, J., Jean, M.M., Hoernle, K., Hauff, F., Maas, R., Woodhead, J.D., and Feig, S.T., 2019, Subduction initiation terranes exposed at the front of a 2 Ma volcanically-active subduction zone: Earth and Planetary Science Letters, v. 508, p. 30–40, <https://doi.org/10.1016/j.epsl.2018.12.011>.
- Pearce, J.A., Ernewein, M., Bloomer, S.H., Parson, L.M., Murton, B.J., and Johnson, L.E., 1995, Geochemistry of Lau Basin volcanic rocks: Influence of ridge segmentation and arc proximity, in Smellie, J.L., ed., Volcanism Associated with Extension at Consuming Plate Margins: Geological Society of London Special Publication 81, p. 53–75, <https://doi.org/10.1144/GSL.SP.1994.081.01.04>.
- Peirce, C., and Watts, A., et al., 2011, R/V *Sonne* SO215 cruise report—The Louisville Ridge–Tonga Trench collision: Implications for subduction zone dynamics: Durham, UK, Durham University, 76 p.
- Pelletier, B., and Auzende, J.-M., 1996, Geometry and structure of the Vitiaz Trench Lineament (SW Pacific): Marine Geophysical Researches, v. 18, p. 305–335, <https://doi.org/10.1007/BF00286083>.
- Pelletier, B., Calmant, S., and Pillet, R., 1998, Current tectonics of the Tonga–New Hebrides region: Earth and Planetary Science Letters, v. 164, p. 263–276, [https://doi.org/10.1016/S0012-821X\(98\)00212-X](https://doi.org/10.1016/S0012-821X(98)00212-X).
- Pelletier, B., Lagabriele, Y., Cabioch, G., Calmant, S., Régnier, M., and Perrier, J., 2000, Transpression active le long de la frontière décrochante Pacifique–Australie: Les apports de la cartographie multifaisceaux autour des îles Futuna et Alofi (Pacifique sud-ouest): Comptes Rendus de l'Académie des Sciences: Series IIA, Earth and Planetary Science, v. 331, p. 127–132, [https://doi.org/10.1016/S1251-8050\(00\)01383-5](https://doi.org/10.1016/S1251-8050(00)01383-5).
- Pelletier, B., Lagabriele, Y., Benoit, M., Cabioch, G., Calmant, S., Garel, E., and Guivel, C., 2001, Newly identified segments of the Pacific–Australia plate boundary along the North Fiji transform zone: Earth and Planetary Science Letters, v. 193, p. 347–358, [https://doi.org/10.1016/S0012-821X\(01\)00522-2](https://doi.org/10.1016/S0012-821X(01)00522-2).
- Petrov, O., Morozov, A., Shokalsky, S., Kashubin, S., Artemieva, I.M., Sobolev, N., Petrov, E., Ernst, R.E., Sergeev, S., and Smelror, M., 2016, Crustal structure and tectonic model of the Arctic region: Earth–Science Reviews, v. 154, p. 29–71, <https://doi.org/10.1016/j.earscirev.2015.11.013>.
- Peucker-Ehrenbrink, B., and Miller, M.W., 2002, Quantitative bedrock geology of the conterminous United States of America: Geochemistry Geophysics Geosystems, v. 3, 8000, <https://doi.org/10.1029/2002GC000366>.
- Peucker-Ehrenbrink, B., and Miller, M.W., 2003, Quantitative bedrock geology of Alaska and Canada: Geochemistry Geophysics Geosystems, v. 4, 8005, <https://doi.org/10.1029/2002GC000449>.
- Peucker-Ehrenbrink, B., and Miller, M.W., 2004, Quantitative bedrock geology of east and south-east Asia (Brunei, Cambodia, eastern and southeastern China, East Timor, Indonesia, Japan, Laos, Malaysia, Myanmar, North Korea, Papua New Guinea, Philippines, far-eastern Russia, Singapore, South Korea, Taiwan, Thailand, Vietnam): Geochemistry Geophysics Geosystems, v. 5, Q01B06, <https://doi.org/10.1029/2003GC000619>.
- Peucker-Ehrenbrink, B., and Miller, M.W., 2007a, Quantitative bedrock geology of Brazil: Geochemistry Geophysics Geosystems, v. 8, Q05014, <https://doi.org/10.1029/2006GC001505>.
- Peucker-Ehrenbrink, B., and Miller, M.W., 2007b, Quantitative bedrock geology of the continents and large-scale drainage regions: Geochemistry Geophysics Geosystems, v. 8, Q06009, <https://doi.org/10.1029/2006GC001544>.
- Phillips, D.A., 2003, Crustal motion studies in the southwest Pacific: Geodetic measurements of plate convergence in Tonga, Vanuatu and the Solomon Islands [Ph.D. thesis]: Honolulu, University of Hawaii, 135 p.
- Regelous, M., Haase, K.M., Freund, S., Keith, M., Weinzierl, C.G., Beier, C., Brandl, P.A., Endres, T., and Schmidt, H., 2014, Formation of the Troodos Ophiolite at a triple junction: Evidence from trace elements in volcanic glass: Chemical Geology, v. 386, p. 66–79, <https://doi.org/10.1016/j.chemgeo.2014.08.006>.
- Resing, J.A., Rubin, K.H., Embley, R.W., Lupton, J.E., Baker, E.T., Dziak, R.P., Baumberger, T., Lilley, M.D., Huber, J.A., Shank, T.M., Butterfield, D.A., Clague, D.A., Keller, N.A., Merle, S.G., Buck, N.J., Michael, P.J., Soule, A., Caress, D.W., Walker, S.L., Davis, R., Cowen, J.P., Reysenbach, A.-L., and Thomas, H., 2011, Active submarine eruption of boninite in the northeastern Lau Basin: Nature Geoscience, v. 4, p. 799–806, <https://doi.org/10.1038/ngeo1275>.
- Rogge, D.M., Rivard, B., Harris, J., and Zhang, J., 2009, Application of hyperspectral data for remote predictive mapping, Baffin Island, Canada: Reviews in Economic Geology, v. 16, p. 209–222, <https://doi.org/10.5382/Rev.16.16>.
- Rubin, K., and the Shipboard Scientific Party, 2018, 2017 NE Lau Basin cruise report: FK171110, R/V *Falkor*, November 10–December 18, 2017, SuBastian dives S085–S105: Honolulu, University of Hawaii, 647 p., <https://doi.org/10.7284/907642>.
- Ruellan, E., and Lagabriele, Y., 2005, Subductions et ouvertures océaniques dans le Sud-Ouest Pacifique: Géomorphologie: Relief, Processus, Environnement, v. 11, p. 121–142, <https://doi.org/10.4000/geomorphologie.307>.
- Ruellan, E., Delteil, J., Wright, I., and Matsumoto, T., 2003, From rifting to active spreading in the Lau Basin–Havre Trough backarc system (SW Pacific): Locking/unlocking induced by seamount chain subduction: Geochemistry Geophysics Geosystems, v. 4, 8909, <https://doi.org/10.1029/2001GC000261>.
- Ryan, W.B.F., Carbotte, S.M., Coplan, J.O., O'Hara, S., Melkonian, A., Arko, R., Weissel, R.A., Ferrini, V., Goodwillie, A., Nitsche, F., Bonczkowski, J., and Zemsky, R., 2009, Global multi-resolution topography synthesis: Geochemistry Geophysics Geosystems, v. 10, Q03014, <https://doi.org/10.1029/2008GC002332>.
- Sabins, F.F., 1999, Remote sensing for mineral exploration: Ore Geology Reviews, v. 14, p. 157–183, [https://doi.org/10.1016/S0169-1368\(99\)00007-4](https://doi.org/10.1016/S0169-1368(99)00007-4).
- Salvador, A., ed., 1994, International Stratigraphic Guide: A Guide to Stratigraphic Classification, Terminology, and Procedure (second edition): Trondheim, Norway, International Subcommission on Stratigraphic Classification of International Union of Geological Sciences, International Commission on Stratigraphy, 214 p.
- Sandwell, D.T., Müller, R.D., Smith, W.H.F., Garcia, E., and Francis, R., 2014, New global marine gravity model from CryoSat-2 and Jason-1 reveals buried tectonic structure: Science, v. 346, p. 65–67, <https://doi.org/10.1126/science.1258213>.
- Sato, T., No, T., Kodaira, S., Takahashi, N., and Kaneda, Y., 2014, Seismic constraints of the formation process on the back-arc basin in the southeastern Japan Sea: Journal of Geophysical Research: Solid Earth, v. 119, p. 1563–1579, <https://doi.org/10.1002/2013JB010643>.
- Scheibner, E., Moore, G.W., Drummond, K.J., Dalziel, I.W., Corvalan, Q.J., Moritani, T., Teraoka, Y., Sato, T., and Craddock, C., compilers, 2013, Tectonic map of the circum-Pacific region, Pacific Basin sheet: U.S. Geological Survey Circum-Pacific Map CP-52, 2 sheets, scale 1:17,000,000, <https://doi.org/10.3133/cp52>.
- Schellart, W.P., Lister, G.S., and Toy, V.G., 2006, A Late Cretaceous and Cenozoic reconstruction of the Southwest Pacific region: Tectonics controlled by subduction and slab rollback processes: Earth–Science Reviews, v. 76, p. 191–233, <https://doi.org/10.1016/j.earscirev.2006.01.002>.
- Schetselaar, E.M., Harris, J.R., Lynds, T., and de Kemp, E.A., 2007, Remote Predictive Mapping 1. Remote Predictive Mapping (RPM): A Strategy for Geological Mapping of Canada's North: Geoscience Canada, v. 34, p. 93–111.
- Schmid, F., Kopp, H., Schnabel, M., Dannowski, A., Heyde, I., Riedel, M., Hannington, M.D., Engels, M., Beniest, A., Klauke, I., Augustin, N., Brandl, P.A., and Devey, C., 2020, Crustal structure and evolution of the Niuafu'ou Microplate in the northeastern Lau Basin, southwestern Pacific: Journal of Geophysical Research: Solid Earth, v. 125, e2019JB019184, <https://doi.org/10.1029/2019JB019184>.
- Schwarz-Schampera, U., Botz, R., Hannington, M., Adamson, R., Anger, V., Cormany, D., Evans, L., Gibson, H., Haase, K., Hirdes, W., Hocking, M., Juniper, K., Langley, S., Leybourne, M., Metaxas, A., Mills, R., Ostertag-Henning, C., Rauch, M., Rutkowski, J., Schmidt, M., Shepherd, K., Stevens, C., Tamburri, K., Tracey, D., and Westernstroer, U., 2007, Cruise report *SONNE* 192/2: MANGO: Marine geoscientific research on input and output in the Tonga–Kermadec subduction zone: Hannover, Bundesanstalt für Geowissenschaften und Rohstoffe, 92 p.
- Sinton, J.M., Johnson, K.T.M., and Price, R.C., 1985, Petrology and geochemistry of volcanic rocks from the Northern Melanesian Borderland, in Brocher, T.M., ed., Geological Investigations of the Northern Melanesian Borderland: Circum-Pacific Council for Energy and Mineral Resources Earth Science Series 3, p. 35–65.
- Sleeper, J.D., and Martinez, F., 2014, Controls on segmentation and morphology along the back-arc Eastern Lau Spreading Center and Valu Fa Ridge: Journal of Geophysical Research: Solid Earth, v. 119, p. 1678–1700, <https://doi.org/10.1002/2013JB010545>.
- Sleeper, J.D., and Martinez, F., 2016, Geology and kinematics of the Niuafu'ou microplate in the northern Lau Basin: Journal of Geophysical Research: Solid Earth, v. 121, p. 4852–4875, <https://doi.org/10.1002/2016JB013051>.
- Sleeper, J.D., Martinez, F., and Arculus, R., 2016, The Fonualei Rift and Spreading Center: Effects of ultraslow spreading and arc proximity on back-arc crustal accretion: Journal of Geophysical Research: Solid Earth, v. 121, p. 4814–4835, <https://doi.org/10.1002/2016JB013050>.
- Smith, W.H.F., and Sandwell, D.T., 1997, Global sea floor topography from satellite altimetry and ship depth soundings: Science, v. 277, p. 1956–1962, <https://doi.org/10.1126/science.277.5334.1956>.

- Staudigel, H., Koppers, A.A.P., Lavelle, J.W., Pitcher, T.J., and Shank, T.M., 2010, Defining the word "seamount": *Oceanography* (Washington, D.C.), v. 23, p. 20–21, <https://doi.org/10.5670/oceanog.2010.85>.
- Stern, R.J., Smoot, N.C., and Rubin, M., 1984, Unzipping of the volcano arc, Japan: *Tectonophysics*, v. 102, p. 153–174, [https://doi.org/10.1016/0040-1951\(84\)90012-X](https://doi.org/10.1016/0040-1951(84)90012-X).
- Stoffers, P., Wright, I., and Shipboard Scientific Party, 1999, Cruise report *SONNE 135*—Havre Trough—Taupo Volcanic Zone: Tectonic, magmatic, and hydrothermal processes: Institut für Geowissenschaften, Universität Kiel, Berichte-Report 1, 249 p., <https://doi.org/10.2312/reports-ifg.1999.1>.
- Stoffers, P., Worthington, T., and Shipboard Scientific Party, 2003, Cruise report *SONNE 167*—Louisville Ridge: Dynamics and magmatism of a mantle plume and its influence on the Tonga-Kermadec subduction system: Institut für Geowissenschaften, Universität Kiel, Berichte-Report 20, 276 p.
- Stoffers, P., Worthington, T.J., Schwarz-Schampera, U., Hannington, M.D., Massoth, G.J., Hekinian, R., Schmidt, M., Lundsten, L.J., Evans, L.J., Vaiomo'unga, R., and Kerby, T., 2006, Submarine volcanoes and high-temperature hydrothermal venting on the Tonga arc, southwest Pacific: *Geology*, v. 34, p. 453–456, <https://doi.org/10.1130/G22227.1>.
- Takahashi, N., Kodaira, S., Tatsumi, Y., Kaneda, Y., and Suyehiro, K., 2008, Structure and growth of the Izu-Bonin-Mariana arc crust: 1. Seismic constraint on crust and mantle structure of the Mariana arc-back-arc system: *Journal of Geophysical Research*, v. 113, B01104, <https://doi.org/10.1029/2007JB005120>.
- Tanaka, K.L., Skinner, J.A., Dohm, J.M., Irwin, R.P., Kolb, E.J., Fortezzo, C.M., Platz, T., Michael, G.G., and Hare, T.M., 2014, Geologic map of Mars: U.S. Geological Survey Scientific Investigations Map 3292, scale 1:20,000,000, 43 p. pamphlet, <https://doi.org/10.3133/sim3292>.
- Tappin, D.R., Bruns, T.R., and Geist, E.L., 1994, Rifting of the Tonga/Lau Ridge and formation of the Lau backarc basin: Evidence from Site 840 on the Tonga Ridge, in Hawkins, J.W., Parson, L.M., Allan, J.F., et al., *Proceedings of the Ocean Drilling Program, Scientific Results, Volume 135*: College Station, Texas, Ocean Drilling Program, p. 367–371, <https://doi.org/10.2973/odp.proc.sr.135.163.1994>.
- Taylor, B., and Karner, G.D., 1983, On the evolution of marginal basins: *Reviews of Geophysics*, v. 21, p. 1727–1741, <https://doi.org/10.1029/RG021i008p01727>.
- Taylor, B., Zellmer, K., Martinez, F., and Goodliffe, A., 1996, Sea-floor spreading in the Lau back-arc basin: Earth and Planetary Science Letters, v. 144, p. 35–40, [https://doi.org/10.1016/0012-821X\(96\)00148-3](https://doi.org/10.1016/0012-821X(96)00148-3).
- Taylor, G.K., Gascoyne, J., and Colley, H., 2000, Rapid rotation of Fiji: Paleomagnetic evidence and tectonic implications: *Journal of Geophysical Research*, v. 105, p. 5771–5781, <https://doi.org/10.1029/1999JB900305>.
- Taylor, P.W., 1991, The geology and petrology of Niuafu'ou Island, Tonga: Subaerial volcanism in an active back-arc basin [M.S. thesis]: Sydney, Australia, Macquarie University, 150 p.
- Thouret, J.-C., 1999, Volcanic geomorphology—An overview: *Earth-Science Reviews*, v. 47, p. 95–131, [https://doi.org/10.1016/S0012-8252\(99\)00014-8](https://doi.org/10.1016/S0012-8252(99)00014-8).
- Tozer, B., Sandwell, D.T., Smith, W.H.F., Olson, C., Beale, J.R., and Wessel, P., 2019, Global bathymetry and topography at 15 arc sec: *SRTM15+ Earth and Space Science*, v. 6, p. 1847–1864, <https://doi.org/10.1029/2019EA000658>.
- Turner, I.M., Peirce, C., and Sinha, M.C., 1999, Seismic imaging of the axial region of the Valu Fa Ridge, Lau Basin—The accretionary processes of an intermediate back-arc spreading ridge: *Geophysical Journal International*, v. 138, p. 495–519, <https://doi.org/10.1046/j.1365-246X.1999.00883.x>.
- van de Lagemaat, S.H.A., van Hinsbergen, D.J.J., Boschman, L.M., Kamp, P.J.J., and Spakman, W., 2018, Southwest Pacific absolute plate kinematic reconstruction reveals major Cenozoic Tonga-Kermadec slab dragging: *Tectonics*, v. 37, p. 2647–2674, <https://doi.org/10.1029/2017TC004901>.
- van der Meer, F.D., van der Werff, H.M.A., van Ruitenbeek, F.J.A., Hecker, C.A., Bakker, W.H., Noomen, M.F., van der Meijde, M., Carranza, J.M., de Smeth, J.B., and Woldai, T., 2012, Multi- and hyperspectral geologic remote sensing: A review: *International Journal of Applied Earth Observation and Geoinformation*, v. 14, p. 112–128, <https://doi.org/10.1016/j.jag.2011.08.002>.
- Volpe, A.M., MacDougall, J.D., and Hawkins, J.W., 1988, Lau Basin basalts (LBB): Trace element and Sr-Nd isotopic evidence for heterogeneity in backarc basin mantle: *Earth and Planetary Science Letters*, v. 90, p. 174–186, [https://doi.org/10.1016/0012-821X\(88\)90099-4](https://doi.org/10.1016/0012-821X(88)90099-4).
- von Stackelberg, U., and Shipboard Scientific Party, 1985, Cruise report *SQ35*—Back-arc hydrothermalism SW-PAC: Hannover, Bundesanstalt für Geowissenschaften und Rohstoffe, 109 p.
- von Stackelberg, U., and Shipboard Scientific Party, 1987, Cruise report *SO48*—Lau Basin hydrothermalism SOPAC: Hannover, Bundesanstalt für Geowissenschaften und Rohstoffe, 122 p.
- von Stackelberg, U., and Shipboard Scientific Party, 1990, R/V *SONNE* cruise report *SO67/2*—Geoscientific investigations in the Lau Basin (southwest Pacific Ocean): Hannover, Bundesanstalt für Geowissenschaften und Rohstoffe, 132 p.
- Wetzel, L.R., Wiens, D.A., and Kleinrock, M.C., 1993, Evidence from earthquakes for book-shelf faulting at large non-transform ridge offsets: *Nature*, v. 362, p. 235–237, <https://doi.org/10.1038/362235a0>.
- Wharton, M.R., Hathway, B., and Colley, H., 1995, Volcanism associated with extension in an Oligocene–Miocene arc, southwestern Viti Levu, Fiji, in Smellie, J.L., ed., *Volcanism Associated with Extension at Consuming Plate Margins*: Geological Society of London Special Publication 81, p. 95–114, <https://doi.org/10.1144/GSL.SP.1994.081.01.06>.
- Wilhelms, D.E., and McCauley, J.F., 1971, Geologic map of the near side of the Moon: U.S. Geological Survey Geologic Investigations Series Map I-703, scale 1:5,000,000, <https://doi.org/10.3133/i703>.
- Wilkinson, B.H., McElroy, B.J., Kesler, S.E., Peters, S.E., and Rothman, E.D., 2009, Global geologic maps are tectonic speedometers: Rates of rock cycling from area-age frequencies: *Geological Society of America Bulletin*, v. 121, p. 760–779, <https://doi.org/10.1130/B26457.1>.
- World Resources Institute, 2011, Reefs at Risk: <https://www.wri.org/our-work/project/reefs-risk> (accessed February 2020).
- Yan, C.Y., and Kroenke, L.W., 1993, A plate tectonic reconstruction of the Southwest Pacific, 0–100 Ma, in Berger, W.H., Kroenke, L.W., Mayer, L.A., et al., *Proceedings of the Ocean Drilling Program, Scientific Results, Volume 130*: College Station, Texas, Ocean Drilling Program, p. 697–709, <https://doi.org/10.2973/odp.proc.sr.130.055.1993>.
- Yeo, I., 2016, Axial volcanic ridges, in Harff, J., Meschede, M., Petersen, S., and Thiede, J., eds., *Encyclopedia of Marine Geosciences*: Dordrecht, Netherlands, Springer, p. 36–39, https://doi.org/10.1007/978-94-007-6644-0_2-2.
- Zellmer, K.E., and Taylor, B., 2001, A three-plate kinematic model for Lau Basin opening: *Geochemistry Geophysics Geosystems*, v. 2, 1020, <https://doi.org/10.1029/2000GC000106>.
- Zhao, D., Xu, Y., Wiens, D.A., Dorman, L., Hildebrand, J., and Webb, S., 1997, Depth extent of the Lau back-arc spreading center and its relation to subduction processes: *Science*, v. 278, p. 254–257, <https://doi.org/10.1126/science.278.5336.254>.
- Zhao, D., Maruyama, S., and Omori, S., 2007, Mantle dynamics of Western Pacific and East Asia: Insight from seismic tomography and mineral physics: *Gondwana Research*, v. 11, p. 120–131, <https://doi.org/10.1016/j.gr.2006.06.006>.